Kinetic Studies of Group VI Metastable Atoms and Molecules

by

William John McElroy

A Thesis presented for the degree
of Doctor of Philosophy in the
Faculty of Science in the
University of Edinburgh
1979

Acknowledgements

I would like to thank the Department of Education for Northern Ireland and Procter and Gamble Ltd. for providing financial support, and Professor C. Kemball and the Department of Chemistry for providing laboratory and technical facilities. The services of Mr. J. Broom for glassblowing, Mr. A. King and the electronic workshop and Mr. J. Ashfield and the mechanical workshop are gratefully acknowledged.

To Dr. R.J. Donovan, who through his patience, enthusiasm and encouragement has helped me throughout the past three years, I am particularly grateful. I am also indebted to Miss J. Champion for help in obtaining the results reported in chapters 4 and 5, Dr. P.R.H. Speakman of Procter and Gamble Ltd. for useful discussions and Mr. E. Lucey of the University of Edinburgh Film Unit for his enthusiastic help and expertise in obtaining high speed films. I have enjoyed the company of my fellow research students, especially Dr. C. Fotakis, Dr. H.M. Gillespie, Mr. J. Garraway and Mr. M.C. Addison. I would like to thank Mrs. J. Gorrie for typing the thesis.

Finally, I thank my parents who have always encouraged and supported me in my studies.

To Stewart and Jenny

Abstract

Kinetic processes involving the low-lying metastable electronically excited states of the group VI atoms, oxygen and sulphur, and diatomics, O_2, S_2 and SO have been investigated.

Singlet molecular oxygen, $O_2(^1\Delta_g)$ was generated by the reaction of hydrogen peroxide with sodium hypochlorite and its subsequent decay monitored by the 'dimol' emission at λ = 633 nm. A simple experimental arrangement is described for determining the rate constants for quenching of $O_2(^1\Delta_g)$ by $O_2(^3\Sigma_g^-)$ and H_2O. It was shown that conditions were readily obtainable under which the decay of $O_2(^1\Delta_g)$ in the bubbles was controlled by quenching in the gas phase, and where gas-surface interactions were negligible.

Singlet sulphur monoxide, $SO(^1\Delta)$ was produced by the reaction of $O(2^1D_2)$ atoms with OCS. The initially rapid removal of ozone in this system was accounted for by the reaction of $SO(^1\Delta)$ with O_3. Rate constants for the reactions of both $SO(^1\Delta)$ and $SO(^3\Sigma^-)$ with O_3 were obtained by computer modelling.

Photolysis of OCS (λ > 200 nm) yields $S(3^1D_2)$ atoms, which react on almost every collision with carbonyl sulphide to produce singlet molecular sulphur, $S_2(^1\Delta_g)$. Both $S_2(^1\Delta_g)$ and $S_2(^3\Sigma_g^-)$ were observed in absorption using kinetic spectroscopy. A rate constant for quenching of $S_2(^1\Delta_g)$ by OCS was obtained from the formation kinetics of ground state sulphur, $S_2(^3\Sigma_g^-)$. This process is discussed qualitatively in terms of electronic to vibrational energy transfer.

Photolysis of O_3 ($\lambda_{u.v.}$ < 310 nm) was employed as a source of $O(2^1D_2)$ atoms. The primary and secondary reactions which follow ozone photolysis were investigated. Ozone was monitored by kinetic absorption spectrophotometry at λ = 253.7 nm. Computer modelling studies were carried out and these provided

a better understanding of the processes involved, and in particular, with regard to the reaction of $O(2^1D_2)$ atoms with ozone.

The reactions of $O(2^1D_2)$ atoms with several chlorofluoromethanes in the presence of ozone were studied. Schemes are presented to account for the observed removal of ozone obtained for CF_3Cl and CF_2Cl_2.

CONTENTS

Chapter 1

Introduction

1.01 Introduction

Absorption of electromagnetic radiation by atoms and molecules in the visible and ultraviolet regions of the spectrum leads to electronic excitation of the absorbing species. The fate of such excited states is often very different from that of the ground state. In recent years the development of sophisticated experimental techniques has led to an increased interest in the chemical behaviour of electronically excited states of atoms and molecules.

In this work the properties of electronically excited atoms and molecules belonging to Group VI have been investigated, particularly those of oxygen and sulphur. The secondary reactions following ozone photolysis in the presence of chlorofluoromethanes have also been studied.

Since the reactions of atomic sulphur and oxygen have been extensively reviewed,[1,2,3] this introduction is primarily concerned with the physical and chemical properties of the low lying electronic states of Group VI diatomic molecules. First, the various techniques commonly employed to study excited molecules are described. A general outline of the main characteristics of Group VI electronic states is then given, followed by a more detailed background discussion of those species which are particularly relevant to the present study.

1.02 Experimental Techniques

Flash Photolysis, developed originally by Norrish and Porter (1949),[4] has largely been responsible for the growth of interest in photochemical phenomena over the past thirty years.

It is still amongst the most powerful and versatile techniques available for the direct study of transient species. Two basic versions of this technique have been developed - kinetic spectroscopy and kinetic spectrophotometry - and both are described in detail in Chapter 2.

The advent of lasers has brought the time resolution of flash photolysis into the picosecond region,[5] as well as providing a highly specific means of exciting a molecule to a selected state or causing photodissociation to give particular products.

Chemical lasers have proved to be useful tools for probing particular chemical systems,although kinetic data can be derived directly by observing the operation of the laser under varying conditions.[6] The a priori requirement of the laser, the formation of a population inversion,means that information can only be obtained from a small number of systems. Low pressure 'discharge flow' systems provide another successful means of studying the reactions of metastable species. Electronically excited atoms and molecules are generated by passing the gas stream through an electric discharge before entering the reaction tube. The tube is typically operated at pressures in the range 13 Nm^{-2} to 1.3 kNm^{-2} with a flow speed of 10 ms^{-1}.[7] Electrodeless discharges are preferred as no electrode material is in contact with the discharge products. Microwave discharges are more stable than radiowave and can be used over a wider range of pressures.

Within a few centimeters of the discharge all short-lived excited states have disappeared and only ground state or metastable atomic and molecular species are left in the carrier gas.

Reactants can be added downstream from the discharge and the progress of the reaction followed by a wide range of analytical techniques. A linear time scale is provided by the distance between the mixing and analysis zones when the flow rate is known. The effects of wall recombination processes, diffusion and turbulence must be considered in the analysis of the experimental results.

Techniques used to study reactions of metastable species in flow systems include mass spectrometry,[8] E.P.R. spectroscopy,[9] absorption spectroscopy,[10] infrared[11] and visible[12] chemiluminescence and also photoelectron spectroscopy.[13]

Modulation techniques have also been used to study the kinetics of excited states. The radiative lifetime of an excited state may be determined using a modulated light source to excite the ground state species, and measuring the phase shift between the fundamental components of the exciting light and the resulting modulated fluorescence. By varying the experimental conditions, rate constants can be determined from measurements of the lifetime and fluorescence intensity.[14]

Molecular modulation spectroscopy was originally developed by Johnston et al.[15] The photolysis light is modulated at a known frequency ($\sim$32 Hz) and the light transmission through the cell at any given wavelength is monitored by phase sensistive detection. Spectra of transient free radicals have been observed in both the infrared and ultraviolet regions for species such as ClO, ClOO,[16] CH_3 and HO_2.[17] Modified versions of the technique have been described by Phillips et al.[18] to determine rate constants for reactions of excited Hg and Xe atoms, and by Parkes[17] to study the

ultraviolet spectra and kinetics of alkyl radicals. Reaction rates are measured by varying the modulation frequency, when it is also possible to pick out transients with different lifetimes when more than one is present. It would seem that phase-shift methods have considerable unrealised potential in the determination of lifetimes, spectra and reaction rates of transient and metastable molecules.

1.03 General Characteristics of Group VI Diatomics

The ground state electronic configuration of Group VI homonuclear diatomics correlates with the combination of two ground state ^3P atoms:-

$$\ldots\ldots (\sigma_g ns)^2 (\sigma_u ns)^2 (\sigma_g np)^2 (\pi_u np)^4 (\pi_g np)^2$$

Thus the highest occupied orbitals are a doubly degenerate antibonding pair, holding only two electrons. For the free diatomic molecule, when orbital angular momentum about the bond is quantised, these two orbitals are denoted as π_+ and π_-, the sign denoting $\pm \hbar$ units of angular momentum.

Three low lying electronic states arise from this configuration, these being $^3\Sigma_g^-$, $^1\Delta_g$ and $^1\Sigma_g^+$. According to Hund's rule, $^3\Sigma_g^-$ is the state of lowest energy since it has the highest spin multiplicity. The $^1\Delta_g$ state is doubly degenerate and has a component of angular momentum $\pm 2\hbar$ about the molecular axis. The $^1\Sigma_g^+$ state lies highest in energy and is diamagnetic, the net angular momentum of the two electrons being zero.

The $^1\Delta_g$ and $^1\Sigma_g^+$ states are metastable, since electric dipole transitions to the ground triplet state are strongly forbidden ($\Delta S \neq 0$) in the absence of some spin-dependent

perturbation. Nuclear exchange symmetry means that the $^1\Sigma_g^+ \rightarrow {}^1\Delta_g$ transition is also forbidden. Magnetic dipole transitions to the ground state are possible for the $^1\Delta_g$ and $^1\Sigma_g^+$ states, although these are rather weak. They have been observed in absorption and emission for oxygen,[7] being known as the "infra-red atmospheric" and "atmospheric" bands respectively. Under normal laboratory conditions, collisional rather than radiative processes are responsible for the removal of these metastable species. However, the efficiency of the radiative processes should increase substantially for the heavier diatomics of the group as Russell-Saunders coupling becomes less important, spin-orbit coupling becoming more so. Table 1 lists known or estimated energies and probabilities for some of these transitions.

Spin-orbit coupling studies for oxygen[19,20] show that the $^1\Sigma_g^+$ and $^3\Sigma_g^-$ states are coupled by a matrix element of $\sim$140 cm^{-1} whereas this does not occur in the case of the $^1\Delta_g$ and $^3\Sigma_g^-$ states. This implies that the radiative lifetime of the $^1\Sigma_g^+$ state should be significantly shorter than that of the $^1\Delta_g$ state. This is well known for oxygen and should be true for the heavier members of the group where spin orbit coupling is stronger.

In the case of heteronuclear diatomics, nuclear exchange symmetry is absent, so that this too should contribute towards shorter radiative lifetimes being observed for the metastable states of these molecules, as opposed to those for homonuclear diatomics.

Table 1: The known or estimated term values for the low lying singlet states of Group VI diatomic molecules, where these are available, and ground state transition probabilities.

Diatomic	State	Te/cm^{-1}	Transition probability(A)/s^{-1}	Ref.
O_2	$a^1\Delta_g$	7882.39	3.7×10^{-4}	22
	$b^1\Sigma_g^+$	13120.91	1.4×10^{-1}	22
S_2	$a^1\Delta_g$	∿4700	-	69
	$b^1\Sigma_g^+$	9090	-	66
SO	$a^1\Delta$	6150	-	167
	$b^1\Sigma^+$	10509.97	-	77

1.04 Singlet Molecular Oxygen

The low lying singlet states of molecular oxygen are amongst the most extensively studied of all metastable molecules. Excellent reviews of the production, reactions and quenching of $O_2(a^1\Delta_g)$ and $O_2(b^1\Sigma_g^+)$ have appeared,[7,21] and only more recent work will be discussed here. The role of these species in atmospheric chemistry will be considered in Chapter 4.

The $^1\Sigma_g^+$ and $^1\Delta_g$ states of oxygen have been observed in emission and lie at 13,121 cm^{-1} and 7882 cm^{-1} respectively above the ground state.[22] Energy pooling processes, which occur on the collision of pairs of excited oxygen molecules, can result in the simultaneous loss of energy from both molecules [1], known as "dimol" emission, or may lead to the formation of $O_2(^1\Sigma_g^+)$ by an "annihilation" reaction [2].[23]

$$O_2(^1\Delta_g) + O_2(^1\Delta_g) \longrightarrow O_2(^3\Sigma_g^-) + O_2(^3\Sigma_g^-) + h\nu \qquad [1]$$

$$O_2(^1\Delta_g) + O_2(^1\Delta_g) \longrightarrow O_2(^1\Sigma_g^+) + O_2(^3\Sigma_g^-) \qquad [2]$$

The weak orange-red emission accompanying a number of reactions,[24,25,26] where $O_2(^1\Delta_g)$ is generated in solution, is due to such simultaneous transitions. Although the probability for these 'dimol' processes is low, the emission provides a suitable means of measuring $O_2(^1\Delta_g)$ concentrations, since the sensitivity of detectors capable of detecting the $^1\Delta_g \rightarrow {}^3\Sigma_g^-$ transition at 1.27μ tends to be poor.[27,28]

Potassium permanganate undergoes aqueous decomposition with formation of up to 6% of oxygen in the singlet delta state,[29] which was monitored by the emission at 1.27μ. Chemiluminescence is also readily observed when a basic potassium chromate solution reacts with peroxide at room temperature[29]. The 1.27μ emission has been detected following irradiation of porphyrins and is strongly quenched on the addition of metalloporphyrins.[30]

Evidence for singlet oxygen involvement in many solution phase reactions has come from product analysis. The intermediacy of $O_2(^1\Delta_g)$ in such oxidation processes is often not the sole possible explanation[31] and participation in a number of enzyme systems now seems unlikely.[32] It has been shown that singlet oxygen is not formed in the decomposition of H_2O_2 in the presence of catalase or horseradish peroxidase,[33] but it may be produced in the base catalysed disproportionation of H_2O_2.[34] The role of $^1O_2$ in organic peroxide systems has been reviewed.[35]

Recently, spectroscopic evidence for the generation of singlet oxygen in NADPH-dependent microsomal lipid peroxidation systems has been produced.[36,37] The light emitted by the system is characteristic of the dimol emission spectrum of singlet oxygen and is quenched in the presence of various radical trappers.

The lifetime of singlet oxygen in solution has been measured by Kearns and the nature of the solvent was found to have a marked effect.[38] Values ranged from 2μs in H_2O to 700μs in CCl_4. A striking parallel between the $^1\Delta_g$ lifetime and the intensity of the solvent absorption near the (0,0) and (0,1) bands of the $^1\Delta_g \rightarrow {}^3\Sigma_g^-$ transition was apparent. To account for this, a simple theory, with no adjustable parameters, was developed[39] in terms of intermolecular electronic to vibrational energy transfer, and gave better than order of magnitude agreement with experimental results. Solution phase rate constants could be used to compute gas phase values. Direct spectroscopic evidence of a deuterium solvent effect on the lifetime of $O_2(^1\Delta_g)$ has been accounted for in terms of this theory.[27] Kearns found the lifetime of $O_2(^1\Delta_g)$ in D_2O to be 20μs

compared with 2μs in H_2O, although the former has recently been determined and to be nearer 30μs[40,41]. More recently the effect of temperature on the lifetime of $O_2(^1\Delta_g)$ has been investigated.[42]

Gas phase quenching rate constants for singlet oxygen have been reviewed.[43,44] Kear and Abrahamson[43] noted a relationship between the highest fundamental vibrational frequency of the quenching molecule and its quenching efficiency for $O_2(^1\Sigma_g^+)$. Davidson and Ogryzlo[44] also noted this correlation and suggested that rate constants could be calculated from the overlap of the absorption spectrum of the quencher with the emission spectrum of the $O_2(^1\Sigma_g^+ \rightarrow {}^1\Delta_g)$ progression. The use of extinction coefficients for the quenching molecule and calculated Franck-Condon factors for the $(^1\Sigma_g^+ \rightarrow {}^1\Delta_g)$ transition, rather than exact overlap integrals, limited the success of the theory.

More recently Ogryzlo et al.[45] have calculated values of k_q based on the assumption that relaxation results from long range interactions between the transition quadrupole of $O_2(^1\Sigma_g^+)$ and the transition quadrupole and dipole of the quencher. The contribution of short range repulsive forces to k_q have been calculated by Kear and Abrahamson[46] using a distorted wave approach. Together, the long and short range interactions provide reasonable agreement between observed and calculated values. Statistical theory[47] has also been used to account for quenching of both $O_2(^1\Sigma_g^+)$ and $O_2(^1\Delta_g)$, including the case where rotational and translational energy contribute to the excitation of the products.

Fewer small quenchers have been studied in the case of $O_2(^1\Delta_g)$ and analysis of the available data is therefore less satisfactory, though not inconsistent with a similar E → V transfer mechanism. Indeed, infrared emission from a number of species[48] including NO[49], CO_2[50] and HF[51] has been observed following deactivation of $O_2(^1\Delta_g)$ and $O_2(^1\Sigma_g^+)$. This confirms energy transfer into the internal modes of the quencher, although Thrush[49,50] has found that near resonance is not generally important in the quenching of singlet molecular oxygen.

The energy gap for the $^1\Delta_g \rightarrow {}^3\Sigma_g^-$ transition is 0.3371 eV greater than that for $^1\Sigma_g^+ \rightarrow {}^1\Delta_g$, so fewer quenching molecules have significant absorptions in this region. Furthermore, the quenching process is spin forbidden. Both these factors account for a decrease in the relaxation probability for $O_2(^1\Delta_g)$ by five orders of magnitude over $O_2(^1\Sigma_g^+)$. Higher values of k_q are observed for non-zero spin species such as NO_2, NO and O_2, when the quenching process becomes spin allowed. A charge transfer mechanism has been invoked to account for the efficiency of species such as sulphides and amines.[52] Little information on the temperature dependence of k_q is available for simple molecules, although Arrhenius parameters have been reported for gas phase cycloaddition reactions[53] and for reactions of $O_2(^1\Delta_g)$ with a number of olefins[54].

Kenner and Khan[55] have reported the molecular oxygen induced fluorescence of polycyclic aromatic hydrocarbons in polymer matrices. Admission of air to a phosphorescing sample gives rise to a burst of light with the same emission spectrum as normal fluorescence of the organic molecule.

$$T_1 + O_2(^3\Sigma_g^-) \rightarrow S_0 + O_2(^1\Delta_g, {}^1\Sigma_g^+) \quad [3]$$

$$T_1 + O_2(^1\Delta_g, {}^1\Sigma_g^+) \rightarrow S_1 + O_2(^3\Sigma_g^-) \quad [4]$$

$$S_1 \longrightarrow S_0 + h\nu_{fluorescence} \quad [5]$$

The singlet oxygen molecule generated in the quenching of the organic triplet,[56] T_1, can by energy transfer excite a second organic triplet molecule to the singlet excited state, S_1, so enhancing fluorescence by a "singlet oxygen feedback mechanism"[57,58].

Irradiation of a mixture of NO_2 and O_2 (λ = 300-590 nm) produces $O_2(^1\Delta_g)$[59] by energy transfer from electronically excited NO_2 to O_2. In the urban environment, high NO_2 concentrations may produce enough O_2 ($^1\Delta_g$) to make a significant contribution to photochemical smog formation.[60,61]

The collisional deactivation of $I(5^2P_{\frac{1}{2}})$ by oxygen has been investigated.[62,63] It has been suggested that

$$I(5^2P_{\frac{1}{2}}) + O_2(^3\Sigma_g^-) \rightarrow I(5^2P_{3/2}) + O_2(^1\Delta_g) \quad [6]$$

the reverse process [6] might be used to pump an iodine atom laser,[64] though obtaining a continuous source of $O_2(^1\Delta_g)$ would appear to be a major difficulty.

Energy transfer from $O_2(^1\Sigma_g^+, {}^1\Delta_g)$ to other diatomic molecules, resulting in emission, has been observed for a number of halogens and interhalogens, where excitation of the B-X system occurs e.g. I_2, Br_2, IF and BrF.[65]

1.05 Singlet Molecular Sulphur

When compared with oxygen, relatively little is known about the low lying metastable states of sulphur. A report of an S_2 laser based on the $^1\Sigma_g^+ \rightarrow {}^3\Sigma_g^-$ transition at 1.1μm has been made,[66] but no other direct observation of emission from the $^1\Sigma_g^+$ or $^1\Delta_g$ states has been reported. Thus only estimates can be made of the energies at which these states lie above the triplet ground state.

Emission to the $^1\Delta_g$ state has been observed under high resolution, via the $f^1\Delta_u \rightarrow a^1\Delta_g$ transition, by Barrow and Duparq.[67,68] Some 28 bands have been assigned to this system by Colin.[69] By comparison with oxygen and parallel extrapolation of the vibrational levels of the $^1\Delta_g$ and $^3\Sigma_g^-$ states, the $^1\Delta g$ state has been estimated to lie ∿4,700 cm^{-1} [69] above the ground state, although there may be an error of ∿800 cm^{-1} in this value.

The $f^1\Delta_u \rightarrow a^1\Delta_g$ system has also been observed in absorption following the photolysis of a number of small sulphur containing molecules[70,71,72] including H_2S, H_2S_2, OCS, CS_2, S_2Cl_2, SPF_3 and SCl_2. Although OCS is a weak absorber in the ultraviolet, it is the cleanest source of $S(3^1D_2)$ atoms.

$$OCS + h\nu_{u.v.} \rightarrow CO(^1\Sigma^+) + S(^1D_2) \qquad [7]$$

$$S(^1D_2) + OCS \rightarrow S_2(^1\Delta_g) + CO(^1\Sigma^+) \qquad [8]$$

$S_2(^1\Delta_g)$ is formed by the subsequent fast reaction of $S(^1D_2)$ with OCS which occurs with almost every collision. The spectrum is short lived and its intensity closely follows the output of the flash lamp.[72] However, there is little

kinetic or mechanistic information available on the removal of $S_2(^1\Delta_g)$. Since the radiative lifetime of $S_2(^1\Delta_g)$ is likely to be comparable with that of $O_2(^1\Delta_g)$, it is to be expected that collisional deactivation to the ground state is the most important removal process. The importance of energy pooling processes, which are comparable with the 'dimol' reactions in oxygen, is not known, although catenation is an important feature of ground state sulphur chemistry.[73] One disadvantage of studying reactions of $S_2(^1\Delta_g)$ in this system is that molecules which might be expected to quench $S_2(^1\Delta_g)$ efficiently are also efficient quenchers of $S(^1D_2)$, so that the yield of the former species is reduced.

1.06 Singlet Sulphur Monoxide

Although $SO(^1\Delta)$ has not been observed either in absorption or emission*, it has been detected by electron paramagnetic resonance when the products of a microwave discharge in oxygen are mixed with small sulphur containing molecules such as OCS and H_2S.[74,75,76] The optical spectrum of the bright blue fluorescence which results from this reaction has been reported[77] and $SO(^1\Sigma)$ has been observed in emission to the ground state[77] at 950 nm. $O(^3P)$ atoms produced by the discharge react with H_2S or OCS to produce $SO(^3\Sigma)$ [9]. Carrington et al.[75] have proposed that direct excitation of $SO(^3\Sigma^-)$ by $O_2(^1\Delta_g)$ occurs by a simple spin allowed energy transfer mechanism [10] to produce $SO(^1\Delta)$ and ground state oxygen.

*Emission from $SO(^1\Delta)$ has recently been reported[167], see Chapter 6.

$$O(^3P) + OCS \rightarrow SO(^3\Sigma^-) + CO(^1\Sigma^+) \quad [9]$$

$$SO(^3\Sigma^-) + O_2(^1\Delta_g) \rightarrow SO(^1\Delta) + O_2(^3\Sigma_g^-) \quad [10]$$

The rate of this reaction is unusually high when compared with most quenching reactions involving $O_2(^1\Delta_g)$ suggesting that the process is near resonant. ($k_{10} = 3.65 \pm .36 \times 10^{-13}$ cm^3 molec^{-1}s^{-1}). The rate constant for reaction [10] was determined by EPR, this technique having the advantage that all four species involved could be detected. Clark and De Lucia[76] have used this reaction to study the microwave spectrum of $SO(^1\Delta)$.

The reaction of metastable oxygen atoms with OCS has been studied,[78] with particular reference to the CO product vibrational energy distribution. Although the product state of SO is not known, orbital correlation rules predict that SO should be formed in either the $^1\Delta$ or $^1\Sigma$ states.

In flow systems, the removal of $SO(^1\Delta)$ is rapid[74] and occurs mainly by deactivation at the walls of the reaction vessel. The efficiency of this process is some four orders of magnitude faster than that for $O_2(^1\Delta_g)$.

The radiative lifetime of $SO(^1\Delta)$ is likely to be very different from that of the homonuclear species already discussed. In O_2, the electric dipole transition between the $^1\Delta_g$ and $^3\Sigma_g^-$ states is forbidden on grounds of spin conservation and nuclear exchange symmetry. The transition is therefore via a magnetic dipole mechanism. In SO, nuclear exchange symmetry is absent, so assuming that some mixing of the π_+^* and π_-^* states occurs, electric dipole transitions will be partially allowed and may even be enhanced by the heavier sulphur atom. Thus the radiative lifetime of $SO(^1\Delta)$ may be several orders of magnitude shorter than that of $O_2(^1\Delta_g)$.

1.07 Singlet Molecular Selenium and Tellurium

Direct observation of $Se_2(a^1\Delta_g)$ in absorption has not been achieved, although its formation has been postulated. The first excited singlet state of atomic selenium has been observed,[79] using time resolved atomic absorption spectroscopy. The reaction of this species with OCSe is expected to yield Se_2 in the $^1\Delta_g$ or $^1\Sigma_g^+$ states. Indirect evidence for this comes from observations of the rate of formation of ground state Se_2 on photolysis of OCSe.[1]

$$OCSe + h\nu \rightarrow CO + Se(4^1D_2) \quad [11]$$

$$Se(4^1D_2) + OCSe \rightarrow CO + Se_2(^1\Delta_g) \quad [12]$$

$$Se_2(^1\Delta_g)(+M) \rightarrow Se_2(^3\Sigma_g^-)(+M) \quad [13]$$

A mechanism similar to that for OCS photolysis suggests that reaction [13] is very fast. It is uncertain whether $Se_2(^1\Delta_g)$ is removed by radiative or collisional processes. If $Se(4^1D_2)$ is partially quenched in the presence of CO_2, then a secondary growth of $Se_2(^3\Sigma_g^-)$ is observed, with a second maximum occuring at ca. 50μs which is consistent with the formation of Se_2 by atomic recombination.

No information is available regarding the low lying electronic states of molecular tellurium. Although singlet atomic tellurium (5^1D_2) has been observed by resonance absorption on photolysis of D_2Te,[80] no analogous reactions to those of $S(^1D_2)$ and $Se(^1D_2)$ are known.

Chapter 2

Experimental Methods

2.01 Introduction

In the study of the kinetics of electronically excited states, several important features are required of the experimental techniques employed. Firstly, the excited species must be generated on a time scale which is short when compared with that for the removal processes. Temperature jump, discharge flow and shock tube techniques are amongst the methods which have been used to produce non equilibrium concentrations of excited species. One of the most successful has been flash photolysis, which makes use of a short, but intense pulse of light. Electronically excited molecules are formed by photodissociation of some parent molecule, by direct excitation, or by a secondary process.

Secondly, the reliability and accuracy of kinetic data derived by any experimental method depends mainly on the signal to noise ratio. The development of large aperture spectrographs and monochromators, sensitive photoelectric detectors and modern data handling facilities - such as fast analogue to digital convertors and signal averaging - has led to remarkable improvements in the signal to noise ratio. However, careful experimental design remains crucial to the success of any method.

Three techniques were employed in this work to study the reactions of electronically excited molecules.

Chemiluminescence:-

The 'dimol' emission at 633 nm, associated with energy pooling processes involving singlet oxygen, provides an ideal means of monitoring this species. Luminescence, arising from the reaction of hydrogen peroxide and sodium hypochlorite, is

readily visible by eye in a darkened room and offers a novel means of studying singlet oxygen kinetics.

Flash Photolysis with Kinetic Spectroscopy:-

A spectroflash of short duration, providing a 'white-light' continuum from 200 nm to the near infrared, is fired at a preset delay (10μs-1s) after the initial photolysis flash. The absorption spectra of the transient intermediates are recorded photographically by a spectrograph, so that a kinetic profile of the reaction is built up over a series of exposures. One advantage of this technique is that transient spectra can be observed within the duration of the primary photolysis flash, and it is particularly useful in preliminary work on a reaction system where the spectra of the transients is either uncertain or unknown.

Flash Photolysis with Kinetic Spectrophotometry:-

A monochromatic light source is focused through the reaction vessel and the attenuation of the incident radiation monitored at a particular wavelength using a photoelectric detector, typically a photomultiplier, and a fast recorder, such as a transient recorder or storage oscilloscope. Species which are only present during the photolysis flash cannot be detected by this method because scattered light from the flash causes interference. However simplicity and accuracy are amongst the advantages of using kinetic spectrophotometry, once the intermediates are known, since a complete concentration time profile can be obtained in a single experiment.

2.02 Chemiluminescence

Many chemiluminescent reactions have been studied in the gas phase using flow systems,[7] where an electric discharge can provide relatively high concentrations of metastable atoms and molecules.

This section describes a novel, yet simple experimental arrangement for determining rate constants for quenching of $O_2(a^1\Delta_g)$ by ground state O_2 and water. Singlet oxygen was formed in solution by the reaction of hydrogen peroxide (100 vol) with sodium hypochlorite and monitored by the 'dimol' luminescence at 633 nm. The intensity of this luminescence has been shown to vary as the square of the $O_2(a^1\Delta_g)$ concentration.[81]

The apparatus (Figure 1) consisted of a three necked flask (250 ml) a burette being mounted on the centre neck. Depending on the experimental requirements, one side arm served as an outlet to a water suction pump and a mercury monometer, or as a gas inlet, while the other served as a gas outlet to a Dreschel Flask.

A photomultiplier, type EMI 9664B, with an enhanced red response was placed directly under the flask. The photomultiplier dynode chain was of standard 9 stage high gain design (Figure 2a), the output being fed into a current to voltage converter and amplified to obtain a suitably large trigger pulse for a signal averager (Datalab DL 4000). Information was stored in a random access integrated circuit memory of 1024 x 20 bit words,with a minimum time resolution of 10μs per sample, signal averaging being carried out by algebraic summation, with a maximum resolution of 12 bits. Data held

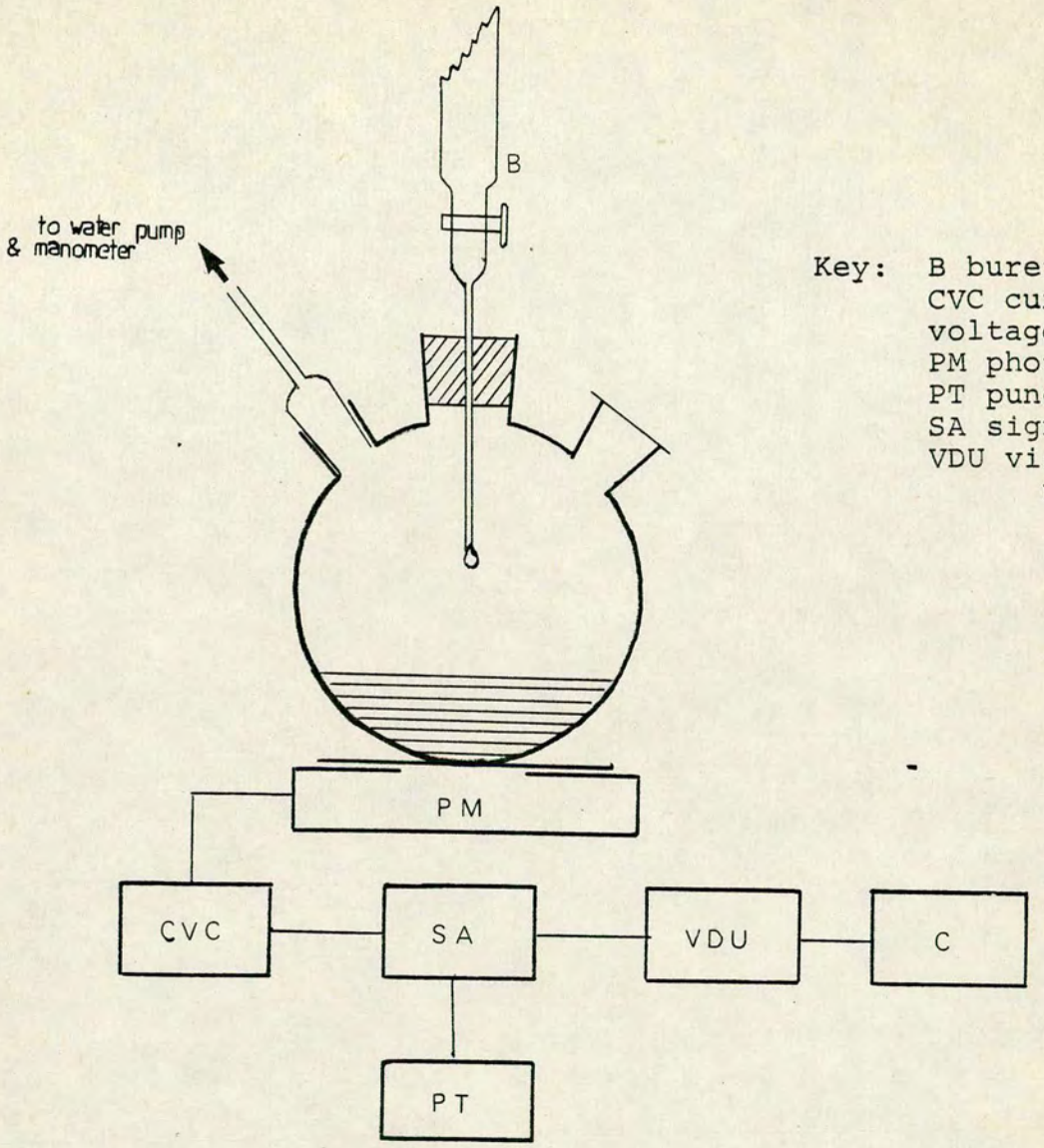

Key: B burette; C camera; CVC current to voltage converter; PM photomultiplier PT punch tape; SA signal averager; VDU visual display unit.

Figure 1: Experimental arrangement for the detection of emission arising from the NaOCl/H_2O_2 reaction.

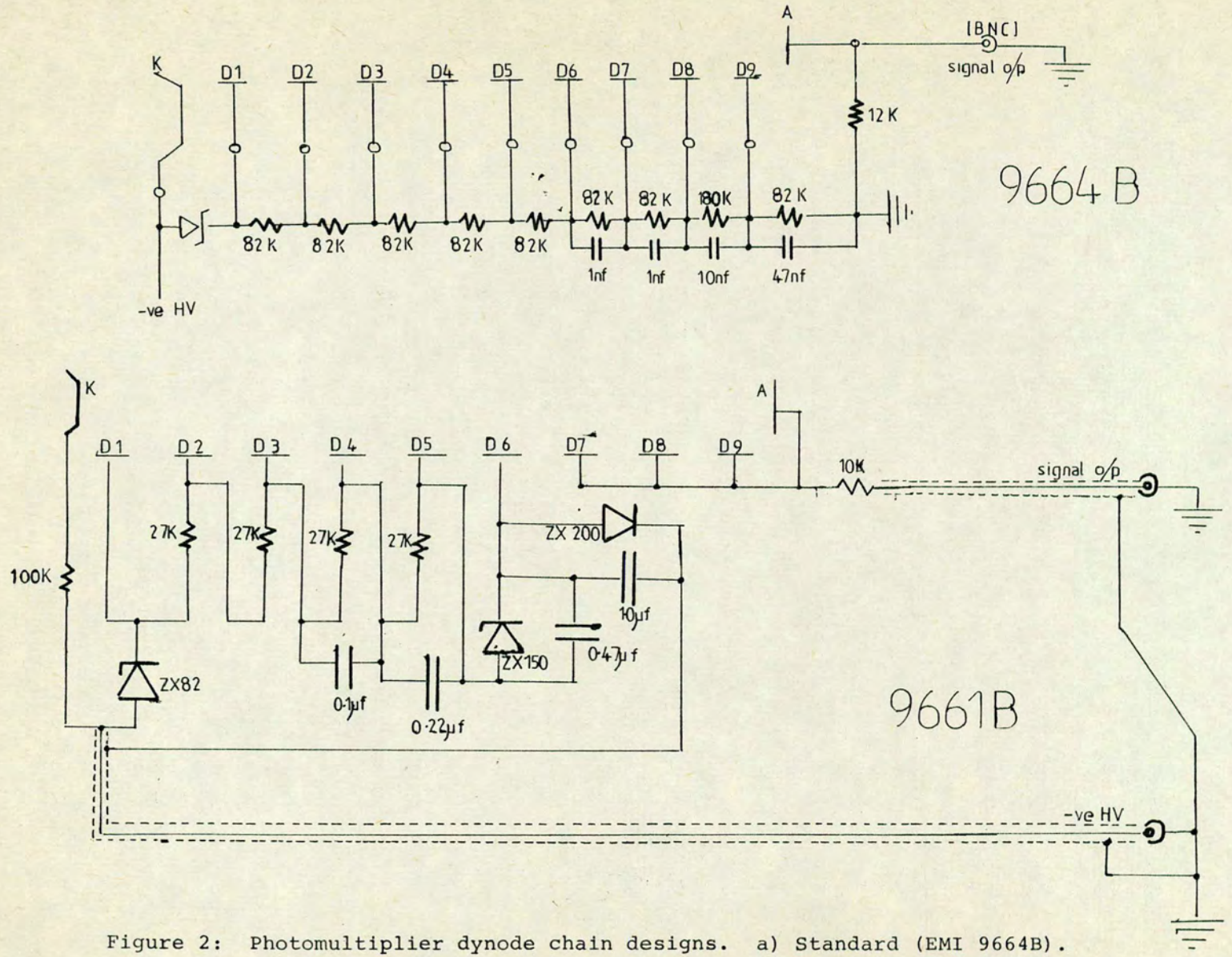

Figure 2: Photomultiplier dynode chain designs. a) Standard (EMI 9664B).
b) Low gain (EMI 9661B).

in the memory was displayed on an oscilloscope (Telequipment DM64) and could be punched out on computer tape (Data Dynamics 1133) using ASC 11 code. A programme contaning a weighted least squares fit and a graph plotting subroutine was written to process the experimental data (see Appendix 3).

In a typical experiment 30 cm^3 of 100 volume H_2O_2 (Fison's SLR) were placed in the three necked flask, and sodium hypochlorite (Fison's technical grade) added dropwise from the burette. By varying the bore of the burette tip, different drop sizes could be obtained. Smaller volumes were added using a microsyringe.

The triggering level of the signal averager was adjusted so that a new recording cycle was initiated with each drop of NaOCl, the number of cycles being preset before each experiment. All possible sources of stray light were eliminated. By inserting various glass filters between the flask and the photomultiplier, different bands of the $[O_2(a^1\Delta_g)]^2$ emission could be detected and this was achieved for the (0,1), (0,0) and (1,0) bands. The flask could also be placed in a heating mantle or ice-bath, so that decay of luminescence was studied over a range of temperatures (273^oK-353^oK) and pressures (20-100 kN m^{-2}).

2.03 High Speed Film Techniques

In order to study the nucleation and growth of oxygen bubbles formed during the H_2O_2/NaOCl reaction, two high speed films of the reaction were made. Although both vertical and horizontal views of the reaction were recorded, only the method for the former will be described in detail (Figure 3).

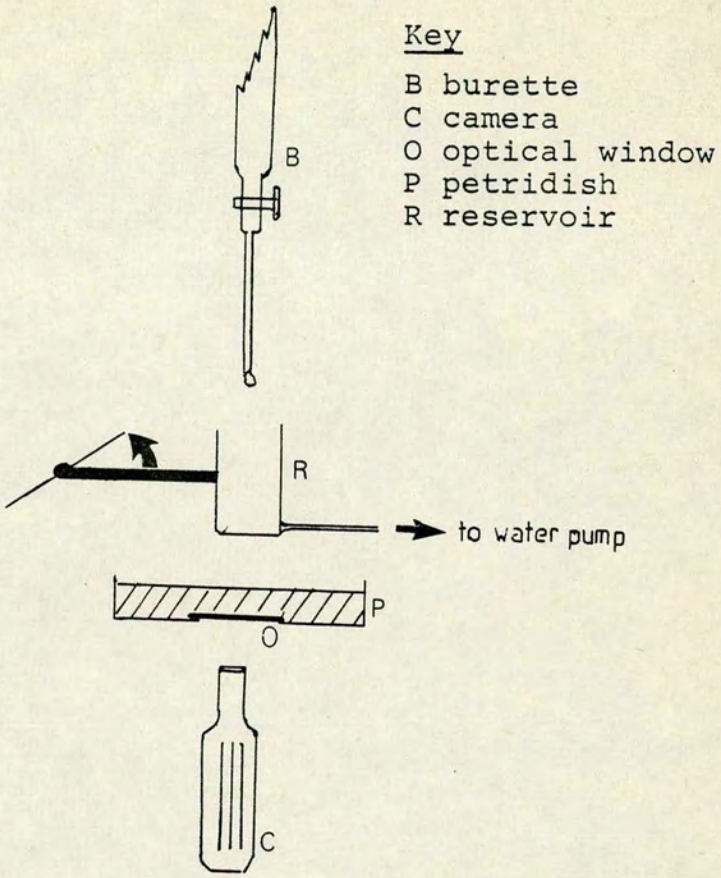

Figure 3: Arrangement for high speed filming of bubble growth in the $NaOCl/H_2O_2$ reaction.

A glass window of high optical quality was mounted on the base of a petri dish (diameter 10 cm) which contained 100 volume hydrogen peroxide solution. NaOCl was allowed to fall dropwise from the burette into a small reservoir, which was connected to a water suction pump. The tip of the burette was positioned directly over the centre of the dish. A high speed camera, containing a 2 mm graticule lens, was mounted vertically below the centre of the window and focused on the brightly illuminated air-liquid interface of the peroxide solution.

On activating a solenoid the reservoir mounting was displaced temporarily, allowing a single drop of NaOCl (0.08 g) to fall into the peroxide solution, while at the same time starting the high speed camera. Thirty metre lengths of gauge 16 film were run at a speed of 8000 frames per second. A mechanism was incorporated in the camera which marked the film at intervals of one millisecond. After developing, prints of selected frames were obtained using a film analyser with an automatic processing unit and a print of the complete film negative was also made.

A similar experimental arrangement was employed in obtaining a horizontal view of the reaction. Prints showing both horizontal and vertical shots of the reaction, at various stages in its development, are included in Chapter 3.

2.04 Flash Photolysis with Kinetic Spectroscopy

Flash photolysis with kinetic spectrsocopy was used to study the physical and reactive quenching of species such as $S_2(a^1\Delta_g)$ and $SO(a^1\Delta)$, following the photolysis of carbonyl sulphide. Since the transient spectra of these species are either unknown or expected to be short lived - their concentration profiles following that of the flash intensity - kinetic spectroscopy would seem to be the method best suited to their study. Since this technique has been described in detail elsewhere,[82] only a brief description is merited here. A diagram of the apparatus is shown in Figure 4.

A one metre system comprising a quartz reaction vessel (i.d. 20 mm) with spectrosil windows and a parallel quartz flash lamp (i.d. 10 mm) was used. Mounted directly behind the reaction vessel was the spectroflash lamp. This was a conventional quartz capillary lamp with the discharge between the tungsten electrodes being mechanically pinched by a narrow quartz capillary (i.d. 2 mm), giving an intense continuum in the ultraviolet. Both flash lamps were thoroughly outgassed before filling with $\sim$900 Nm^{-2} of krypton. New lamps required to be filled a number of times before a single filling would last for several hundred discharges.

The photolysis lamp was normally discharged at 8 kV from a 10μf capacitor, while the spectroflash lamp was fired at 10 kV from a 1μf capacitor, resulting in flash energies of 320J and 50J respectively. A delay unit incorporating an ignitron, built in the departmental workshop, was used to control the time interval between the photolysis and spectroflashes (Figure 5). The photolysis lamp was discharged by means of a low inductance mechanical plunger, and a signal from a photocell in close proximity to the lamp was amplified and

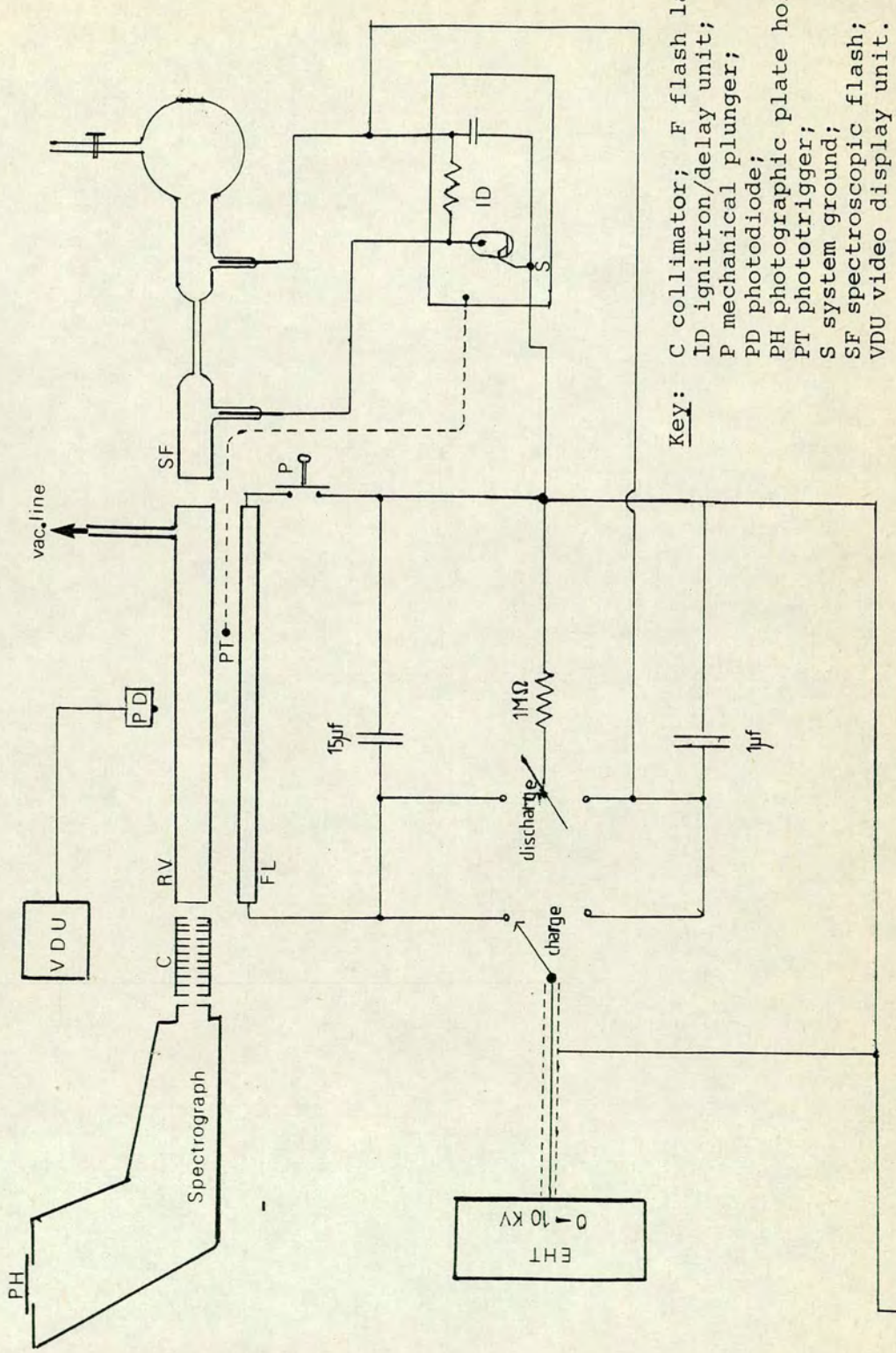

Figure 4: Experimental arrangement for studies using flash photolysis with kinetic spectroscopy

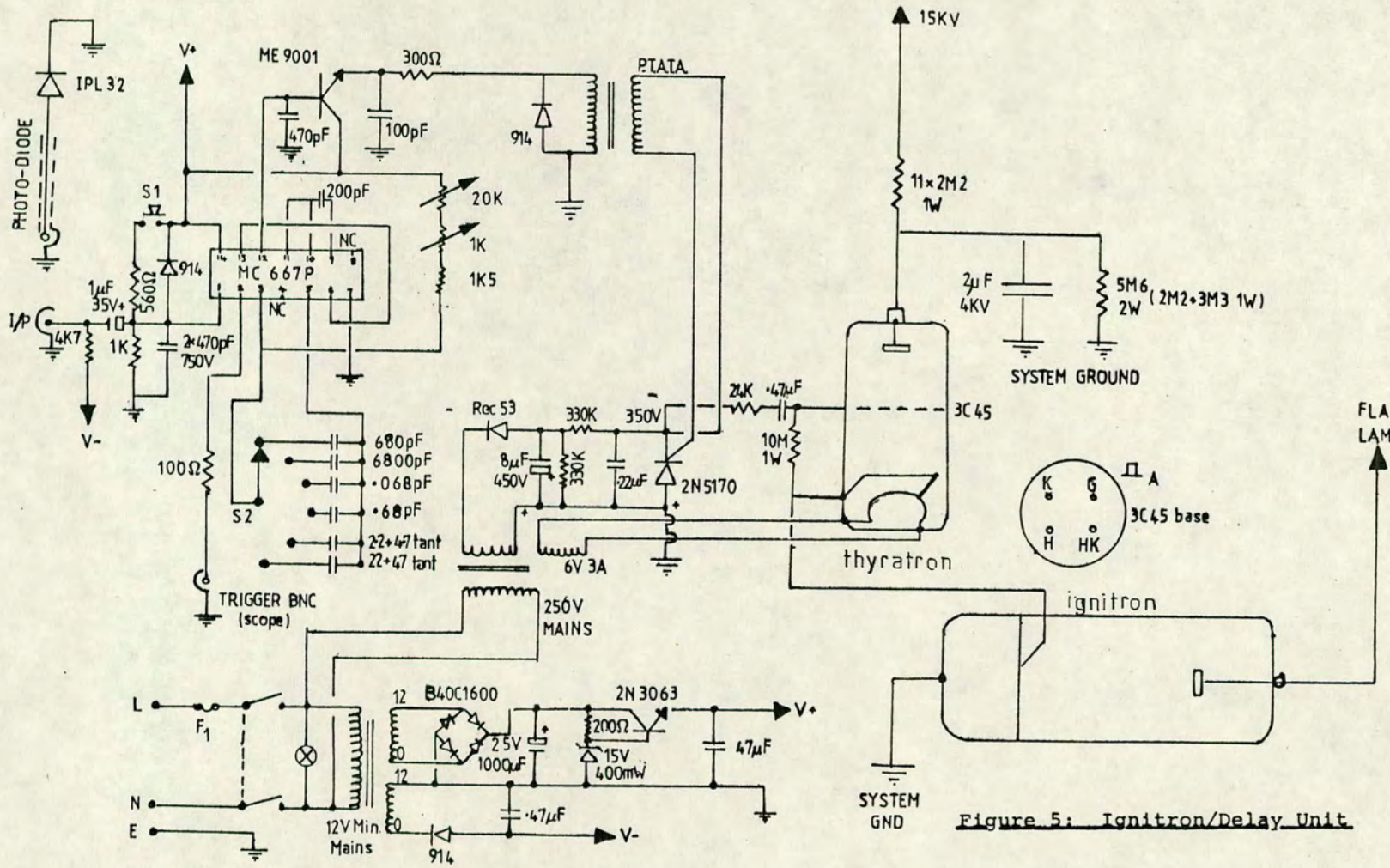

Figure 5: Ignitron/Delay Unit

delayed for a preset time (1μs-1s) before a 100 V spike was passed to the grid of an ignitron, allowing the latter to conduct and discharge the spectroflash lamp. The delay was checked using a photodiode connected to a storage oscilloscope (Tektronix Type 549).

Aluminium foil wrapped around the reaction vessel and flash lamp acted as a reflector and a series of collimators between the reaction vessel and spectrograph helped to minimise the amount of scattered light falling on the entrance slits. The Hilger and Watts medium quartz spectrograph (Type E486) was used with slits set at a width of 60μm and a height of 3 mm. Alignment of the spectroflash lamp with the spectrograph slits such that it did not 'see' the walls of the reaction vessel was achieved by using a helium-neon laser.

Kodak Panchro Royal film was found to be perfectly adequate for wavelengths longer than 230nm, without sensitation to ultraviolet light using sodium salicylate. Plates were developed in Ilford Contrast FF developer (1+4) for 5 minutes at 20°C, with continuous agitation. Sensitized plates appeared to give better image density but resulted in a rather grainy emulsion,which gave a poor signal to noise ratio when densitometered.

The characteristic curve, which is a plot of the optical density versus the logarithm of the exposure, is obtained by subjecting the photographic plate to a series of exposures, each greater by a constant factor than that of the preceding one, and measuring the resultant optical densities.

For quantitative work it is necessary to work in the linear region of the curve, scattered light from the photolysis flash normally being sufficient to take images into this region. However, if one of the reagents has a particularly strong continuum absorption, then the image may no longer lie on the linear section of the curve for that particular region of the spectrum.

Plates were densitometered on a Joyce Loebl Double Beam Recording Microdensitomer MKIII and optical densities of absorption bands obtained by comparing the plate densities D_o, before the photolysis flash ($t = 0$), and D_t, at some subsequent time t. If the Beer Lambert Law applies, then

$$\text{Peak Height} = D_o - D_t = \gamma \log I_o/I = \gamma \varepsilon C_t l$$

where γ is the slope of the linear section of the characteristic curve, l is the path length through the absorber of concentration C_t at time t and ε is molar absorption coefficient. γ is inversely proportional to the microdensitometer wedge factor. Thus the peak height is directly proportional to concentration, except when plate saturation occurs.

In attempting to model the growth in the concentration of a transient species within the duration of the flash, by computer simulation, it is necessary to know the photolysis flash intensity profile. The flash was focused onto the slits of a monochromator by means of a concave front-surfaced mirror. Carbonyl sulphide absorbs in the ultraviolet with a maximum absorbance at 236 nm, so that this wavelength was selected to monitor the flash profile. The signal from a photomultiplier (Type EMI 9661B) was transferred to a transient recorder (DL 905) and subsequently plotted out using an XYT recorder. The time constant for the circuit was estimated

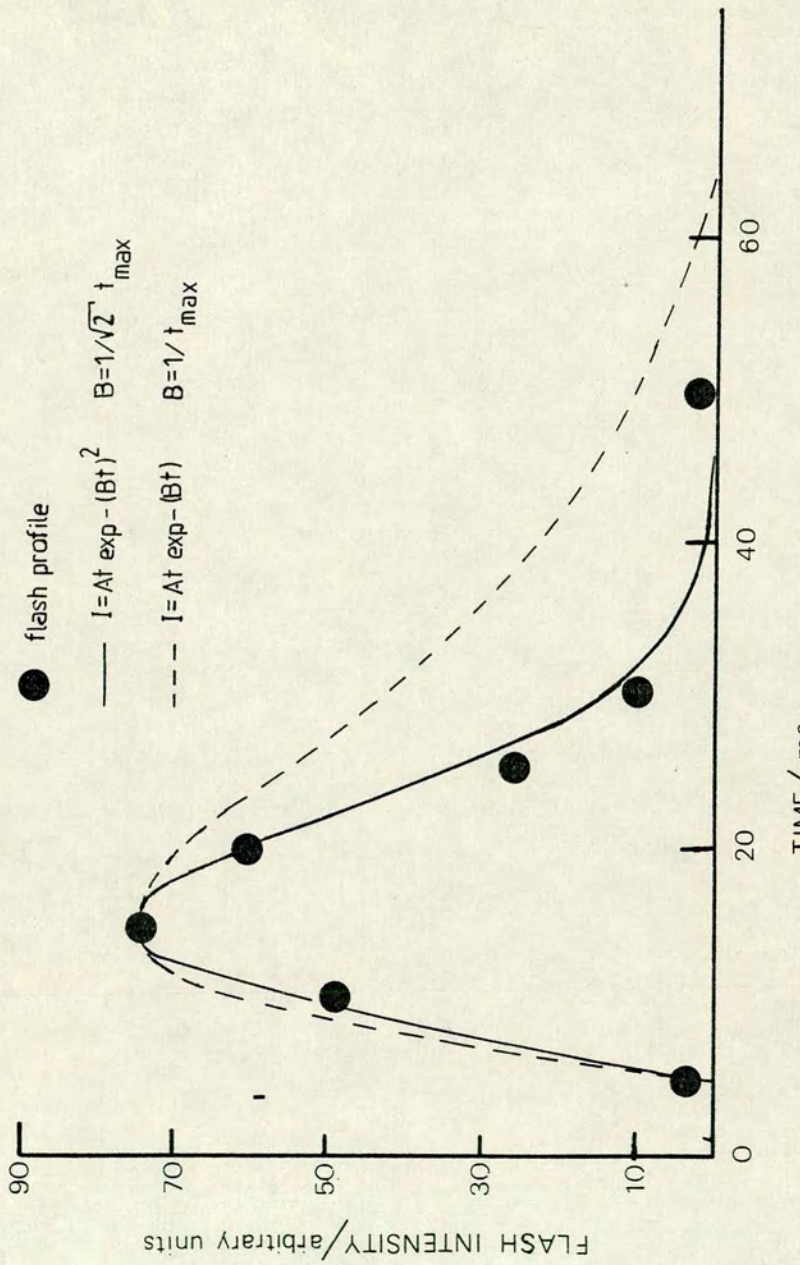

Figure 6: Experimental and computed flash profiles

to be 0.5μsec.

The flash profile is often found to fit an expression of the type:-

$$I = At \exp(-\beta t); \quad \beta = {}^{1}/t \text{ max}$$

where I is the intensity at time t, β is inversely proportional to the time at which the intensity is at a maximum and A is a constant of proportionality. In this case the flash was found to decay rapidly so that the above expression was modified.

$$I = At \exp-(\beta t)^2 ; \quad \beta = {}^{1}/_{\sqrt{2}}\ t \text{ max}$$

The intensity is effectively described by the photomultiplier output voltage. A plot showing the experimental and fitted curves is given in Figure 6. Later simulation studies suggested that the time constant for the detector circuit may have been underestimated so that some distortion of the true profile may have occurred (see chapter 7), and the time constant should have been further decreased. However, an expression of the second form is still applicable if the fast decay of the flash is to be accounted for.

2.05 Flash Photolysis with Kinetic Spectrophotometry

Kinetic spectrophotometry was used to study the secondary reactions following ozone photolysis. This technique has been widely used and is described in detail elsewhere.[82] Only those aspects of the design which relate to the present study will be described in the following sections. Figure 7 shows a diagram of the apparatus.

Reaction vessel and Flash lamp :-

As ozone is a strong absorber in the ultraviolet ($\lambda > 200$nm), the dimensions of the reaction vessel are important,

Key:

A atomic emission lamp;

ADC analogue to digital converter;

B black glass filter;

C collimator;

FL Flash lamp;

L lens;

M microwave cavity;

MC monochromator;

MWG microwave generator;

P mechanical plunger;

PM photomultiplier;

RV reaction vessel;

S shutter;

VDU video display unit;

XYT XYT recorder.

Figure 7: Experimental arrangement for studies using flash photolysis with kinetic spectrophotometry

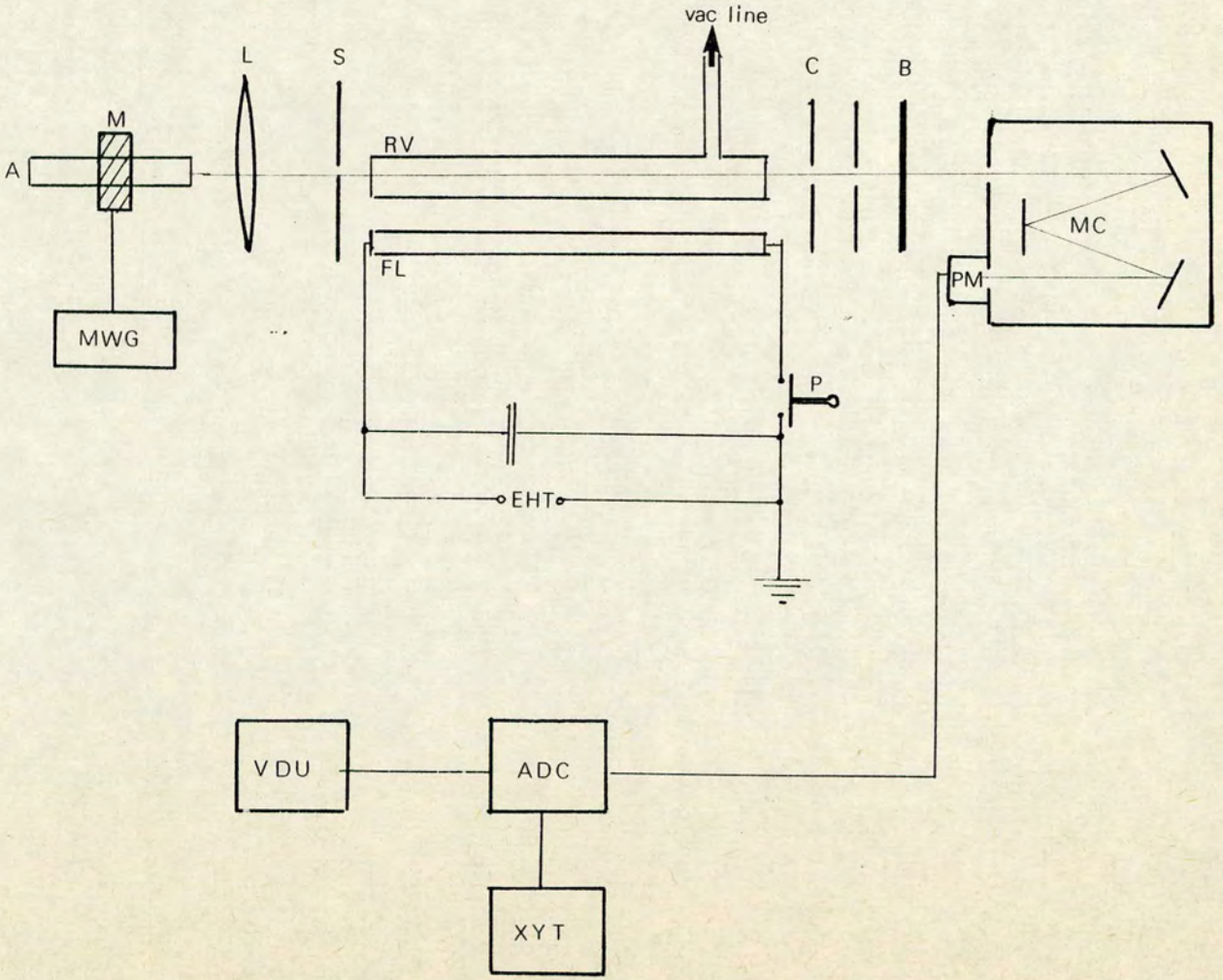

both in optimising the extent of photolysis and also the extent to which the monitoring signal is attenuated. The diameter of the reaction vessel must be small enough to prevent the formation of significant concentration gradients (greater than 1:10) following photolysis,which would lead to noticeable diffusion effects within the time scale of reaction. However it is necessary to avoid too small a diameter,which would lead to heterogeneous processes having important effects on the observed decay of ozone, since the walls of the reaction vessel would lie within the observation zone.

Although it is desirable to have a long path length through the absorbing medium in order to optimise the S/N ratio, complete absorption may occur, due to the high extinction coefficient of ozone at the monitoring wavelength (253.7nm).

A cylindrical quartz reaction vessel was constructed (l = 125mm, i.d. = 20mm) to minimise these various effects. Quartz windows were mounted at each end, using araldite. A conventional glass vacuum line serviced the reaction vessel.

The flash lamp, also constructed of quartz (l = 202mm, i.d. = 15mm), lay parallel to the reaction vessel and was filled with Krypton to a pressure of 933 Nm^{-2}. Flash energies of ca. 60J were obtained by discharging a 1.5μf capacitor at 7kV, the flash being initiated by a mechanical plunger.

Aluminium foil wrapped around the reaction vessel and flash lamp acted as a condenser, noticeably increasing the amount of photolysis, as well as reducing the amount of scattered light. Such interference has already been mentioned and in this work it was particularly important that as short a photomultiplier dead-time as possible should be obtained following the flash. Backward extrapolation of the ozone concentration to just after the end of the flash has to be

employed to obtain the amount of O_3 removed by the flash. To achieve a meaningful degree of accuracy, the extent of this extrapolation must be kept to a minimum. Two collimators (5mm) and a black glass filter, with transmission between 230 and 400nm, were inserted between the reaction vessel and the monochromator slits and reduced the dead-time from 2ms to approximately 600μs. Although this could be further reduced by narrowing the slit-width, a decrease in the S/N ratio resulted so that a compromise was made between the two factors. As reproducibility was an essential criterion of the experiment, the system was rigidly clamped.

The products of ozone photolysis are wavelength dependent and, in order to determine their relative amounts, the spectral output of the photolysis lamp was investigated. Figure 8 shows the photomultiplier output voltage over the wavelength range 200-600nm after correction for the quantum efficiency of the detector. At wavelengths longer than 350nm a Pyrex filter was placed in front of the monochromator entrance slits to avoid interference from higher spectral orders.

Detection of Ozone : Hg lamp

Ozone was monitored by measuring the absorption of light at 253.7nm from a mercury atomic lamp. Mercury has a vapour pressure of ca. 0.23 Nm^{-2} at room temperature (293°K), and is thus ideal for use in a sealed microwave lamp. The construction of this type of lamp has been described by Little.[83] Several drops of mercury were placed in the tube and thoroughly outgassed before being filled with Krypton (1.3 kNm^{-2}) and sealed. The inert gas stabilised the discharge and an outer Pyrex jacket

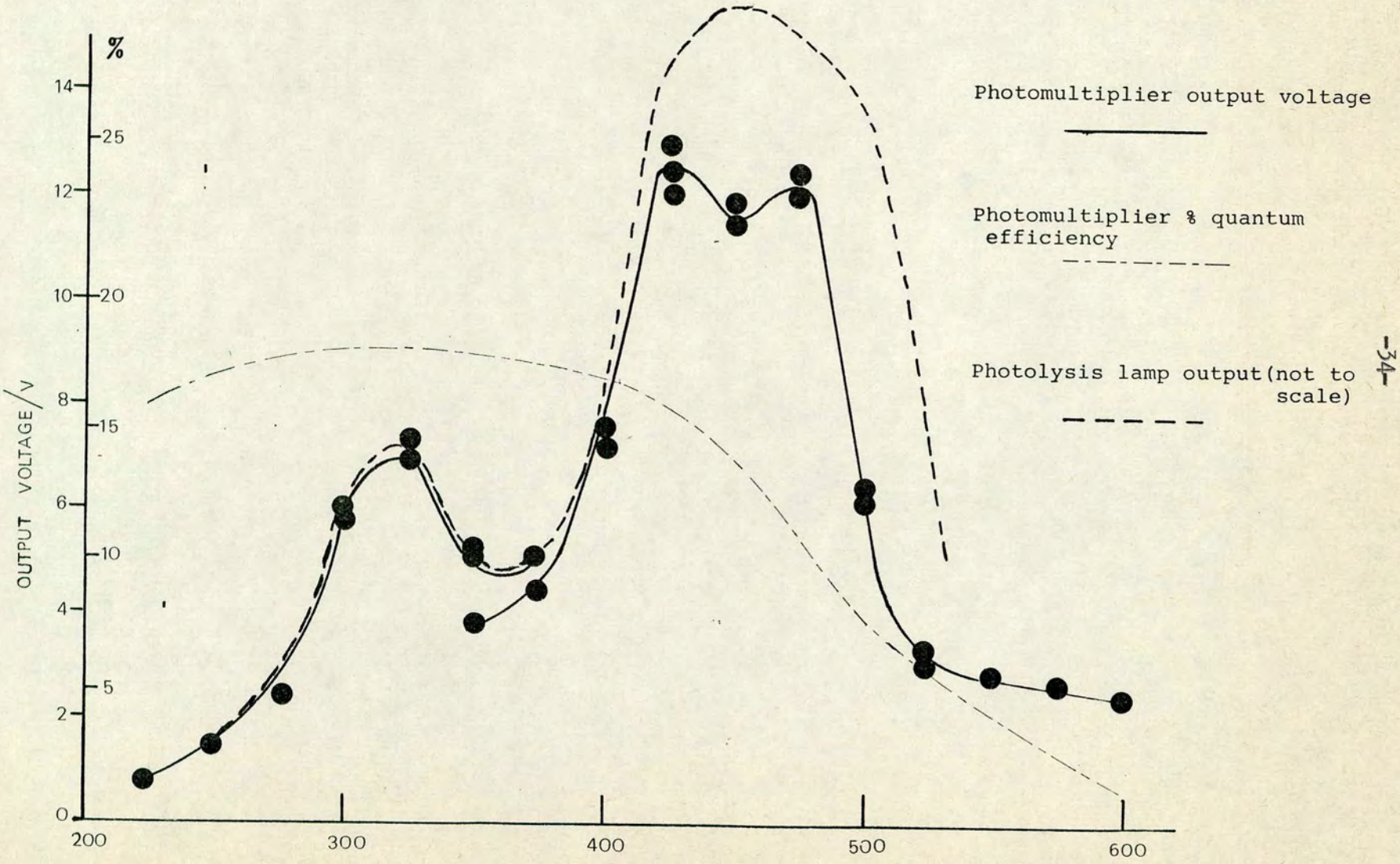

Figure 8: Photolysis lamp output over the wavelength range 200-600 nm

acted as an ultraviolet shield,as well as helping to maintain thermal equilibrium. A standard Evenson cavity was tuned to give optimum conditions of operation with incident powers of 50-75W. The 2450 MHz microwave generator (EMS Microtron 200 Mk II) had extra DC smoothing and stabilisation to prevent the superimposition of 50 Hz mains ripple on the lamp output. The emission was focused through the reaction vessel onto the monochromator entrance slits. To prevent photolysis of ozone while the reaction vessel was being filled and before the flash lamp was discharged, a shutter was placed between the emission lamp and the lens.

The monochromator was a Hilger and Watts Monospek 1000 Grating Scanning Spectrometer fitted with a D410 plane grating blased at 1.0μ and, in this case, operated in the second order with slit widths of 250μ. Absorption signals were detected by means of an EMI 9661B photomultiplier tube, mounted at the exit slit of the monochromator. This photomultiplier is an improved 9-stage side window tube having a Corning 9741 glass envelope which transmits down to 200 nm, the ceasium-antimony cathode having an S-5 type spectral response. Conventional whole dynode chain circuits are designed for situations where a high gain is required. In this case the intensity of the Hg emission was such that a detector with high sensitivity was not required and indeed a photomultiplier circuit with relatively low gain was more suitable. Thus only the first six dynodes of the photomultiplier were used, the remaining three acting as the anode. This allowed high incident light levels to be used,thus ensuring a high photocathode current and optimising the signal to noise ratio, without causing excessive

anode currents which would have resulted in a non linear response. The circuit diagram is shown in Figure 2b. The tube was typically run at 650-750V (Brandenburg 472R Power Supply), with the output of the photomultiplier developed across a 10kΩ resistor, before being fed to a fast analogue to digital converter (Datalab DL905). This has an 8 bit x 1024 word integral memory. Signals were inspected on a visual display unit (Telequipment DM64) before transfer to an XY plotter for analysis.

The Beer Lambert Law

The attenuation of radiation through an absorbing medium is normally described by means of the Beer Lambert Law.

$$\ln I_o/I = \alpha c l$$

I_o and I are the incident and transmitted light intensities through an absorbing medium of concentration C and path length l. The constant of proportionality, α, is known as the extinction coefficient.

2.06 Gas Handling

Reagents were handled using a conventional glass vacuum line, evacuated by a liquid N_2 cryogenic trap and a mercury diffusion pump backed by a rotarypump, giving a vacuum better than 2×10^{-2} Nm^{-2}, measured with a pirani gauge. Gas pressures were measured using a glass spiral gauge (1-15 kNm^{-2}) or a mercury manometer (13-100 kNm^{-2}). Lower pressures were measured by using sharing ratios. The line was fitted with a highly efficient mechanical mixing vessel and reagents were allowed to mix for at least five minutes before carrying out an experiment. All bulbs used for ozone storage were aged before use and were well protected from room light by black cloth. Details of sources,

preparation, purification and handling of all reagents used are given in Appendix 1.

Contamination of the vacuum line by mercury vapour was occasionally a problem in experiments where ozone was monitored by absorption of radiation at 253.7 nm. The effect of the photolytic flash was to drive mercury atoms off the walls of the reaction vessel into the field of observation, so causing an apparent transient absorption, even in the absence of any reagent mixture. By monitoring other mercury transitions which are not optically connected to the ground state, it could be confirmed that this was the cause of the transient signal. Thus special care was taken, so as to minimise the pressure of mercury vapour in the vacuum line. Gold wire, placed in the main manifold, removed mercury by forming an amalgum and the columns of the mercury manometer were covered by silicon oil (20 mm). The line was flushed several times before use with air (10 kNm^{-2}), so as to prevent contamination by mercury from the diffusion pump. A 5% solution of hydrofluoric acid removed traces of mercury from the walls of the reaction vessel.

Chapter 3

Singlet Molecular Oxygen

3.01 Introduction

In this chapter, rate constants for quenching of $O_2(^1\Delta_g)$ by $O_2(^3\Sigma_g^-)$ and H_2O have been obtained using an extremely simple experimental method. It has been found that when concentrated solutions of sodium hypochlorite and hydrogen peroxide (100 vol) are reacted, the decay of $O_2(^1\Delta_g)$, in the rapidly evolved oxygen bubbles, is controlled by quenching in the gas phase and that gas-surface interactions are negligible.

The weak red-orange chemiluminescence accompanying the reaction of the hypochlorite ion with hydrogen peroxide [1] was first observed by Mallet[84] in 1927.

$$H_2O_2 + OCl^- \rightarrow O_2(^1\Delta_g) + H_2O + Cl^- \qquad [1]$$

Groh and Kirrman[85] proposed that the emission at 633 nm was due to the energy pooling of two electronically excited oxygen molecules [2], and this was later confirmed by Ogryzlo et al.[26]

$$2O_2(^1\Delta_g) \rightarrow 2O_2(^3\Sigma_g^-) + h\nu(\lambda = 633 \text{ nm}) \qquad [2]$$

The complete emission spectrum of the reactions in the range 450-800 nm has been analysed by Khan and Kasha.[86] Table 2 lists the observed bands. From the analysis of the rotational structure it was shown that the emission from $O_2(^1\Sigma_g^+)$ at 762 nm arises from the bubbles.[86] No emission from singlet oxygen molecules <u>in solution</u> has been observed.[27]

Isotopic labelling has confirmed the chloroperoxy ion as the intermediate[87] in reaction [1]. A spin correlation diagram[25] for the chloroperoxy ion, giving oxygen and chloride ion as products, correlates with $O_2(^1\Delta_g)$ and not $O_2(^3\Sigma_g^-)$.

Table 2: Bands observed in the oxygen emission spectrum of the $NaOCl/H_2O_2$ reaction in the wavelength range 450-800 nm (after ref. 86).

Process giving rise to observed band	Wavelength/nm
$^1\Delta(v'=0)+{}^1\Sigma(v'=0)\rightarrow{}^3\Sigma(v''=0)+{}^3\Sigma(v''=0)$	478.0
$^1\Delta(v'=1)+{}^1\Delta(v'=0)\rightarrow{}^3\Sigma(v''=0)+{}^3\Sigma(v''=0)$	577.0
$^1\Delta(v'=0)+{}^1\Delta(v'=0)\rightarrow{}^3\Sigma(v''=0)+{}^3\Sigma(v''=0)$	633.4
$^1\Delta(v'=0)+{}^1\Delta(v'=0)\rightarrow{}^3\Sigma(v''=0)+{}^3\Sigma(v''=1)$	703.2
$^1\Sigma(v'=0)\rightarrow{}^3\Sigma(v''=0)$	762.0
$^1\Delta(v'=0)+{}^1\Delta(v'=0)\rightarrow{}^3\Sigma(v''=2)+{}^3\Sigma(v''=0)$	786.0

Table 3: Rate constants for deactivation of $O_2(^1\Delta_g)$ in units of $cm^3molec^{-1}s^{-1}$. Temperature = 293 ± 5^oK

Author (ref)	Quenching Gas	
	$O_2(^3\Sigma_g^-)$	H_2O
This work	$1.7 \pm 0.4 \times 10^{-18}$	$4.0 \pm 1.0 \times 10^{-18}$
Becker (94)	$1.7 \pm 0.1 \times 10^{-18}$	$4.0 \pm 1.0 \times 10^{-18}$
Becker (97)	$1.47 \pm 0.05 \times 10^{-18}$	
Wayne (101)	$2.3 \pm 0.2 \times 10^{-18}$	$1.4 \pm 0.3 \times 10^{-17}$
Findlay (98)	$2.17 \pm 0.12 \times 10^{-18}$	
Steer (102)	$2.04 \pm 0.23 \times 10^{-18}$	
Wohra (103)	1.7×10^{-18}	
Heustis (91)	2.19×10^{-18} (calc)	
Borrell(104)	$1.56 \pm 0.04 \times 10^{-18}$	

Higher states of the chloroperoxy ion correlate with $O_2(^1\Sigma_g^+)$ and the ratio of $O_2(^1\Sigma_g^+)$ to $O_2(^1\Delta_g)$ has been found to be less than 10^{-6} [89]. The rate of reaction [1] is highly pH dependent and Kearns et al.[27,88] have shown the emission intensity to be highest in the pH range 8-10, contrary to earlier work by Seliger.[90]

3.02 Results and Discussion

In these experiments, sodium hypochlorite (Fisons technical grade) was added dropwise to hydrogen peroxide (100 vol), as described in section 2.02. The weight of a single drop was 0.083 g, except where luminescence was studied over a range of drop sizes (0.007-0.102g). Signals were averaged over 32 single shots, thus giving a five-fold reduction in signal to noise ratio.

Figure 9 shows a typical averaged decay of the 'dimol' emission obtained at room temperature (296°K) and atmospheric pressure. From this signal it can be seen that the rate of formation of singlet oxygen was much faster than its decay. Using information obtained by Kearns et al.[27], k_1, the rate constant for overall formation of $O_2(^1\Delta_g)$, can be estimated to be 3.3×10^{-16} cm^3 $molecule^{-1}s^{-1}$ at pH 10. This is several orders of magnitude faster than most gas phase quenching processes of $O_2(^1\Delta_g)$.

In solution $O_2(^1\Delta_g)$ is efficiently quenched by H_2O, having a half-life of 2μs.[27] Thus, although singlet oxygen is the dominant product of reaction [1], only a fraction of the oxygen molecules in a bubble will be in an excited state.

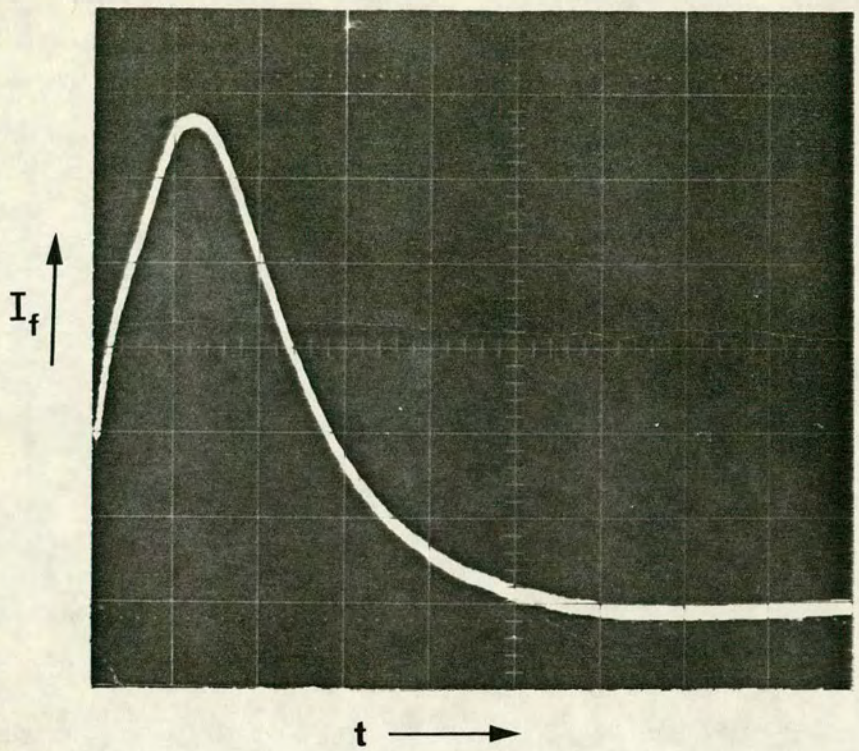

Figure 9. The rise and decay of "dimol" emission (λ = 634 nm) from $O_2(^1\Delta g)$, produced by the reaction of hydrogen peroxide solution (100 vol.) with a concentrated solution of sodium hypochlorite. The experiment was carried out at atmospheric pressure and at room temperature (296 K). The signal shown has been averaged over 32 separate runs; t = 10 ms per major division; $k' = 47\ s^{-1}$.

The most important removal processes for $O_2(^1\Delta_g)$ in the bubbles should be quenching by H_2O [3] and $O_2(^3\Sigma_g^-)$ [4], wall removal [5] and 'dimol' processes [2,6].

$$O_2(^1\Delta_g) + O_2(^1\Delta_g) \rightarrow 2\ O_2(^3\Sigma_g^-) + h\nu \quad [2]$$

$$O_2(^1\Delta_g) + H_2O \rightarrow O_2(^3\Sigma_g^-) + H_2O \quad [3]$$

$$O_2(^1\Delta_g) + O_2(^3\Sigma_g^-) \rightarrow 2\ O_2(^3\Sigma_g^-) \quad [4]$$

$$O_2(^1\Delta_g) + \text{Wall} \rightarrow O_2(^3\Sigma_g^-) + \text{Wall} \quad [5]$$

$$O_2(^1\Delta_g) + O_2(^1\Delta_g) \rightarrow O_2(^1\Sigma_g^+) + O_2(^3\Sigma_g^-) \quad [6]$$

Rate constants for reactions [3] and [4] are given in Table 3. The best literature values for processes [2] and [6] are $2.6\text{-}5.0 \times 10^{-23}$ $cm^3molec^{-1}s^{-1}$ [91] and $0.2\text{-}5.0 \times 10^{-17} cm^3molec^{-1}s^{-1}$ [92,93] respectively.

The effect of 'dimol' emission processes [2] on the decay will be negligible, so that this provides an ideal means of monitoring $O_2(^1\Delta_g)$. Although the rate constant for annihilation [6] is of the same magnitude as that for quenching by H_2O and $O_2(^3\Sigma_g^-)$ the low concentration of $O_2(^1\Delta_g)$ means that this process will only have a very small effect. The quenching efficiency of H_2O [3] is a factor of three greater than $O_2(^3\Sigma_g^-)$ [4].[94] Since the vapour pressure of water at S.T.P. is 2.3 kNm^{-2} [95] (17τ), under normal conditions it would only account for < 8% of the total gas phase quenching of $O_2(^1\Delta_g)$. However, at higher temperatures, water would become the most abundant species in the bubble.

At room temperature, removal of $O_2(^1\Delta_g)$ is controlled by wall deactivation and gas phase quenching by $O_2(^3\Sigma_g^-)$. Since both of these processes are first order in $O_2(^1\Delta_g)$ [7], and the intensity of dimol emission, I, is proportional to the square of the singlet oxygen concentration [8], a plot of the logarithm of $I^{\frac{1}{2}}$ versus time, t, should be linear, if second order processes are unimportant [9].

$$-\frac{d}{dt}[O_2(^1\Delta_g)] = (k_5[M] + k_4[O_2(^3\Sigma_g^-)])[O_2(^1\Delta_g)] \quad [7]$$

$$(I)^{\frac{1}{2}} \propto [O_2(^1\Delta_g)] \quad [8]$$

$$\ln(I)^{\frac{1}{2}} = -k't + \text{constant} \quad [9]$$

where $k' = k_5[M] + k_4[O_2(^3\Sigma_g^-)]$

Figure 10 shows a computerised plot of the pseudo first order decay. Monitoring the decay either by the (0,0) or (0,1) bands, at 633 and 702 nm respectively, gave rise to the same rate coefficients. Furthermore, when the reaction vessel was flushed with oxygen or nitrogen, no detectable change in k' was observed. A small decrease in k' within experimental error, in the case of flushing with helium, could not be accounted for. Thus no apparent contribution to k' came from surface losses of $O_2(^1\Delta_g)$

The logarithm of the concentration, $\ln I^{\frac{1}{2}}$, was plotted against time, t, over four half-lives of the decay and no evidence of second order kinetics was apparent, as this would have resulted in non-linear behaviour.

The diffusion coefficient for self diffusion of oxygen can be expressed as a function of temperature ($T/^oK$) and pressure (P/mm Hg) [10].

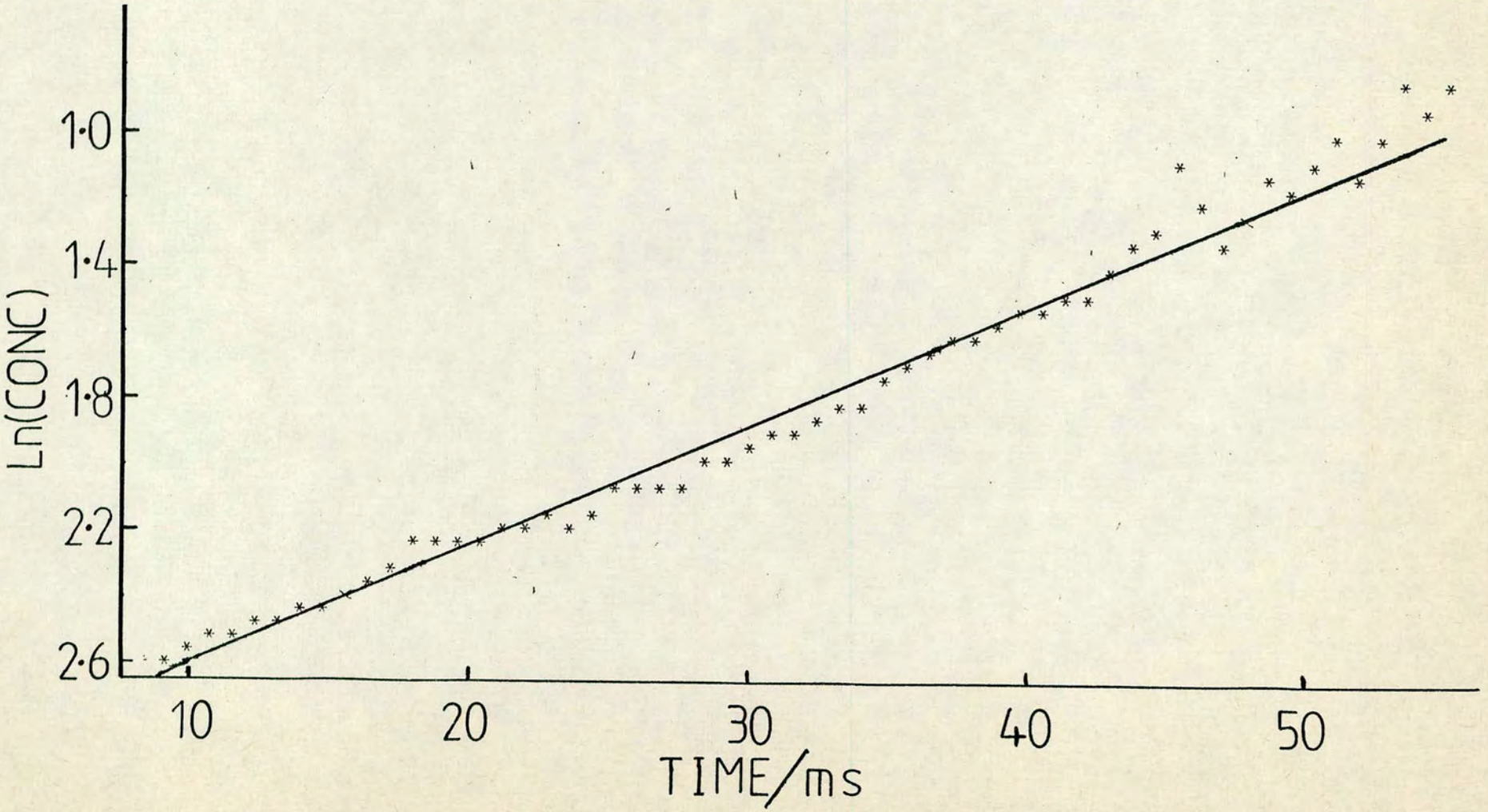

Figure 10: A computerised plot of the pseudo first order decay of $O_2(^1\Delta g)$

$$D_{O_2\text{-}O_2} = 3.07 \times 10^{-6} T^{3/2} P^{-1} (m^2 s^{-1}) \qquad [10]$$

This expression was calculated from simple diffusion theory and compares well with the experimentally determined value for $O_2(^1\Delta_g)$ in $O_2(^3\Sigma_g^-)$ by Wayne,[96] which gives $D^*_{O_2\text{-}O_2}$ as $2.01 \times 10^{-5} m^2 s^{-1}$ at 1 atmosphere pressure and 298°K. Thus for bubbles with a diameter less than 1 mm, diffusion to the walls probably accounts for most of the deactivation of $O_2(^1\Delta_g)$, whereas for larger diameters gas phase quenching should be dominant.

By varying the bore of the burette tip, a range of drop sizes of NaOCl could be obtained. Even when observed by eye, the average bubble size appeared to be considerably reduced for the smaller drops. Pseudo first order decay coefficients were obtained for drop weights in the range 0.007-0.102g and these are shown in Figure 11. Higher removal rates of $O_2(^1\Delta_g)$ are observed for small drop sizes and are probably accounted for by wall deactivation. For drops weighing more than 0.7g, the decay rate levels off as gas phase quenching becomes dominant due to the formation of larger bubbles.

Thus, the standard drop weight (0.083g) used in these experiments lies in the region where gas phase quenching, rather than wall deactivation, controls the removal rate. Further evidence for this comes from high speed film of the reaction. A single drop of sodium hypochlorite (0.083g) was allowed to fall into 100 volume H_2O_2 and the rapid growth of oxygen bubbles recorded at a film speed of 8000 frames per second. The reaction is illustrated, at various stages in its development, by a series of prints showing vertical and horizontal views of the reaction zone (Figures 12 and 13).

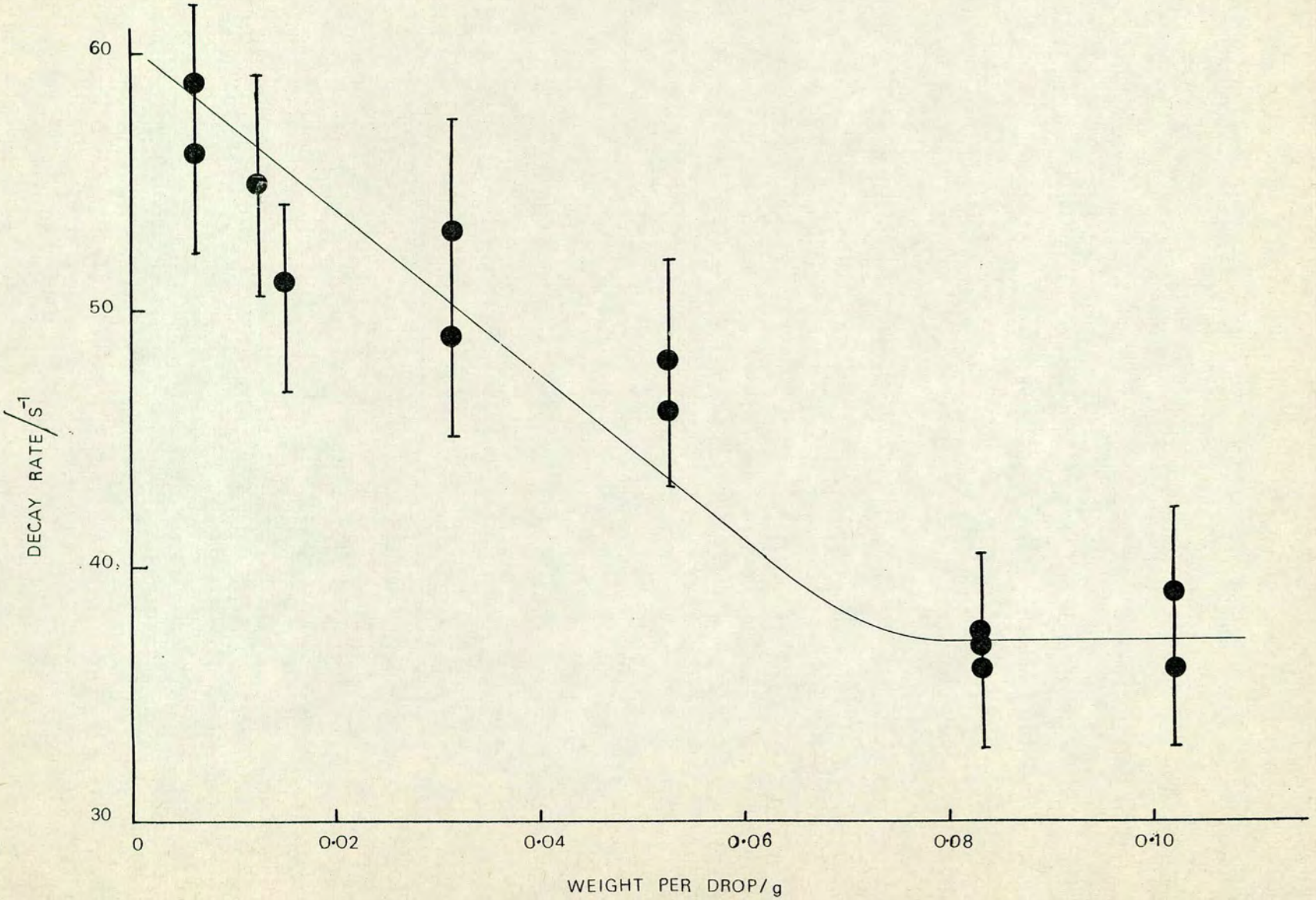

Figure 11 : A plot of the pseudo first order decay decay coefficient for quenching of $O_2(^1\Delta g)$ versus NaOCl drop weight

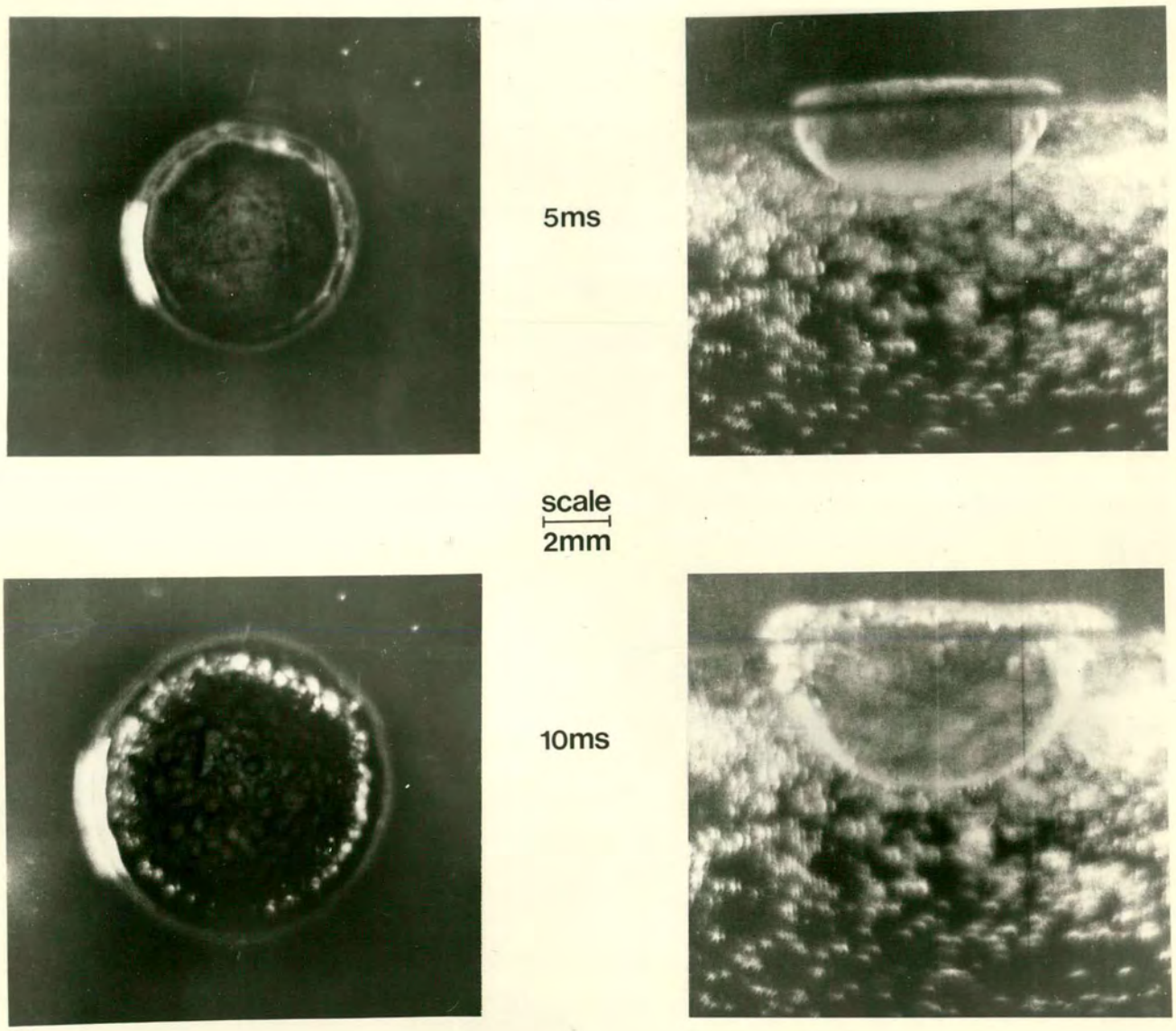

Figure 12: Vertical and side views of the $NaOCl/H_2O_2$ reaction at 5 and 10 ms

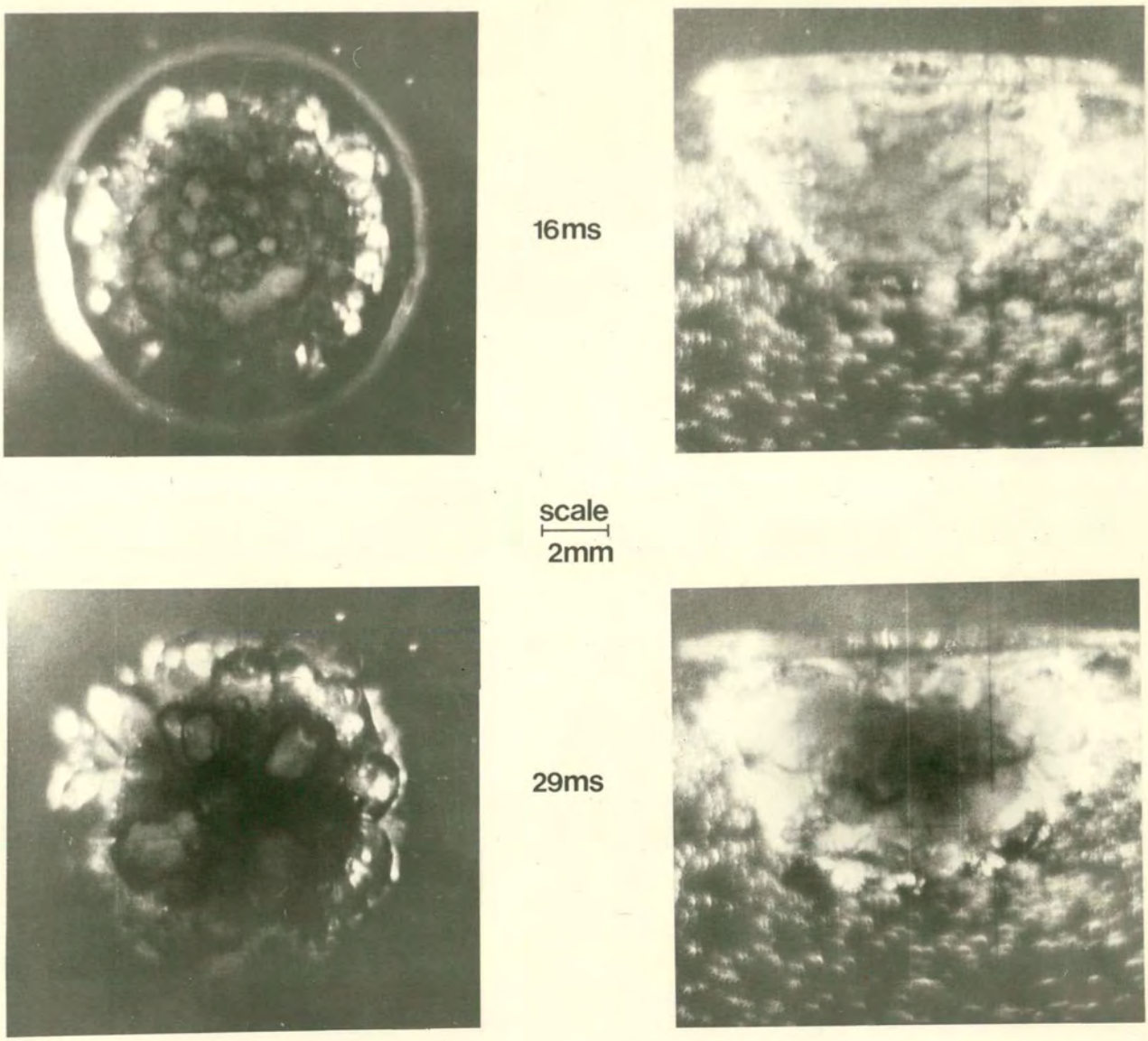

Figure 13: Vertical and side views of the $NaOCl/H_2O_2$ reaction at 16 and 29 ms

A number of important features are immediately apparent. Not only is the reaction confined to a specific, localised region of the solution, but, for at least 40 ms after its initiation, there appears to be no escape of oxygen due to bubbles breaking at the gas/liquid interface. Thus, there is no contribution to the observed chemiluminescent decay due to escape of $O_2(^1\Delta_g)$ at the liquid surface. Since the reaction is localised, occurring within a volume of ca. 2 cm^3, the photomultiplier can view the complete reaction zone.

In studying the various stages of the reaction as illustrated in Figures 12 and 13, it is interesting to compare these with the decay of 'dimol' emission shown in Figure 9.

Within several milliseconds (Fig.12 a) of the drop of NaOCl falling into the peroxide solutions, a well defined region of activity is discernable, being bounded by a wave moving out from the point of impact. At 10 ms (Figure 12b) this region is still growing rapidly in volume while the $NaOCl/H_2O_2$ reaction proceeds just within the radially expanding boundary. Individual bubbles are now recognisable in the centre of the reaction zone and many have diameters approaching 0.5 mm. The emission intensity is at a maximum at 13 ms, when the formation and removal processes for $O_2(^1\Delta_g)$ proceed at nearly equal rates. After 16 ms (Figure13a) the reaction has progressed to that section of the decay where first order kinetics are applicable. The active volume is no longer increasing, although the wave can still be seen moving further out from its centre of origin. The volume of O_2 liberated at STP on the complete reaction of 0.083 g of NaOCl solution

(8% available chlorine) with H_2O_2 is 1.70 cm^3. This compares favourably with an estimate of 1.85 cm^3 for the volume of the reaction zone at 16 ms, made using the prints in Figure 13a Most bubbles now have diameters greater than 1 mm and are merging together to become even larger. This is further evidence that only gas phase removal processes are important for NaOCl drop sizes greater than 0.07g. After 29 ms the emission intensity has dropped considerably and the reaction is in its final stages. Bubbles as large as 5 mm in diameter can be observed, but there is still no sign of movement towards the surface until at least 40 ms after the point at which the drop broke the peroxide surface.

The high speed film provides conclusive evidence that the observed emission arises only from within the bubbles, and not from the solution. Also, under the standard experimental conditions, it is mainly gas phase removal of $O_2(^1\Delta_g)$ that is important and any contributions to the observed decay by surface losses or a poorly defined observation zone are minimal.

Thus, it was possible to obtain the rate constant for quenching by $O_2(^3\Sigma_g^-)$ by simply varying the pressure above the surface of the peroxide solution as this should vary the bubble oxygen pressure by the same amount. Figure 14 shows a plot of the pseudo first order rate coefficients for quenching of $O_2(^1\Delta_g)$ against the pressure of $O_2(^3\Sigma_g^-)$. Linear behaviour was indeed found and the graph yields a value for k_4 of $(1.7 \pm 0.4) \times 10^{-18} cm^3$ $molec^{-1}s^{-1}$, which is in agreement with the values obtained by Becker et al,[94,97] the most recent of these being obtained by using an improved detection system.[97] Current literature values for k_4 are shown in Table 3.

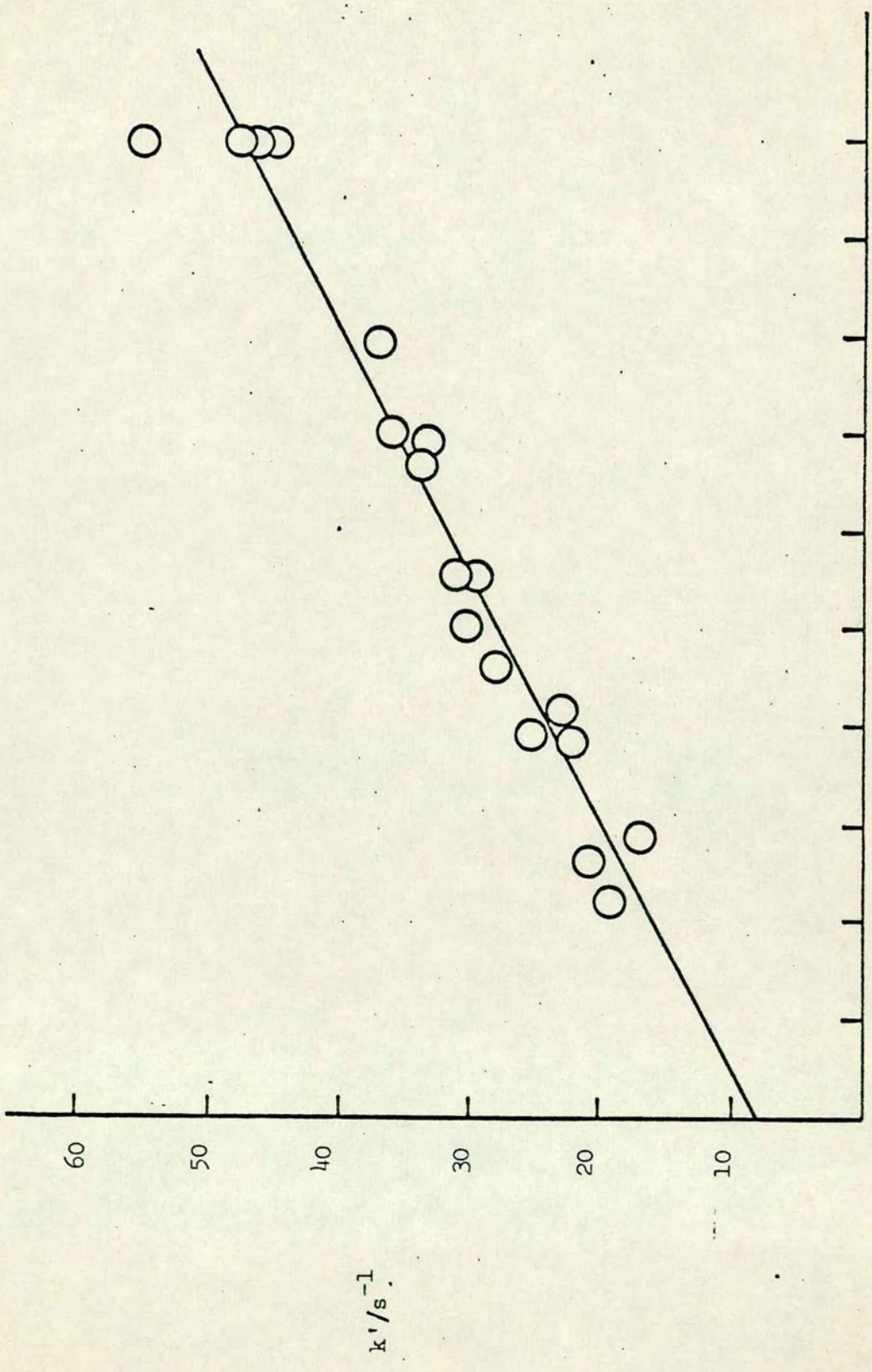

Figure 14. Plot of the pseudo-first-order rate coefficients (k') for quenching of $O_2(a^1\Delta_g)$ against the pressure of $O_2(X^3\Sigma_g^-)$.

If the oxygen in the bubbles was almost entirely present in the $^1\Delta_g$ state, this rate constant might be attributable to the 'dimol' annihilation process [6]. However, no second order trends were observed for the original 'dimol' luminescence decays. Also, since the lifetime of $O_2(^1\Delta_g)$ in aqueous solution is only ca. 2μs, it is extremely improbable that the proportion of singlet oxygen in the bubbles should be greater than several percent. To confirm this a computer model of the system was used and gave good agreement with the experimental data for pseudo first order removal of $O_2(^1\Delta_g)$.

Pressure variation of the pseudo first order quenching rate was also investigated for a drop weight of 0.007 g, a factor of 12 smaller than the standard weight. In decreasing the pressure from 100 kNm^{-2} (760τ) to 15 kNm^{-2} (110τ), the rate did not show any negative pressure dependence and may indeed have increased slightly, confirming that diffusion controlled wall deactivation accounts almost entirely for the removal of $O_2(^1\Delta_g)$ under such conditions.

Since H_2O is approximately three times more efficient in quenching $O_2(^1\Delta_g)$ than $O_2(^3\Sigma_g^-)$, once the partial pressure of H_2O inside the bubbles is greater than 25 kNm^{-2} (190τ), quenching by this species will be dominant. The simplest available means of increasing the vapour pressure of water in this system was to heat the peroxide solution before adding NaOCl from the burrette. Even at the highest temperatures used (360°K) the effect of adding 32 drops of NaOCl, maintained at room temperature, was only to decrease the overall temperature of the solution by 2 to 3°K. Over the middle of the temperature

range (300-330^{o}K) the exothermic nature of the reaction helped to maintain the temperature of the solution at a constant value. The greatest effect was observed for the lowest temperature (263^{o}K), where the warmer NaOCl solution and the reaction's exothermicity both served to increase the temperature of the H_2O_2 solution by approximately 5^{o}K. Thus, the mean of the initial and final temperatures was used to calculate the partial pressure of H_2O in conjunction with literature data on H_2O vapour pressure.[95]

In using this simple method of varying P_{H_2O}, and hence of obtaining a value of the quenching rate constant of $O_2(^1\Delta_g)$ by H_2O, it was important to consider the temperature dependence of k_3 and k_4. Any large effect could invalidate the procedure. Finlay and Snelling[98] determined k_4 at three temperatures, 285, 299.5 and 322^{o}K, the rate constant being expressed in the form, $k_4 = 2.22 \pm 0.09 \times 10^{-18}(T/300)^{0.78 \pm 0.32}$ $cm^3molec^{-1}s^{-1}$, where T is in ^{o}K. A more recent experiment, by Heustis et al,[91] on laser excited liquid oxygen extended this information to 77^{o}K, and was consistent with a $T^{\frac{1}{2}}$ dependence, such that $k_4 = 2.22 \times 10^{-18}$ $(T/300)^{\frac{1}{2}} cm^3molec^{-1}s^{-1}$. In the range 260-360^{o}K, k_4 varies from 2.0×10^{-18} to 2.43×10^{-18} $cm^3molec^{-1}s^{-1}$. This variation in the quenching rate constant for $O_2(^3\Sigma_g^-)$ lies well within the quoted error limits for k_4 determined in this work and could be considered unimportant for the purposes of this investigation. No determination of the Arrhenius parameters for quenching of $O_2(^1\Delta_g)$ by H_2O has been reported, but it was assumed that k_3 shows the same temperature dependence as k_4.

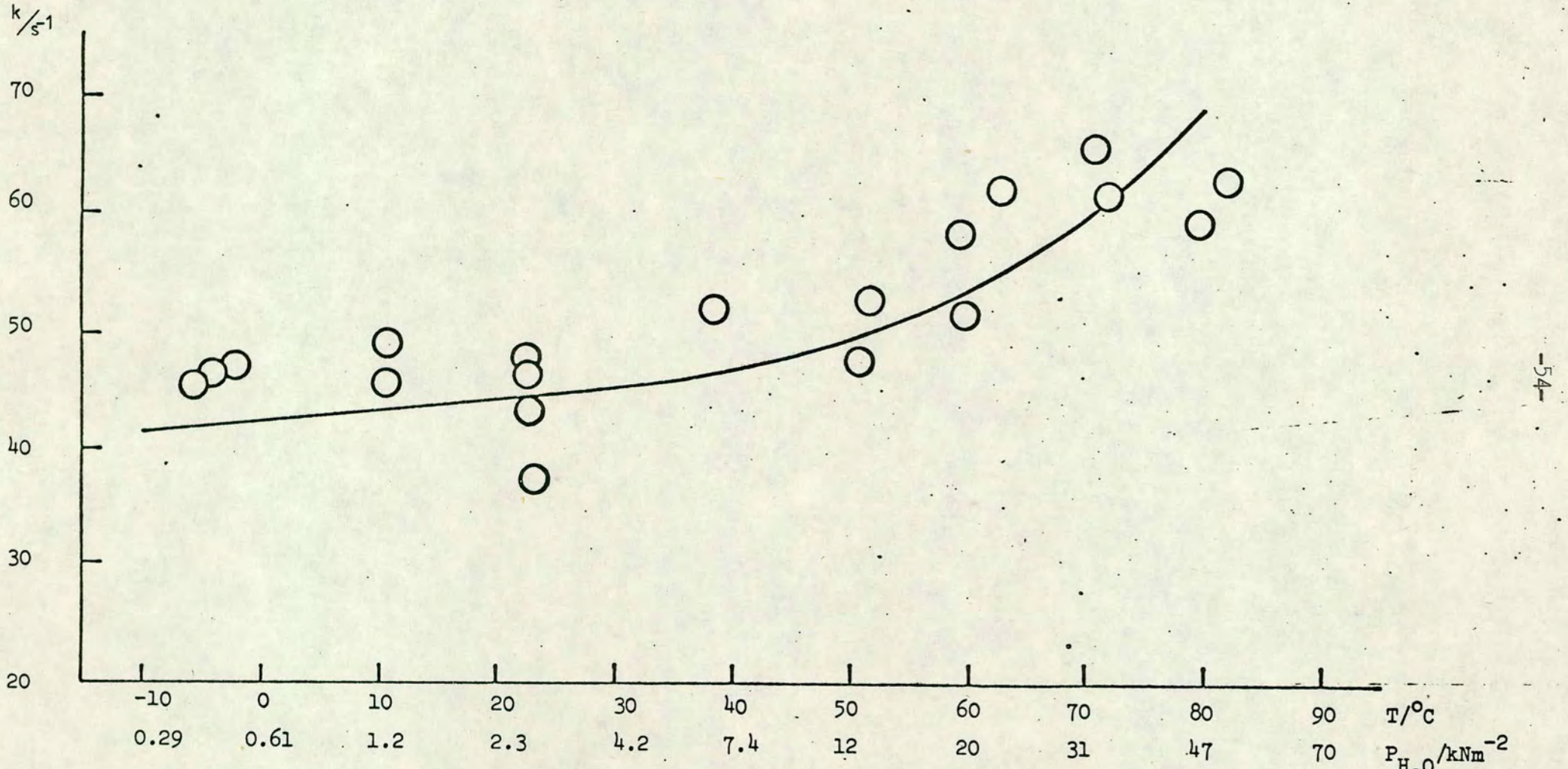

Figure 15. Plot of pseudo-first-order rate coefficients for quenching of $O_2(a^1\Delta_g)$ against the partial pressure of H_2O (and the temperature of the solution). The solid line is calculated from previous data.

The pseudo first order rate coefficient, k", for quenching of $O_2(^1\Delta_g)$ is related to the H_2O partial pressure by an equation of the form [11].

$$k'' = k_3[H_2O] + k_4[O_2] + k_5 \qquad [11]$$

A plot of $k''/[O_2]$ versus $[H_2O]/[O_2(^3\Sigma_g^-)]$ was found to be linear and the slope gave a value for k_3 of $4.0 \pm 1.0 \times 10^{-18} cm^3 molec^{-1}s^{-1}$ which is again in agreement with that obtained by Becker et al.[94] (Table 3). The intercept gave a value for k_4 of $1.9 \times 10^{-18} cm^3 molec^{-1}s^{-1}$, which agrees with the previous determination, assuming negligible contribution from wall processes [5].

$$k_{O_2} = k_4 = (1.7 \pm 0.4) \times 10^{-18} cm^3 molec^{-1}s^{-1}$$

$$k_{H_2O} = k_3 = (4.0 \pm 1.0) \times 10^{-18} cm^3 molec^{-1}s^{-1}$$

Figure 15 shows a plot of the pseudo-first order rate coefficients for quenching of $O_2(^1\Delta_g)$ against the partial pressure of H_2O. The solid line was calculated using the experimentally determined values shown above. Although there appears to be a wide scatter in the results, there is a definite trend in k" which is attributable to the increased contribution to quenching by H_2O at higher temperatures.

3.03 Spectroscopic Detection of $O_2(^1\Delta_g)$ in other Chemical Systems

The sodium salt of N-chloro-N Methyl σ-sulpho benzamide (a), reacts in akaline hydrogen peroxide as shown [12].

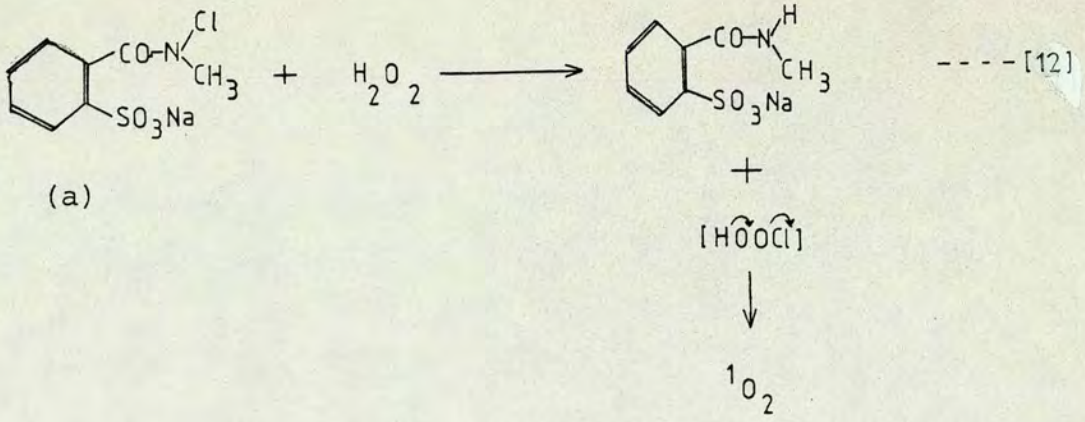

(a)

Singlet oxygen has been chemically trapped,[99] but product analysis experiments are often ambiguous. Salt (a) was prepared by the reaction of N-Methyl-o-sulphobenzamide with hypochlorous acid. A sample of (a) (36.4 mg) in water (20 cm^3) containing acetic acid (10 cm^3) was treated with KI (2g) and a piece of solid carbon dioxide. The liberated iodine was titrated against standard thiosulphate (0.1N) and the available chlorine from (a) was determined to be 24.8%.

An aqueous solution of (a) (1.0 M) was added dropwise (0.085 g) to 100 vol H_2O_2. No emission was detected over the pH range 8-10, even after the detection system had been optimised using the NaOCl-H_2O_2 reaction. Reaction [12] proceeds slowly and generates very small bubbles of oxygen, so that any singlet oxygen would be quenched in the solution. This technique is unsuitable for studying the evolution of $O_2(^1\Delta_g)$ under conditions where the rate of removal is more than two orders of magnitude slower than the rate of formation. Similarly no emission was detected from the decomposition of hydrogen peroxide in the presence of the enzyme catalase, although the generation of $O_2(^1\Delta_g)$ in this system has been discounted.[34]

The oxidation of formaldehyde by alkaline peroxide in the presence of pyrogallol, the Trautz reaction, has been shown to evolve singlet oxygen.[100] Hydrogen peroxide (100 vol) was added to a solution of pyrogallol (2.2 g) in 37% formalin. The reaction was exceedingly vigorous and chemiluminescence was readily observed. Emission was detected at 633 nm and 702 nm. The pyrogallol/formalin solution absorbs in the red, so that luminescence, following addition of a single drop of H_2O_2, could not be detected, and it was only when volumes of 1 cm^3 or more were added that a decay was observed. Poor signal to noise ratios were obtained, and the difficulty of reproducibly adding 1 cm^3 volumes of H_2O_2, together with the highly exothermic nature of the reaction made signal averaging impracticable.

Chapter 4

Primary and Secondary Processes in the Photolysis of Ozone

4.01 Introduction

The photolysis of ozone in the near ultraviolet Hartley band ($\lambda < 310$ nm) is an important source of metastable $O(^1D)$ atoms in the atmosphere [1]. There is much current interest in the subsequent reactions of $O(^1D)$ atoms, because of the important role this species plays in the initiation of stratospheric chemistry.

$$O_3 + h\nu(\lambda < 310 \text{ nm}) \rightarrow O(^1D) + O_2(^1\Delta_g) \qquad [1]$$

The main features in the absorption spectrum of ozone[105] consist of the strong Hartley band in the near ultraviolet (200-300 nm) centred at 254 nm, the Huggins band (300-360 nm) and the much weaker Chappius band (440-850 nm).

Photolysis of ozone in the red region of the spectrum ($\lambda > 610$ nm) is well understood[106] and yields both an oxygen atom and an oxygen molecule in their ground electronic states [2].

$$O_3 + h\nu(\lambda > 610 \text{ nm}) \rightarrow O(^3P) + O_2(^3\Sigma_g^-) \qquad [2]$$

$$O(^3P) + O_3 \rightarrow 2O_2 \qquad [3]$$

A further molecule of ozone is removed by reaction with $O(^3P)$ [3] produced in the initial photolysis step [2]. Thus the overall quantum yield, Φ_f is 2.

Photolysis of O_3 in the near ultraviolet produces $O(^1D)$ as the main atomic fragment and also yields oxygen molecules in the metastable $^1\Delta_g$ state. Thermodynamic calculations[107] show the lower energy limit for the production of $O(^1D)$ and $O_2(^1\Delta_g)$ from O_3 is 387 ± 2 kJ mole^{-1}, which corresponds to a threshold wavelength of 310 nm. Wavelength limits for the

production of various electronic states of O_2 and O and the energies of these states are shown in tables 4 and 5.

$$O_3 + h\nu(\lambda < 410 \text{ nm}) \rightarrow O(^1D) + O_2(^3\Sigma_g^-) \quad [4]$$

$$O_3 + h\nu(\lambda < 611 \text{ nm}) \rightarrow O(^3P) + O_2(^1\Delta_g) \quad [5]$$

$$O_3 + h\nu(\lambda < 463 \text{ nm}) \rightarrow O(^3P) + O_2(^1\Sigma_g^+) \quad [6]$$

Studies of the photolysis of ozone at 340 nm have shown that only processes [5] and [6] occur, [4] being unimportant.[108,109]

In the wavelength range 300-320 nm [1], conflicting results have been obtained for the production of $O(^1D)$.[110] Above 300 nm, the $O(^1D)$ yield falls off to zero. Even though the absorption cross section of O_3 is also rapidly decreasing in this threshold region,[105] the nature of this fall off is important in the troposphere and lower atmosphere, due to lack of radiation at wavelengths shorter than 300 nm. Some of the results which have been obtained are shown in figure 16.[110,111,112]

The quantum efficiency for the production of $O(^1D)$ from O_3 photodissociation has been accepted as unity below 300 nm.[113,114,115] However, recent results obtained by Lawrence et al.[116] suggest that this may not be the case and show that $\Phi_{O(^1D)}$ decreases steadily from 0.93 to 0.87 in the wavelength region 300-274 nm.

The reaction of $O(^1D)$ with O_3

The overall quantum yield, Φ_f, for the removal of ozone on photolysis at shorter wavelengths (λ < 300 nm) is considerably higher than that found for longer wavelengths. There is, however, considerable disagreement as to the exact value.

Table 4: The energies of the electronically excited states of oxygen atoms and molecules

O			O_2		
State	E/kJ mol^{-1}	E/eV	State	E/kJ $mole^{-1}$	E/eV
^3P	0	0	$^3\Sigma_g^-$	0	0
^1D	190.0	1.97	$^1\Delta_g$	94.3	0.98
^1S	402.8	4.18	$^1\Sigma_g^+$	151.7	1.57

Table 5: Long wavelength limits (nm) for the production of various states of O_2 and O in the photolysis of O_3

O \ O_2	$^3\Sigma_g^-$	$^1\Delta_g$	$^1\Sigma_g^+$	$^3\Sigma_u^+$	$^3\Sigma_u^-$
^3P	1180	611	463	230	170
^1D	411	310	266	167	150
^1S	234	196	179	129	108

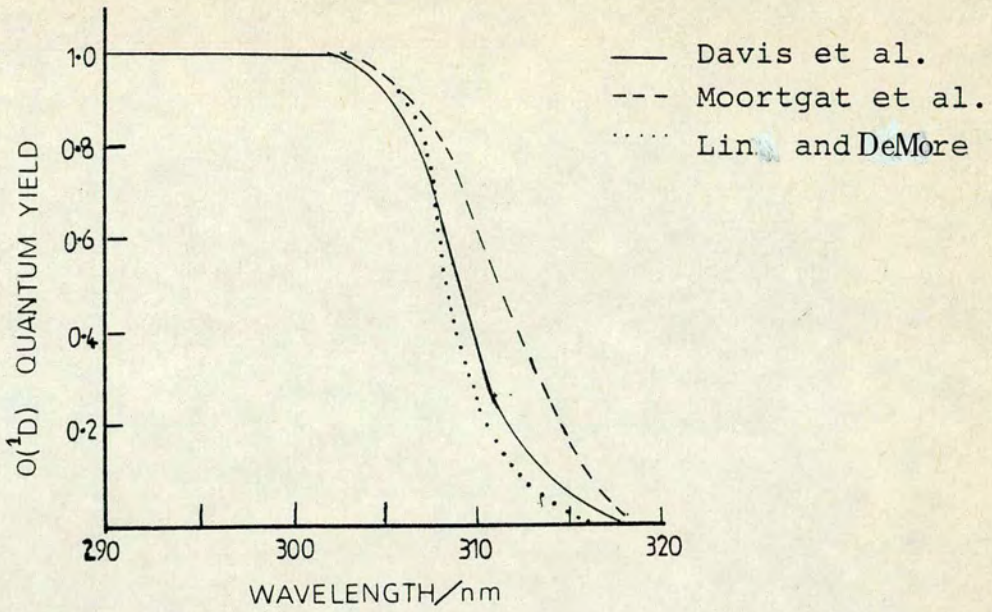

Figure 16: The quantum yield for $O(^1D)$ production from ozone photolysis for wavelengths in the range (290-320)

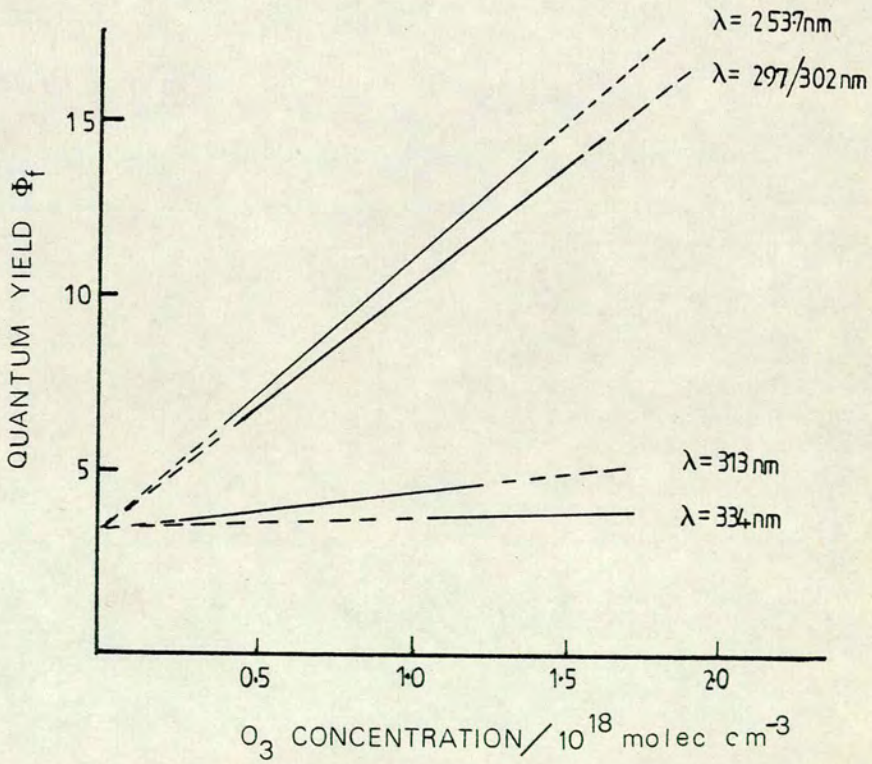

Figure 17: The dependence of Φ_f for pure ozene on concentration for a number of wavelengths (after ref. 108).

Heidt and Forbes[117] found values of up to 6.7 in O_3/O_2 mixtures, while Norrish and Wayne[118] obtained values as high as 16 in pure ozone (λ = 253.7 nm). Jones and Wayne[108] obtained high pressure values of 16 or 17 (λ = 254 nm) extrapolating to a zero pressure value of 4 for all wavelengths, whereas Schumacher et al.[119] found a value of 6 in pure ozone over a wide range of pressures. Lissi and Heicklen[114] found no evidence for $\Phi_f > 6$ at 300 nm for pure ozone pressures up to 350 Nm^{-2}. Such diversity has resulted in considerable confusion as to the nature of the chemical processes involved in the degradation of pure ozone and, in particular, with regard to the products of the reaction of $O(^1D)$ with O_3.

To account for the pressure dependence of Φ_f, as shown in Figure 17, McGrath and Norrish[120] proposed a chain mechanism ([7]-[11]) initiated by $O(^1D)$ [7] and propagated by $O_2^\dagger$ [8], some energy rich state of molecular oxygen. Chain termination is by wall and gas phase quenching of $O_2^\dagger$ [11].

$$O_3 + h\nu(\lambda < 300 \text{ nm}) \rightarrow O(^1D) + O_2(^1\Delta_g) \qquad [1]$$

$$O(^1D) + O_3 \rightarrow O_2^\dagger + O_2 \qquad [7]$$

$$O_2^\dagger + O_3 \rightarrow 2\,O_2 + O(^1D) \qquad [8]$$

$$O_2(^1\Delta_g) + O_3 \rightarrow 2\,O_2 + O(^3P) \qquad [9]$$

$$O(^3P) + O_3 \rightarrow 2\,O_2 \qquad [10]$$

$$O_2^\dagger + M \rightarrow O_2 + M \qquad [11]$$

Extrapolation to $[O_3] = 0$ for this scheme yields $\Phi_f = 4$, assuming only processes [1], [7], [9] and [10] occur. These assumptions are not altogether convincing and do not support the values of Schumacher et al.[119] or Lissi and Heicklen[114] at low O_3 pressures. It is important to note that Jones and Wayne[108] obtained no values of Φ_f below 6 over the pressure range used and the validity of their extrapolation may therefore be in doubt.

McGrath and Norrish[120] have found $O_2(^3\Sigma_g^-)$, $v'' < 17$, on photolysis of pure ozone, which they explained by the high exothermicity of reaction [12]

$$O(^1D) + O_3 \rightarrow 2\ O_2 + 580\ kJ\ mole^{-1} \qquad [12]$$

$$O(^3P) + O_3 \rightarrow 2\ O_2 + 400\ kJ\ mole^{-1} \qquad [10]$$

although [10] is also highly exothermic and could account for $O_2(^3\Sigma_g^-)$ up to $v'' = 27$. Bair et al.[121] have found $O_2(^3\Sigma_g^-)$, $v'' < 30$, suggesting $27 < v'' < 30$, formed from reaction [12], is at least a minor product. Reaction [8] becomes thermoneutral for $v'' = 17$ and the low concentration of $O_2(^3\Sigma_g^-)$, $v'' > 17$ observed by McGrath and Norrish[120] led them to propose $O_2^\dagger$, $v'' > 17$ as the chain carrier, though the transfer of 17 quanta of energy is unlikely, even for near resonant processes.

The argument that an electronically excited state of O_2, such as $^3\Sigma_u^+$, might be the chain carrier is improbable since the lifetime of this species is too short to have an effect within the experimental time scale.[122] Gunther and Snelling[123] have shown that $O_2(^1\Sigma_g^+)$ formation is an unimportant product of the reaction of $O(^1D)$ with O_3, so that this species, too, is not the chain carrier. Bair et al.[121,122] have proposed reaction [13] as the major path, which results in an overall

$$O(^1D) + O_3 \rightarrow 2\,O(^3P) + O_2 \qquad [13]$$

quantum yield prediction of 6 for pure ozone which decreases by a factor of $^2/3$ in the presence of gases which quench $O(^1D)$. Lissi and Heicklen[114] have found that in the presence of N_2, CO_2 or N_2O at high pressures Φ_f falls to almost 4.0, supporting this scheme. However, these workers proposed reaction [14], with some quenching of $O_2^{\dagger}$, to account for a value of $\Phi_f = 5.0 \pm 0.3$ in pure ozone.

$$O_2^{\dagger} + O_3 \rightarrow 2\,O_2 + O(^3P) \qquad [14]$$

Giachardi and Wayne[124] studied the photolysis of ozone using both a conventional flow system and resonance fluorescence measurements of $[O(^3P)]$. Both techniques depended on the grouping of the secondary reactions following ozone photolysis into 'fast' and 'slow' processes. Conditions employed were such, that when reactions involving $O(^1D)$, $O_2(^1\Sigma_g^+)$ and $O_2^{\dagger}$ had almost gone to completion, those involving $O(^3P)$ and $O_2(^1\Delta_g)$ had barely begun. Hence it was possible to obtain an intermediate quantum yield, Φ_i, which only accounted for the removal of ozone by $O(^1D)$, $O_2(^1\Sigma_g^+)$ and $O_2^{\dagger}$.

In the presence of excess N_2, when $O(^1D)$ is rapidly quenched , the intermediate quantum yield, Φ_i, is 1.0. For pure ozone, assuming reaction [13] is the major channel, a value of $\Phi_i = 2.0$ would be predicted. The involvement of processes such as [14] would give a value of $\Phi_i > 2.0$. An experimental value of $\Phi_i = 1.89 \pm 0.03$ was obtained, assuming a value of $\Phi_i = 1.0$ for nitrogen. However, Giachardi and Wayne[124] made no allowance, in the case of excess nitrogen, for the removal of some 3-7% of $O(^1D)$ by reaction with O_3 rather than by physical quenching. Thus their experimental value of Φ_i in pure ozone was probably closer to 2.0.

This result suggests reaction [13] is the major path and that the production of electronically or vibrationally excited molecular oxygen species is only of minor importance.

Giachardi and Wayne[124] calculated an overall quantum yield of $\Phi_f = 4.7$, which can be compared with the value $\Phi_f = 5.0 \pm 0.3$ obtained by Lissi and Heicklen,[114] although this result was explained using the assumption that $O_2^{\dagger}$ is produced by reaction [7], only a fraction of which reacts with O_3. Schumacher et al.[119] found $\Phi_f = 6.0$ over a wide range of pressures and, although this does not support the values of $\Phi_i = 1.9$ and $\Phi_f = 4.7$ as obtained by Wayne,[124] it does suggest that $O(^1D)$ reacts with O_3 entirely by process [13]. The overall quantum yields, Φ_f, obtained by various workers are summarised in Table 6.

<u>The reaction of $O(^3P)$ with O_3</u>

$$O(^3P) + O_3 \rightarrow O_2 + O_2 \qquad [10]$$

$$O(^3P) + O_3 \rightarrow O_2(^1\Delta_g) + O_2 \qquad [15]$$

$$O(^3P) + O_3 \rightarrow O_2(^1\Sigma_g^+) + O_2 \qquad [16]$$

The reaction of $O(^3P)$ with ozone is well understood and seems to proceed entirely by process [10]. Although reaction [15] is allowed on grounds both of spin conservation and thermochemistry, the absence of any chain reaction[106] [9,15] following visible photolysis of O_3 seems to rule this possibility out. Similarly, $O_2(^1\Sigma_g^+)$ has not been observed[125] as a product of reaction [16].

Table 6. Final quantum yields for O_3 removal as found by other workers

Author	P_{O_3}/kNm^{-2}	Φ_f	System Studied	Comments	Ref.
McGrath and Norrish	0.27-6.7	16.7	O_3/He	Chain mechanism postulated to account for Φ_f	120
Norrish and Wayne	0	4.0	O_3/He	at high pressures of O_3	118
	0.27	2.0	O_3/N_2	Extrapolation to $[O_3] = 0$ yields $\Phi_f = 4$. $\Phi_f = 2$ in the presence of N_2	
Jones and Wayne	0.005-0.27	4.0	O_3/O_2	O_2 added in partial pressures from 10-90%. Φ_f remained constant	108
	0.013	4.5 ± 0.3	O_3/He		
Schumacher et al.	1.3-13	6.0	O_3/He	Φ_f remained constant over a wide range of O_3 pressures	119
Lissi and Heicklen	0.013-0.36	5.5 ± 0.5	O_3/He	O_2^+ postulated to account for Φ_f in pure ozone	114
		4.2 ± 0.4	O_3/N_2		
Webster and Bair	0.027		O_3/He	$\Phi_i(O_3/He) = 2\Phi_i(O_3/N_2)$	122
			O_3/N_2		
Giachardi and Wayne	6.7-67 Nm^{-2}		O_3/He	Φ_i incorrectly calculated for O_3/He system	124

The reaction of $O_2(^1\Delta_g)$ with O_3

$$O_2(^1\Delta_g) + O_3(^1A_1) \rightarrow O(^3P) + 2\ O_2(^3\Sigma_g^-) \qquad [9]$$

Although this reaction [9] is about 12.1 kJ mol^{-1} endothermic, it is spin allowed, and occurs in preference to physical quenching.

The quenching of $O(^1D)$

$O(^1D)$ is known to be efficiently quenched by N_2, CO_2 and O_2[3], the products

$$O(^1D) + N_2 \rightarrow O(^3P) + N_2^* \qquad [17]$$

of this highly exothermic process [17] being $O(^3P)$ and vibrationally excited quencher.

Quenching by O_2, however, can lead to formation of $O_2(^1\Sigma_g^+)$ by energy transfer as well as vibrationally excited $O_2(^3\Sigma_g^-)$ [18,19]. Literature estimates of the fraction, α, of $O(^1D)$ quenched to give $O_2(^1\Sigma_g^+)$ vary from 0.01 to 1.0. Giachardi and Wayne[20] suggest $0.5 < \alpha < 0.6$, whereas Young and Black[126] prefer a value for α of 1.0.

$$O(^1D) + O_2(^3\Sigma_g^-) \rightarrow O(^3P) + O_2(^1\Sigma_g^+) \qquad [18]$$

$$O(^1D) + O_2(^3\Sigma_g^-) \rightarrow O(^3P) + O_2(^3\Sigma_g^-) \qquad [19]$$

$O(^1D)$ is not efficiently quenched by gases such as He and SF_6. The three body recombination of $O(^1D)$ with N_2 to give N_2O [20] is also unimportant.[127]

$$N_2 + O(^1D) + M \rightarrow N_2O + M \qquad [20]$$

The present study of ozone photolysis was undertaken in an attempt to resolve the discrepancies which exist, regarding the chemical processes involved in determining the intermediate and final quantum yields for O_3 removal. Most of the uncertainty

centres around the products of the reaction of $O(^1D)$ with O_3.

The three possible outcomes of this reaction, which have already been discussed, are summarised below, together with the respective values of Φ_i.

$$\text{(i)} \quad O(^1D) + O_3 \rightarrow O(^3P) + O(^3P) + O_2 \qquad \Phi_i = 2$$

$$\text{(ii)} \quad O(^1D) + O_3 \rightarrow O_2^{\dagger} + O_2 \qquad \Phi_i > 2$$

$$O_2^{\dagger} + O_3 \rightarrow O_2 + O_2 + O(^3P)$$

$$O_2^{\dagger} + M \rightarrow O_2 + M$$

$$\text{(iii)} \quad O(^1D) + O_3 \rightarrow O_2^{\dagger} + O_2 \qquad \Phi_i >> 2$$

$$O_2^{\dagger} + O_3 \rightarrow O_2 + O_2 + O(^1D)$$

The importance of three body recombination processes in determining the value of Φ_f is considered. Computer modelling studies were carried out to obtain a fuller understanding of all the processes involved and their relative significance.

4.02 Results and Discussion

Ozone was monitored in absorption at 253.7 nm using kinetic spectrophotometry, as described in section 2.05.

Preparation was by the method of Clough and Thrush[128] and ozone purity was checked using an ultraviolet spectrophotometer (Perkin-Elmer 402). Concentrations were determined from the absorption coefficients of Griggs.[105]

In carrying out an experiment, the zero and incident (I_0) light intensities were plotted out first of all. The reaction vessel was filled so that the partial pressure of ozone was 26 Nm^{-2} (0.2 τ) and the capacitor charged. After opening the shutter, the flash lamp was discharged and the ozone absorption signal monitored over a period of 20 ms.

The pretriggering facility of the transient recorder was used to check the ozone concentration immediately prior to the flash. The shutter was closed to prevent further photolysis and after the decay had been plotted out, the final ozone concentration was recorded. After pumping out the reaction vessel the incident light intensity was again checked to make certain that no change had occurred within the period of the experiment.

The ozone decay curve was extrapolated back to ca. 40μs after the flash, so as to obtain an estimate of the ozone concentration removed by primary processes.

In order to determine the yield of $O(^3P)$ from ozone photolysis, the product of the corrected flash intensity (Figure 8) and the ozone absorption coefficient was integrated over the wavelength range 200-600 nm (Figure 18). From this, it was shown that ca. 99% of the light absorbed on photolysis was of shorter wavelength than 310 nm. Hence, assuming the quantum yield for $O(^1D)$ production to be unity for wavelengths shorter than 300 nm,less than 1% of oxygen atoms were produced in the ground ^3P state.

In the preliminary stages of this investigation, experiments were carried out for both the O_3/He and O_3/He/N_2 systems using a total pressure of 2.6 kNm^{-2} (20 τ). Final to intermediate quantum yield ratios (Φ_f/Φ_i) were found to be ca. 2.8 and ca. 3.8 respectively. These results are in agreement with those of Lissi and Heicklen[114] for both cases, assuming a value of $\Phi_i = 2$ in the case of ozone in helium.

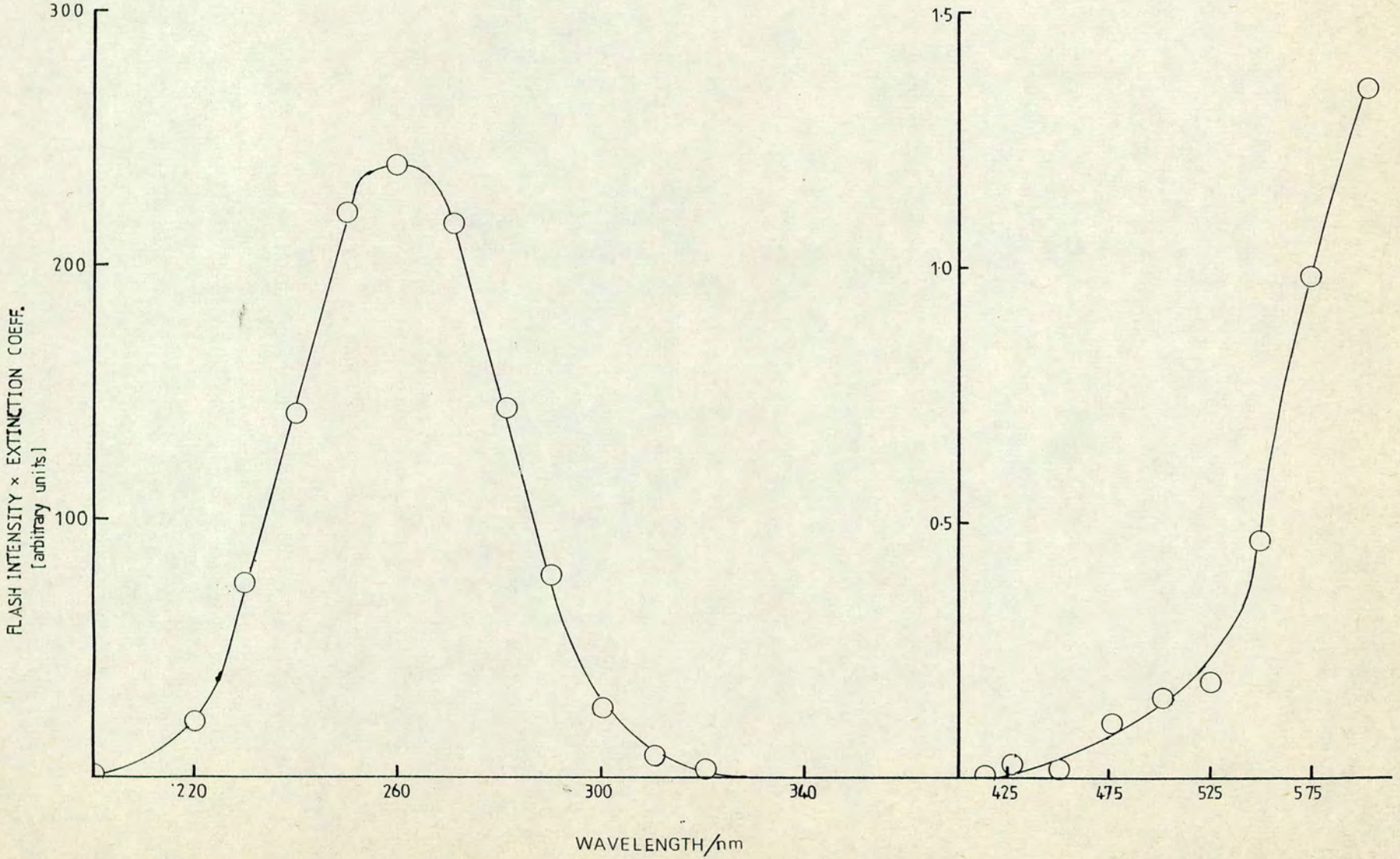

Figure 18: The intensity of absorption of the photolysis flash by ozone over the wavelength range 200-600 nm.

There appeared to be some diffusion of ozone back into the centre of the reaction vessel at longer times so that the final ozone concentration, $[O_3]_f$, was taken as the minimum in the decay curve. Such diffusion effects could be readily understood if the low heat capacity, particularly in the presence of helium was considered (Table 7). Rapid expansion of gas in the reaction zone, due to the highly exothermic nature of the processes involved, was followed by cooling at the wall of the reaction vessel and the flow of gas back into the centre.

The rate of removal of ozone under the above conditions was very rapid during the first 10 ms, due to the large increase in the temperature of the system. Thus it was very difficult to obtain an accurate extrapolation of the absorption signal. Furthermore, the lack of information concerning the Arrhenius parameters for the reactions involved, together with the difficulty of estimating the temperature rise in the system made analysis of the experimental results and their simulation very difficult.

The high heat capacity of SF_6 (Table 7) and its low efficiency as a quencher of $O(^1D)$, made it an ideal buffer gas in the study of O_3 photolysis. By varying the pressure of SF_6 in the reagent mixture over a wide range (0-26 kNm^{-2}), in both the O_3/SF_6 and $O_3/N_2/SF_6$ systems, the optimum conditions were obtained under which the decay of O_3 could be analysed. The slope of each decay curve, in units of s^{-1}, was calculated at a fixed time of 2.4 ms after the flash. Figures 19 and 20 show the effect of both SF_6 and N_2 pressures on the pseudo first order rate of removal of ozone.

Table 7. Heat Capacities of various gases at 298°K

Gas	C_p/J $K^{-1}mole^{-1}$	C_v/J $K^{-1}mole^{-1}$
N_2	29.12	20.81
O_2	29.36	21.05
SF_6	97.60	89.29
He	21.15	12.84

Table 8. Experimental results for the depletion of O_3 following photolysis in the presence of SF_6, SF_6 and excess N_2, SF_6 and excess O_2 (average of ≥15 experiments).

System	P_{O_3}	P_{O_2}	P_{N_2}	P_{SF_6}	P_{He}	Avg. intermediate % O_3 depletion	Avg. Final % O_3 depletion	Φ_f/Φ_i
O_3/SF_6	26 Nm^{-2}	6.7 Nm^{-2}	-	16.4 kNm^{-2}	180 Nm^{-2}	19.9 ± 1.8	36.3 ± 2.7	1.84 ± 0.23
$O_3/SF_6/N_2$	26 Nm^{-2}	6.7 Nm^{-2}	2.45 kNm^{-2}	14.0 kNm^{-2}	180 Nm^{-2}	10.5 ± 0.8	26.4 ± 1.0	2.48 ± 0.11
$O_3/SF_6/O_2$	26 Nm^{-2}	2.67 kNm^{-2}	-	13.8 kNm^{-2}	180 Nm^{-2}	2.0 ± 0.8	2.0 ± 0.8	1.0 ± 0.5

errors represent 2 Standard Deviations.

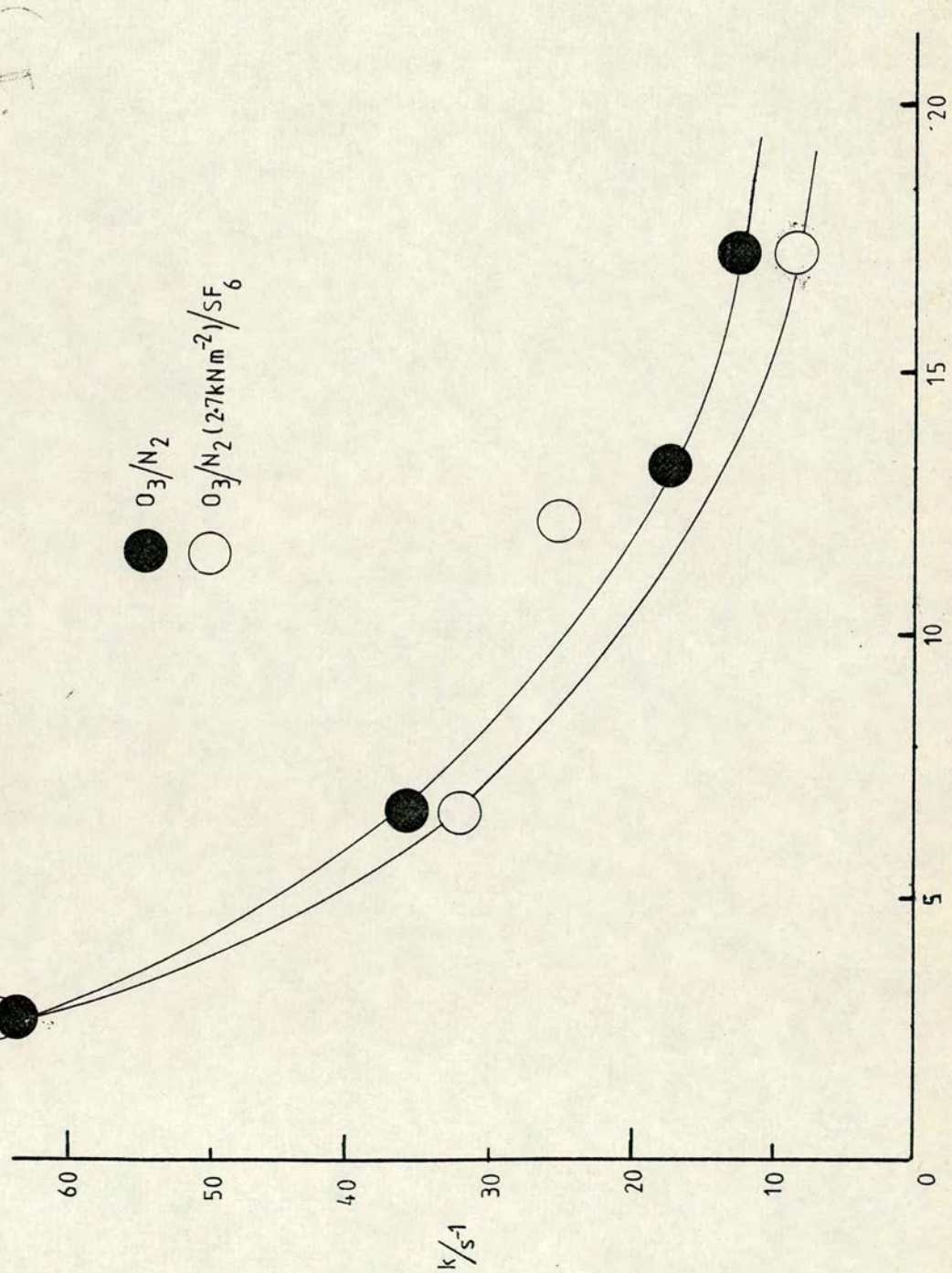

Figure 19: A plot of pseudo 1st order decay coefficient versus total pressure for the $O_3/SF_6/N_2$ systems.

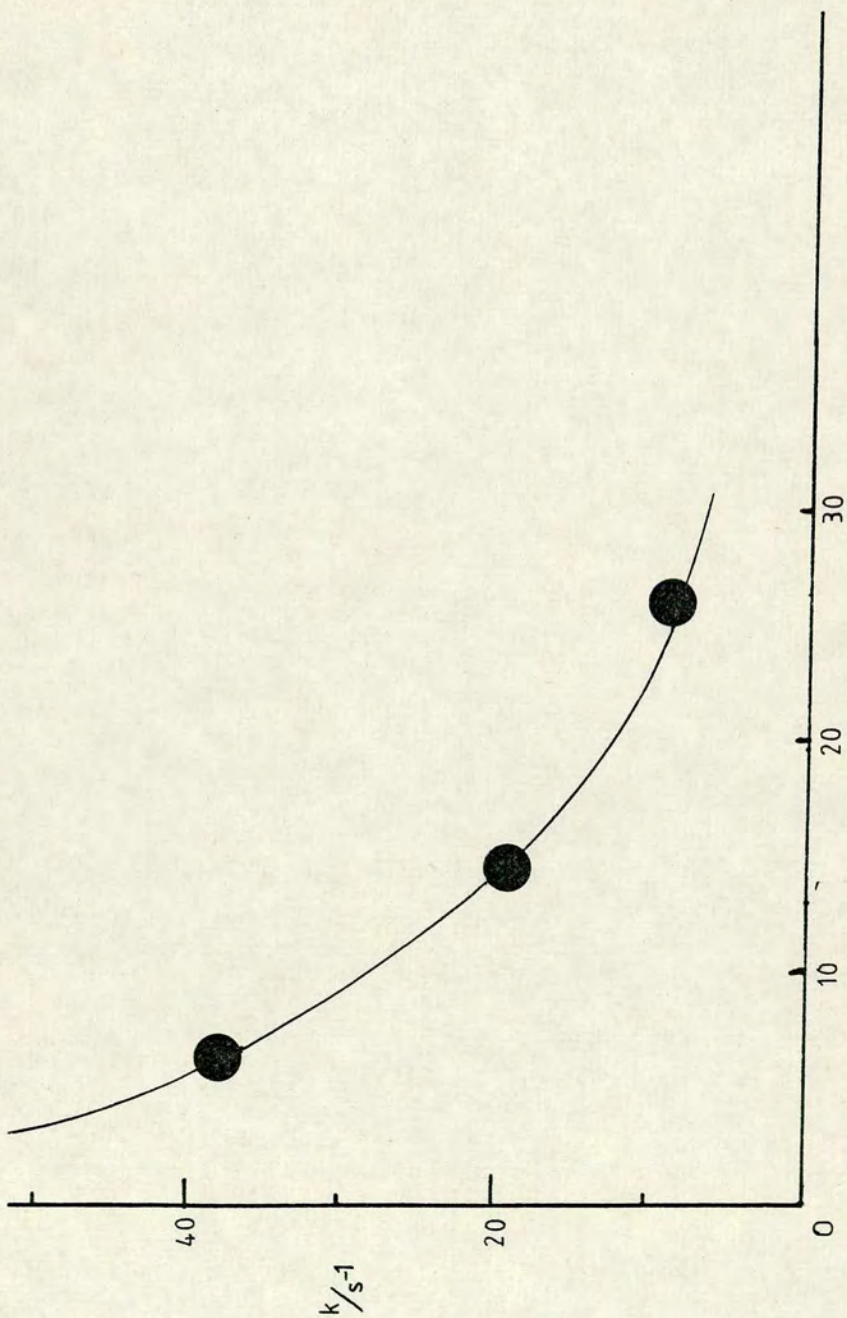

Figure 20: A plot of the pseudo 1st order decay coefficient versus total pressure for the O_3/SF_6 system.

Increasing the pressure of N_2 had a significant effect on the ozone removal rate, although the effect of SF_6 was somewhat greater, but not as large as might have been expected from the four-fold increase in heat capacity. At high pressures of SF_6 (>13 kNm^{-2}) there was at least a five-fold decrease in the removal rate, compared with the result at 2.6 kNm^{-2}. A value of the O_3 removal rate, in agreement with room temperature estimates, was obtained for the $O_3/N_2/SF_6$ system, with SF_6 pressures in excess of 13 kNm^{-2} (P_{N_2} = 2.6 kNm^{-2}). As a result of this investigation, all further experiments were carried out at a total pressure of 16.7 kNm^{-2} (125 τ), so reducing the temperature rise in the system, while maintaining the number of experiments which could be carried out from a single mixture at a reasonable level (4-5). Although some heating still appeared to occur in the O_3/SF_6 system under these conditions, O_3 diffusion was no longer expected to be a problem.

The photolysis of O_3 (26 Nm^{-2}) was studied at high pressures of SF_6 (total pressure = 16.7 kNm^{-2}) and also in the presence of N_2 (2.6 kNm^{-2}) and O_2 (2.6 kNm^{-2}). A large number of experiments were carried out in each case and those decays where the measured initial O_3 pressure was not within 5% of the correct value (26 Nm^{-2}) were discarded. Experiments were alternated between the O_3/SF_6 and $O_3/SF_6/N_2$ systems so that the consistency of the flash lamp output could be checked. The results are shown in Table 8, with typical decays illustrated in Figure 21.

Assuming an intermediate quantum yield of unity (Φ_i = 1.0) in the presence of N_2 gave a value of Φ_i = 1.90 in pure ozone. However this assumption does not consider that quenching of

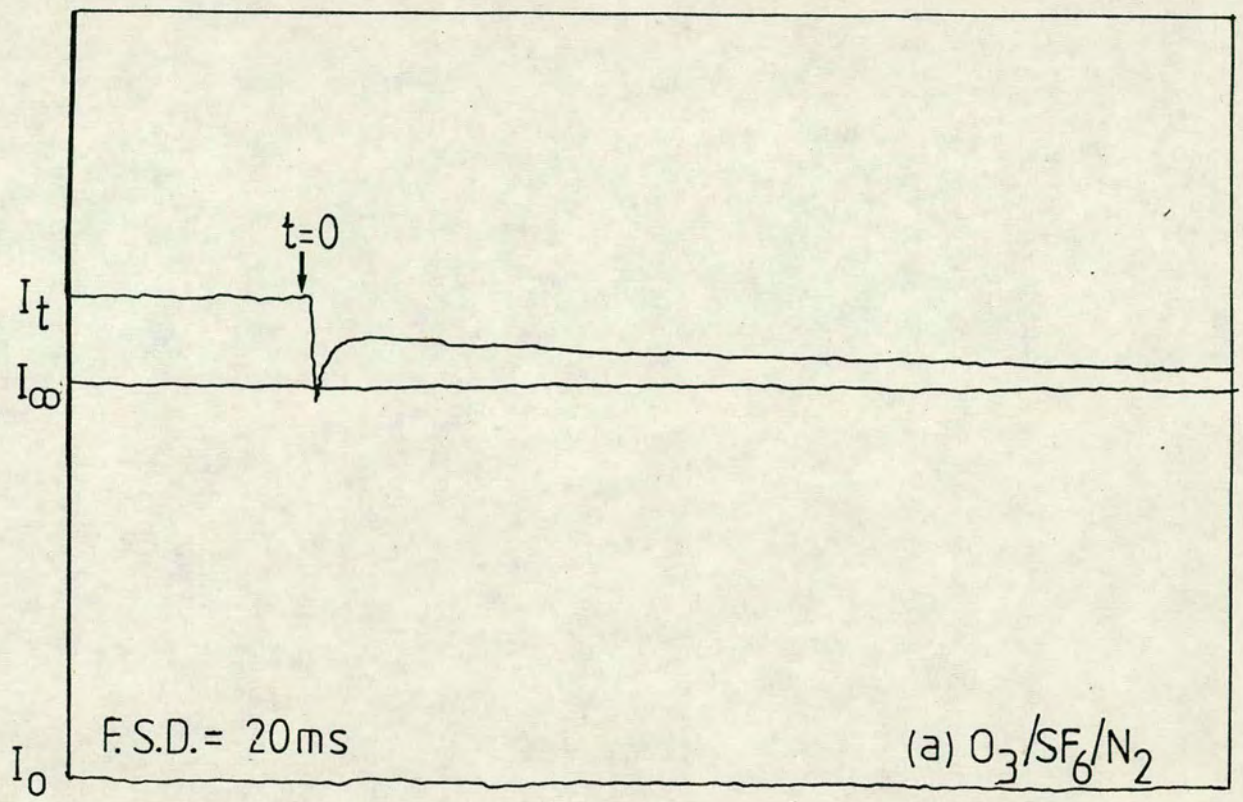

Figure 21: Typical experimental ozone decays

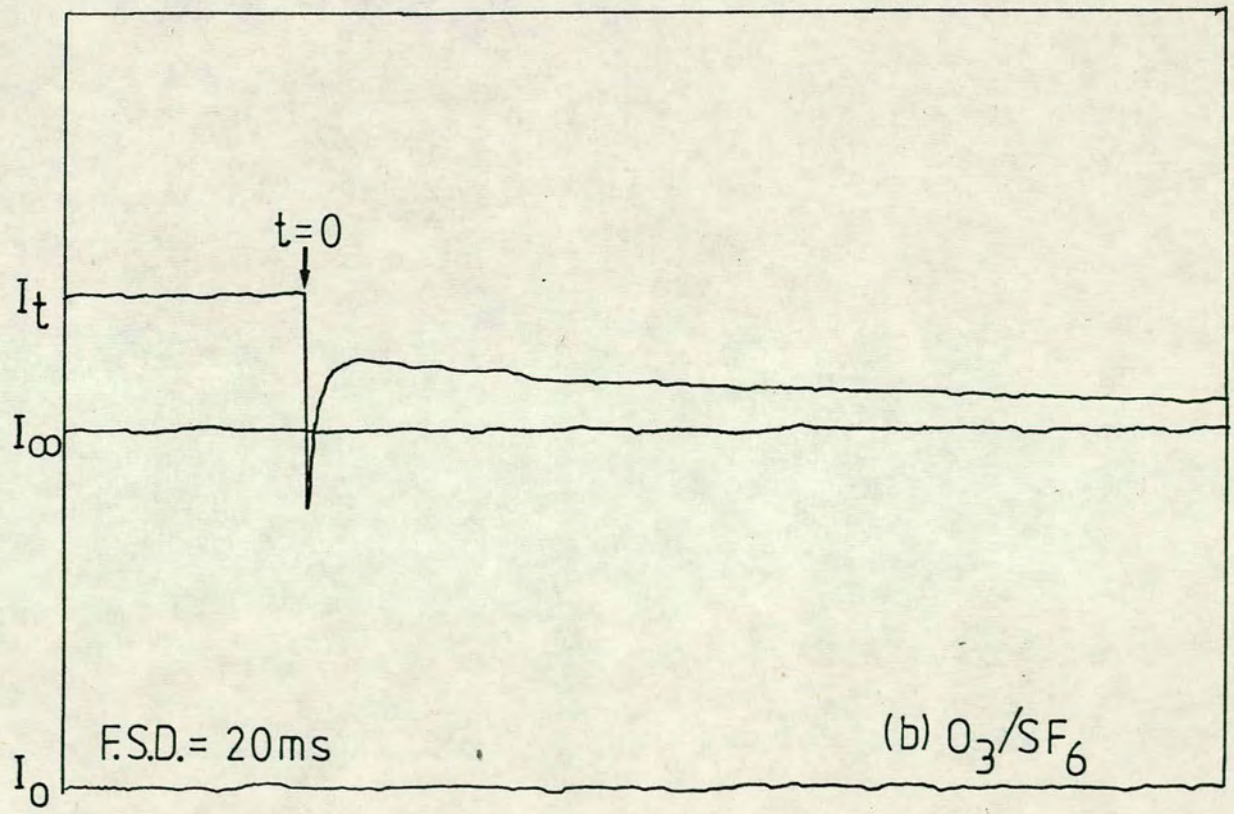

$O(^1D)$ by N_2 was not 100% efficient. A comparison of the relative rates of removal of $O(^1D)$ by both O_3 and N_2 (see Table 9) shows that, under the experimental conditions employed, only 95% of $O(^1D)$ produced in the primary photolysis was quenched by N_2. Taking this into consideration, the corrected value of Φ_i for ozone in the presence of SF_6 alone was 2.00 ± 0.23. This value for Φ_i supports the argument that the dominant channel, in the reaction of $O(^1D)$ atoms with O_3, leads to the formation of two ground state $O(^3P)$ atoms [13] and not some excited form of O_2 [7]. It also suggests $< 10\%$ $O(^3P)$ production from ozone photolysis at wavelengths shorter than 300 nm, in support of the results of Lawrence et al.[116]

Taking an intermediate quantum yield of 2.0 for ozone removal in the presence of SF_6 (total pressure = 16.7 kNm^{-2}), as calculated above, the final quantum yield, Φ_f, was in this case 3.66 ± 0.46 compared with 2.48 ± 0.11 in the presence of SF_6 and N_2 (2.6 kNm^{-2}). These values are much less than in the previous low pressure experiments, suggesting that SF_6 has a significant effect on the rate of secondary processes, where it is an effective third body under high pressure conditions [21], [22].

$$O(^3P) + O(^3P) + M \rightarrow O_2 + M \qquad [21]$$

$$O(^3P) + O_2 + M \rightarrow O_3 + M \qquad [22]$$

From these results, it can be seen that any computer model of O_3 photolysis, apart from considering the basic primary and secondary processes leading to the destruction of ozone, must take account of third body recombination reactions leading to the formation of ozone and the removal of reactive species such as $O(^3P)$.

4.03 Computer Modelling Studies

The chemical simulation package, 'CHEK', developed by Curtis and Chance,[129] together with several additional sub-routines, was used to model the primary and secondary reactions involved in the photolysis of ozone. Appendix 3 contains a full description of the program and its applications.

For the simulation to be successful, it must generate a reliable flash intensity profile as well as providing a good fit to the experimental decay curve and the measured values of Φ_i and Φ_f. It was found that the simulated flash profile, outlined in Appendix 3, predicted correctly the initial percentage depletion for O_3 photolysis in the presence of N_2. When incomplete quenching of $O(^1D)$ was taken into consideration, the agreement obtained was within 0.02% of the experimental value.

Assuming that $O(^1D)$ atoms react with O_3 to produce two oxygen atoms and an oxygen molecule in their respective ground states, the following scheme was used to predict values of Φ_i for both the O_3/SF_6 and $O_3/SF_6/N_2$ systems.

$$O_3 + h\nu(\lambda < 310 \text{ nm}) \rightarrow O(^1D) + O_2(^1\Delta_g) \qquad [1]$$

$$O(^1D) + N_2 \rightarrow O(^3P) + N_2 \qquad [17]$$

$$O(^1D) + O_3 \rightarrow 2\,O(^3P) + O_2 \qquad [13]$$

The various reactions considered in this system, together with literature values of rate constants, are listed in Table 9. The actual values used in the model are marked (*). Using a flash profile which gave 9.98% photolysis of ozone, the intermediate depletion in the presence of N_2 and SF_6 was 10.3(5)% whereas in the absence of N_2, the value was found to be 18.8(5)%,

Table 9: Reactions considered in the simulation of ozone photolysis together with literature values of rate constants

Reaction no.	Reaction	Rate/ $cm^3 molec^{-1} s^{-1}$	Method	Author	Ref.
[13]	$O(^1D)+O_3 \rightarrow$	2.7×10^{-10}	FP-KS	Husain	130*
		$5.3\pm2.6\times10^{-10}$	eval.	Cvetanovic	131
[17]	$O(^1D)+N_2 \rightarrow O(^3P)+N_2$	5.4×10^{-11}	eval.	Cvetanovic	131*
		6.9×10^{-11}	FP-KS	Husain	130
		$2.0\times10^{-11}\exp(\frac{107}{T})$	FP-CL	Streit	132
[23]	$O(^1D)+O_2 \rightarrow O(^3P)+O_2(^1\Sigma)$	7.4×10^{-11}	eval.	Cvetanovic	131*
		7.0×10^{-11}	FP-KS	Husain	130
		$2.9\times10^{-11}\exp(\frac{67}{T})$	FP-CL	Streit	132
[27]†	$O(^1D)+He \rightarrow O(^3P)+He$	$<7\times10^{-16}$		Husain	133
[24]	$O_2(^1\Sigma)+O_3 \rightarrow 2O_2+O(^3P)$	2.3×10^{-11}	FP-KS	Snelling	134
[27]	$O_2(^1\Sigma)+O_2 \rightarrow O_2(^1\Delta)+O_2$	1.4×10^{-16}	eval.	Demerijian	135
[9]	$O_2(^1\Delta)+O_3 \rightarrow 2O_2+O(^3P)$	$4.5\times10^{-18}\exp(\frac{5600}{RT})$	eval.	Schofield	136*
		4.03×10^{-15}	FP-KS	Donovan	137

Table 9: (contd.)

Reaction no.	Reaction	Rate/ $cm^3 molec^{-1} s^{-1}$	Method	Author	Ref.
[26]†	$O_2(^1\Delta)+O_2 \rightarrow O_2+O_2$	2.0×10^{-18}	eval.	Demerijian	135
		1.7×10^{-18}	KS	Becker et al	94*
[25]†	$O_2(^1\Delta)+O_2(^1\Delta) \rightarrow O_2+O_2(^1\Sigma)$	2.0×10^{-18}		Schofield	138
		2.0×10^{-18}	CL	Heustis	91*
[10]†	$O(^3P)+O_3 \rightarrow O_2+O_2$	1.3×10^{-14}	FP-KS	Husain	139
		9.6×10^{-15}	FP-KS	Davis	140
		$1.9 \times 10^{-11} \exp(\frac{4600}{RT})$	eval.	Hampson	115*
[21]	$O(^3P)+O(^3P)+M \rightarrow O_2+M$	Rate/ $cm^6 molec^{-2} s^{-1}$			
(a)†	$M = O_2$	48×10^{-34}			141*
		72×10^{-34}		Johnston	142
(b)†	$M = N_2$	28×10^{-34}	DF	Morgan	143
		48×10^{-34}	DF	Campbell	144*
(c)†	M = He	9×10^{-34}	DF	Morgan	143
(d)	$M = SF_6$	84×10^{-34}	DF	Morgan	143*
[22]	$O(^3P)+O_2+M \rightarrow O_3+M$				

Table 9: (contd.)

Reaction no.	Reaction	Rate/ $cm^3 molec^{-6} s^{-2}$	Method	Author	Ref.
[22]		87×10^{-35}	TD-DF	Mulcahy	146
(a)†	$M = O_2$	50×10^{-35}	FP	Snelling	134
		65×10^{-35}	DF	Kaufman	147*
(b)†	M = He	32.3×10^{-35}	TD	Benson	145
		40×10^{-35}	DF	Kaufman	147*
(c)†	$M = N_2$	33.7×10^{-35}	TD	Benson	145
		61×10^{-35}		Huie	148
		56×10^{-35}	DF	Kaufman	147
(d)	$M = SF_6$	34×10^{-34}	DF	Kaufman	147

Notation: * preferred rate constant

† can be omitted from model without any significant effect

eval evaluation

DF discharge flow

FP flash photolysis

KS kinetic spectroscopy

TD thermal decomposition

in good agreement with the experimental values. However, in this scheme, the presence of oxygen impurities has also to be considered.

$$O(^1D) + O_2 \rightarrow O(^3P) + O_2(^1\Sigma_g^+) \quad [23]$$

$$O_2(^1\Sigma_g^+) + O_3 \rightarrow O(^3P) + 2O_2 \quad [24]$$

As the major source of O_2 was impurity in O_3 (80% pure), the low concentration of this species could only account for a maximum of 10% of the total $O(^1D)$ removal. If the fraction, α, of $O(^1D)$ giving $O_2(^1\Sigma_g^+)$ is unity, the effect on Φ_i should be negligible. If, however, α approaches zero, the experimental value of Φ_i should be nearer 1.9. The present experimental results suggest that α is closer to unity than zero in agreement with the prediction of Young and Black.[126] However, the low concentrations of oxygen present in these systems prevented the determination of an accurate value of α.

Reaction considered to be of importance in the 'slow' secondary decay of ozone are as follows:-

$$O(^3P) + O_3 \rightarrow O_2 + O_2 \quad [10]$$

$$O_2(^1\Delta_g) + O_3 \rightarrow O_2 + O_2 + O(^3P) \quad [9]$$

$$O(^3P) + O(^3P) + M \rightarrow O_2 + M \quad [21]$$

$$O(^3P) + O_2 + M \rightarrow O_3 + M \quad [22]$$

Other $O_2(^1\Delta_g)$ removal processes, [25,26] were unimportant, being for very slow, and accounted/less than 1% of the removal of this species.

$$O_2(^1\Delta_g) + O_2(^1\Delta_g) \rightarrow O_2(^1\Sigma_g^+) + O_2(^3\Sigma_g^-) \quad [25]$$

$$O_2(^1\Delta_g) + O_2(^3\Sigma_g^-) \rightarrow 2\ O_2(^3\Sigma_g^-) \quad [26]$$

The total ozone removal by these 'slow' processes depends on the relative importance of direct removal processes, [9] and [10], and recombination reactions which remove $O(^3P)$, [21] and [22]. The latter process [22], leads to the production of O_3, and was important in the final stages of the reaction.

Arrhenius parameters are known for the removal of ozone by both $O(^3P)$[141] and $O_2(^1\Delta_g)$[136], and the temperature of the reaction system would appear to have an appreciable effect on the rate of these processes. Little is known about $O(^3P)$ recombination in the presence of SF_6,[150] although rate constants for reactions [21] and [22] are available, with N_2, O_2 and He as the third body. Since SF_6 was the dominant third body in this work and was expected to be more efficient than O_2 or N_2, some revision of the available literature values for k_{21} and k_{22} was necessary.

The effect of temperature on the rate of processes [9] and [10], for the $O_3/SF_6/N_2$ system, is shown in Table 10. The model predicted that the heat released by the 'fast' primary reactions should have a significant effect on the final quantum yield, Φ_f. Simulated ozone decays over the temperature range 298-315^oK are shown in Figure 22. The best fit occurred for a temperature of 310^oK.

Although a good fit obtained for the first 8 ms of the decay (Figure 22a), there was still considerable divergence between the computed and experimental values of the final % O_3 depletion. The results shown in Table 10 were calculated using

Table 10: The effect of temperature on the value of Φ_f for the $O_3/SF_6/N_2$ system over the range 298-315°K. Φ_f has been corrected to allow for quenching of $O(^1D)$ by nitrogen.

Temp./ °K	k_{10}/ $10^{15}cm^3molec^{-1}s^{-1}$	k_9/ $10^{15}cm^3molec^{-1}s^{-1}$	Intermediate % O_3 depletion	Final % O_3 depletion	Φ_f
298	8.40	3.40	10.3(4)	29.0(4)	2.85
305	9.60	4.37	10.3(5)	29.9(4)	2.93
310	10.9	5.07	10.3(6)	30.6(6)	3.01
315	12.2	5.85	10.3(7)	31.3(7)	3.07

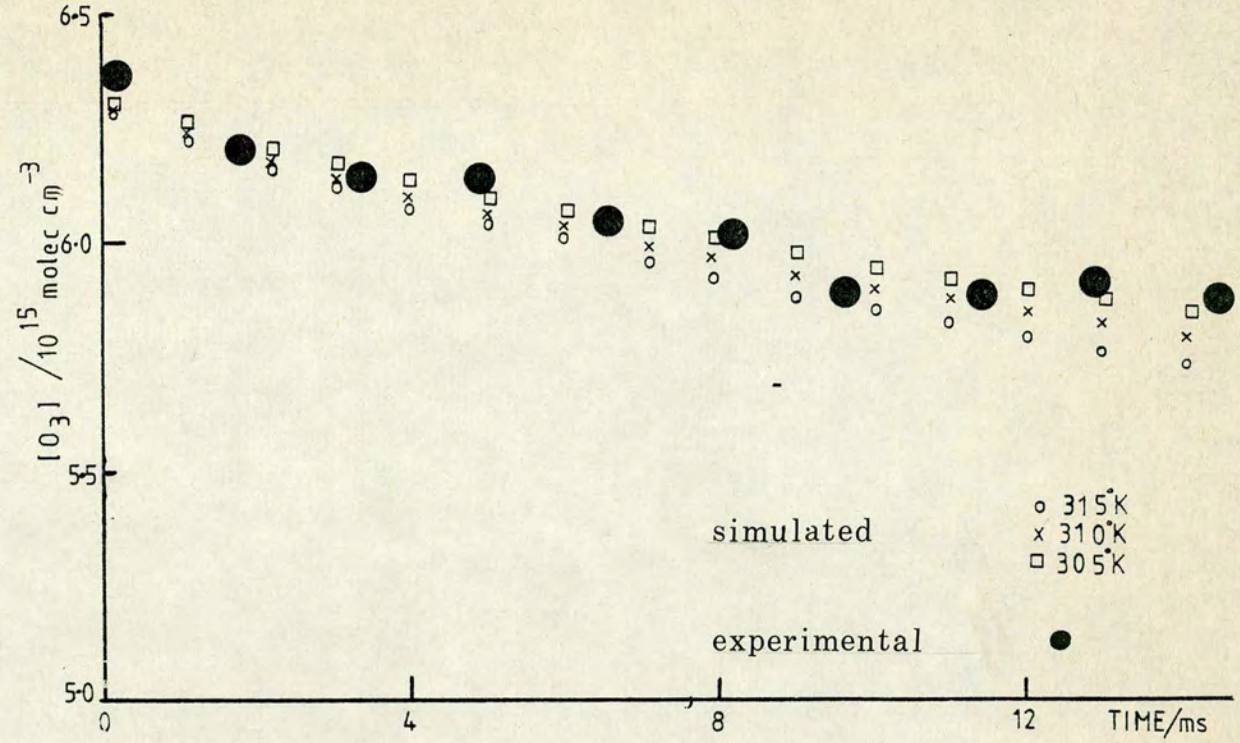

Figure 22(a): The effect of temperature on the simulated ozone decay in the $O_3/SF_6/N_2$ system.

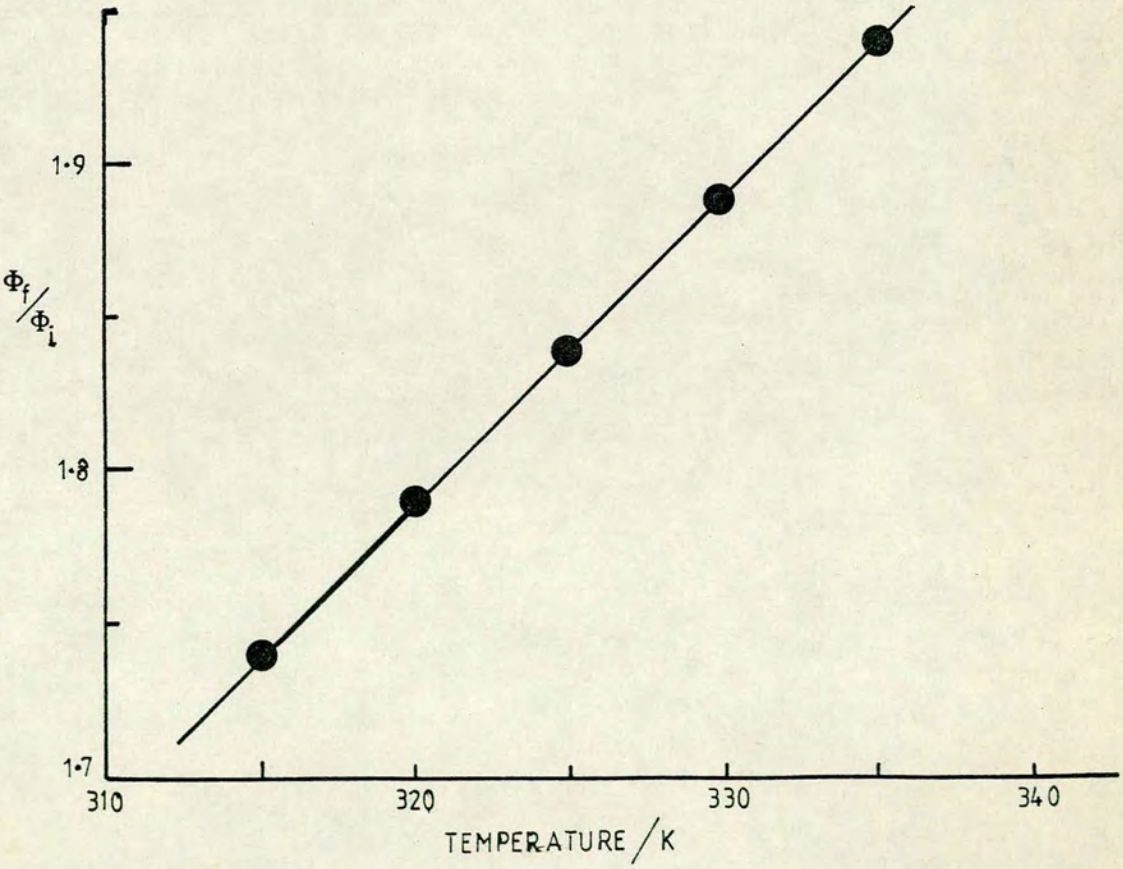

Figure 22(b): A plot of Φ_f/Φ_i versus temperature for the O_3/SF_6 system.

the literature rate constants for processes [21] and [22], where M = SF_6. Since the rate of [21] depends on the square of the $O(^3P)$ concentration, it was important only in the early stages of the decay, whereas the rate of process [22] depends on the O_2 concentration, which was greatest in the final stages of the reaction. Figure 23 shows the effect of varying both k_{21} and k_{22} on Φ_f for the $O_3/SF_6/N_2$ system. The greatest effect occurred on varying k_{22}, since the O_2 concentration was very much higher than that of $O(^3P)$. Agreement between the experimental and simulated values of Φ_f for O_3 photolysis in the presence of N_2 was obtained for values of k_{21} and k_{22} (M = SF_6) as follows:-

$$k_{21} = 8.4 \times 10^{-33} cm^6 molec^{-2} s^{-1}$$

$$k_{22} = 2.5 \times 10^{-33} cm^6 molec^{-2} s^{-1}$$

Figure 24(a) shows the final simulated and experimental decays.

On taking the model presented above for the $O_3/SF_6/N_2$ system as a basis for the O_3/SF_6 model, the only adjustable parameter which remained was temperature. A fit to the experimental decay was obtained by varying k_9 and k_{10}, using the Arrhenius parameters measured by Schofield[136] and Hampson.[141] Figure 22b shows the effect of temperature on Φ_f over the range 315-335°K. A good overall fit was obtained for a temperature of between 325-330°K. A plot of the experimental decay together with the best simulated fit is shown in Figure 24(b).

When a subroutine (PATCH 1) was added to the 'CHEK' program, employing the Beer-Lambert Law to convert the simulated O_3 concentrations into transmitted light intensities, I_t, the simulated and experimentally observed decays could be directly compared for both the $O_3/SF_6/N_2$ and O_3/SF_6 systems.

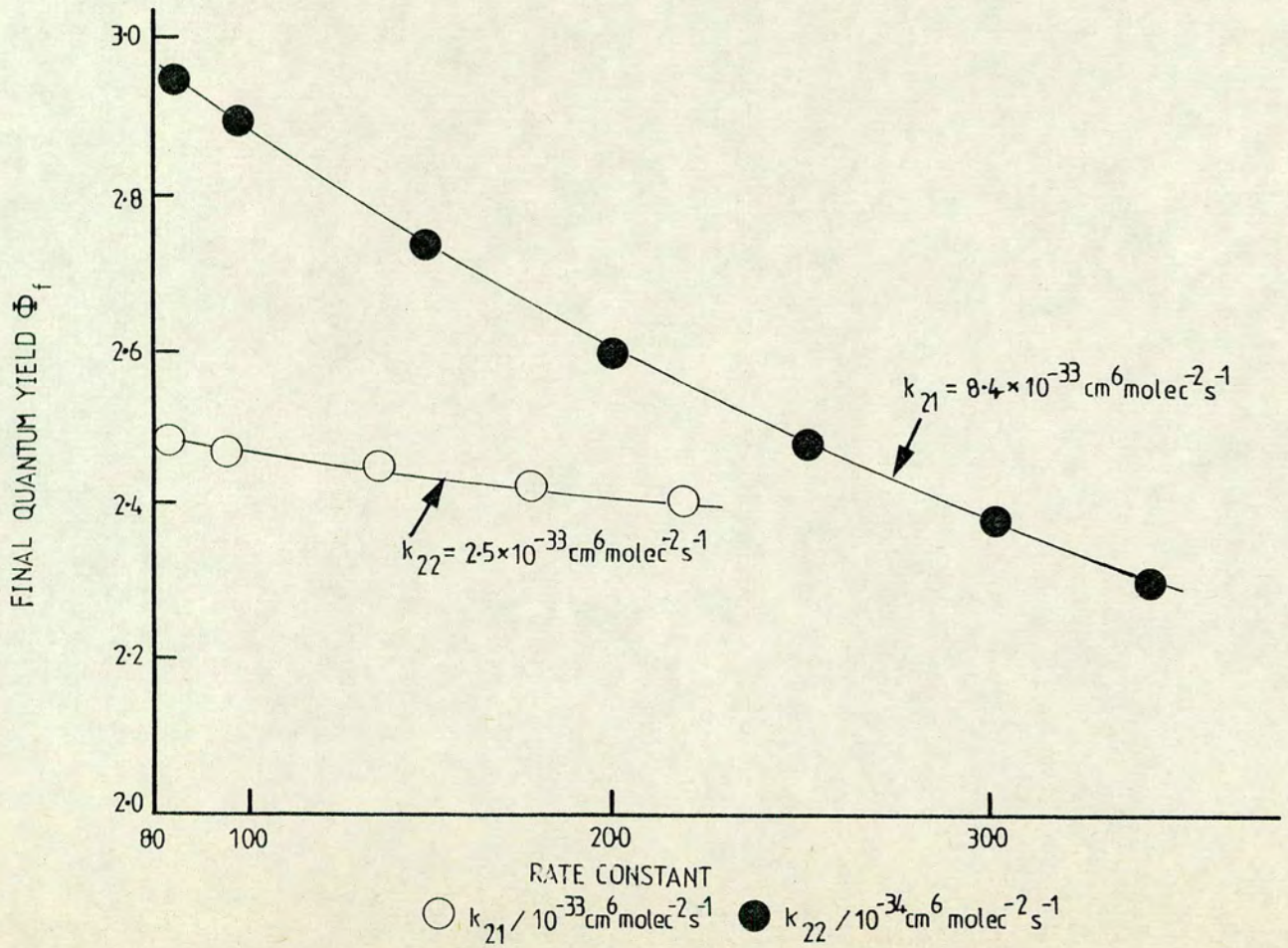

Figure 23: The effect on Φ_f of varying k_{21} and k_{22} for the $O_3/SF_6/N_2$ system.

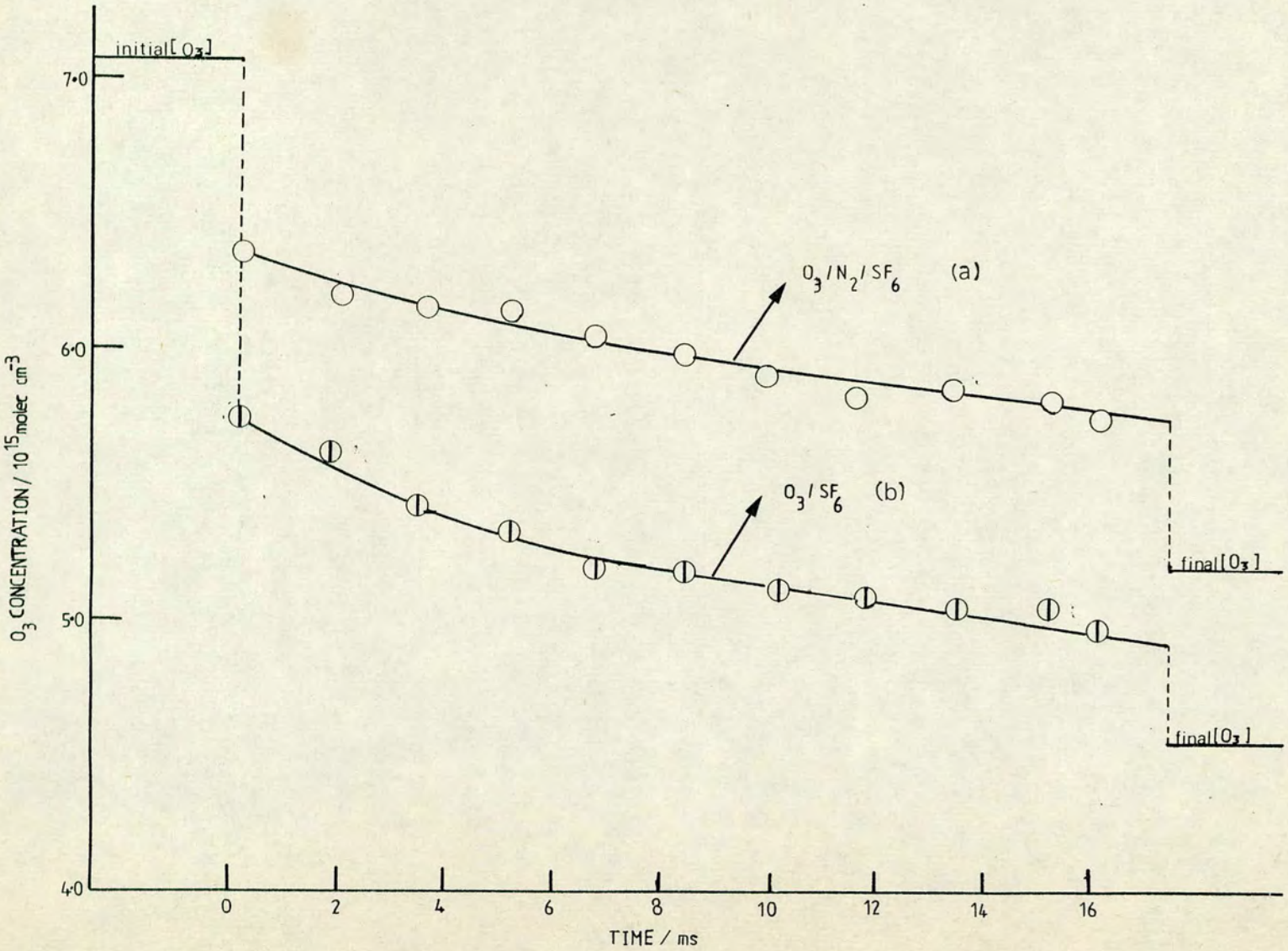

Figure 24: The best computer simulated fits (solid lines) for the removal of O_3 in the $O_3/SF_6/N_2$ and O_3/SF_6 systems - experimental decays are represented by ◐, ○.

On photolysing ozone in the presence of a 100 fold excess of oxygen, it was found that very little depletion occurred, and that this was limited entirely to the early stages of reaction (Table 8). Every O_3 molecule removed, either by photolysis or reaction, eventually resulted in the formation of an $O(^3P)$ atom, which recombined with O_2 in the presence of a third body to form another O_3 molecule. However, during the flash, when the $O(^3P)$ atom concentration was highest, some recombination of oxygen atoms to form O_2 occurred and it was this process which ultimately accounted for the observed depletion of ozone. The simulation model previously described gave a reasonable fit when applied to the $O_3/O_2/SF_6$ system, although the comparison with experimental results was more difficult, in this instance, because of the error involved in measuring such a small ozone depletion.

An estimate of the temperature rise in the various systems studied could be made by measuring the slope of the experimental decay curves at a fixed time of 2.4 ms after the flash. Pseudo first order rates for ozone removal calculated over a wide range of temperatures compared most favourably with the observed rates when the temperature agreed with the simulated value.

Furthermore, an attempt was made to calculate the expected temperature rise in the O_3/SF_6 and $O_3/SF_6/N_2$ systems, also at a time of 2.4 ms after the photolysis flash. Heat capacities of the various gases and relevent heats of reaction are listed in Tables 7 and 11 respectively.

For 2.6 kNm^{-2} of N_2 (20 τ) in 14 kNm^{-2} of SF_6 (105 τ) a rise in temperature of 1^oK is equivalent to a heat release of ca. 48 kJ $mole^{-1}$. At 2.4 ms after the flash the calculated heat

Table 11: Heats of reaction (ΔH^{o}_{298}) at 298°K

Reaction	ΔH^{o}_{298} / kJ mole^{-1}
[17] $O(^1D) + N_2 \rightarrow O(^3P) + N_2$	−190
[13] $O(^1D) + O_3 \rightarrow 2\ O(^3P) + O_2$	− 82
[10] $O(^3P) + O_3 \rightarrow 2\ O_2$	−392
[22] $O(^3P) + O_2 + M \rightarrow O_3 + M$	−195
[21] $O(^3P) + O(^3P) + M \rightarrow O_2 + M$	−498
[9] $O_2(^1\Delta_g) + O_3 \rightarrow O_2 + O_2 + O(^3P)$	12.1
[1] $O_3 + h\nu_{260nm} \rightarrow O(^1D) + O_2(^1\Delta_g)$	− 74

release of ca. 380 kJ $mole^{-1}$ suggests that the temperature rise in the system was ca. $8^{o}K$. This is incompatible with the temperature of $310^{o}K$, derived from the computer simulation of the observed decay. Together with the evidence presented in Figure 19, this suggests that the available heat capacity of SF_6 was not as high as the literature value, and that this molecule was only slightly more efficient than N_2 as a buffer gas. Assuming a $17^{o}K$ temperature rise, the effective heat capacity of SF_6 can be estimated as 38 ± 5 J $mole^{-1}K^{-1}$.

For the photolysis of ozone in SF_6 (16.7 kNm^{-2}), the calculated heat release at 2.4 ms was ca. 680 kJ $mole^{-1}$. Assuming the corrected value for the effective heat capacity of SF_6, a temperature rise of $29 \pm 4^{o}K$ would be expected, which compares favourably with that determined by modelling this system.

Thus from the above energy calculations, the high temperature rise observed in both these systems can be explained in terms of an apparent deviation from the accepted heat capacity of SF_6. Alternatively, it may be possible to account for the fast removal of ozone by the formation, in a non thermal equilibrium, of vibrationally excited O_3 or $O_2(^1\Delta_g)$.

Table 12 summarises the experimental and computed results obtained for the various ozone systems. A number of the reactions originally included in the simulation model could be eliminated, without any significant effect (< 1.0%) on the simulated results and these are marked (†) in Table 9.

Table 12: Summary of experimental and computer simulated results for O_3 photolysis

System (Temperature)	Experimental Result				Simulated Result			
	% O_3 depletion		Φ_i (corrected)	Φ_f	% O_3 depletion		Φ_i	Φ_f
	intermed.	final			intermed.	final		
O_3/SF_6 (325°K)	19.9 ± 1.8	36.3 ± 2.7	2.0 ±0.23	3.66 ±0.46	18.8	35.5	2.0	3.63
$O_3/SF_6/N_2$ (310°K)	10.5 ± 0.8	26.4 ± 1.0	1.0	2.66 +0.10	10.3	25.8	1.0	2.64
$O_3/SF_6/O_2$ (300°K)	2.0 ± 0.8	2.0 ± 0.8	0.20 ±0.08	0.20 ±0.08	1.1	1.1	0.11	0.11

Chapter 5

The Reaction of $O(2^1D_2)$ Atoms with Chlorofluoromethanes

5.01 Introduction

In 1974 Rowland and Molina[150] developed a theory concerning the adverse impact of chlorofluoromethanes (CFM) on the earth's ozone shield. There are detectable concentrations of these molecules in the atmosphere,[151] particularly CCl_3F (Freon-11) and CF_2Cl_2 (Freon-12). CFMs are inert in the troposphere and are transported into the stratosphere, where photodissociation in the atmospheric window between about 190-210 nm produces free chlorine atoms. This could eventually lead to a depletion of ozone in the upper atmosphere by way of the ClO_x cycle

$$Cl + O_3 \longrightarrow ClO + O_2 \qquad [1]$$

$$ClO + O \longrightarrow O_2 + Cl \qquad [2]$$

$$O + O_3 \longrightarrow O_2 + O_2 \qquad [1] + [2] = [3]$$

Thus there is much current interest in the primary and secondary processes which occur when ozone is photolysed in the presence of CFMs. The reaction of $O(^1D)$ with Freons 11-13 is known to give rise to ClO radicals,[152] thus providing a means of direct entry into the ClO_x cycle. A number of other channels have been proposed for the reaction of $O(^1D)$ with molecules of the type CF_xCl_{4-x}[153].

$$O(^1D) + CF_xCl_{4-x} \rightarrow ClO + CF_xCl_{3-x} \qquad [4]$$

$$\rightarrow Cl + CF_xCl_{3-x}O \qquad [5]$$

$$\rightarrow O(^3P) + CF_xCl_{4-x} \qquad [6]$$

$$\rightarrow CF_xCl_{2-x}O + Cl_2 \qquad [7]$$

$$\rightarrow CF_{x-1}Cl_{3-x}O + FCl \qquad [8a]$$

$$\rightarrow CF_{x-1}Cl_{3-x}O + F + Cl \qquad [8b]$$

Apart from the rapid primary formation of ClO[6], Donovan et al.[152] also observed the secondary release of ClO in systems containing CF_2Cl_2 and $CFCl_3$. This secondary formation of ClO involves reaction or reactions of the methyl fragment. The mass spectroscopic observation of CFClO and FCl[154] following photolysis of $CFCl_3/O_3$ mixtures, provides direct evidence for channel [8]. Thus secondary formation of ClO might be explained by the reactions

$$CFCl_2 + O_3 \longrightarrow CFCl_2O^{\ddagger} + O_2 \qquad [9]$$

$$CFCl_2O^{\ddagger} \longrightarrow CFClO + Cl \qquad [10]$$

$$Cl + O_3 \longrightarrow ClO + O_2 \qquad [11]$$

(where ‡ denotes vibrational excitation).

Indirect evidence suggests that channel [5] accounts for no more than 20% of the total reaction cross section, even though it is more exothermic than channel [4] by ca. 200 kJ $mole^{-1}$. (For CF_3Cl, $\Delta H^{o}_{298}[5] \approx -293$ kJ $mole^{-1}$ whereas $\Delta H^{o}_{298}[4] = -98$ kJ $mole^{-1}$ Various workers have shown that quenching of $O(^1D)$ by Freons 12 and 13 is negligible [6].[155]

End product analysis has produced evidence for the formation of CF_2O following photolysis of O_3 in the presence of CF_2Cl_2[7].[154] Pitts et al.[155] proposed reactions [8a] and [7] as respective major channels for Freons 12 and 13. It is also thermodynamically possible that halogen atoms may be produced directly via channel [8b] in the case of CF_3Cl.[158]

Absolute rate constants for the reaction of $O(^1D)$ with the most common CFMs have been determined by Fletcher and Husain, using atomic absorption spectroscopy in the vacuum ultraviolet.[156a]

These authors report two sets of absolute values depending on which value of γ is selected in the modified Beer-Lambert expression $I = I_o \exp[-\varepsilon(Cl)^{\gamma}]$, used to interpret their resonance absorption measurements. The use of $\gamma = 0.41$ is preferred by Fletcher and Husain[156a], but more recent work by Davidson et al. is only in agreement if $\gamma = 1$, and there are theoretical reasons for favouring this choice.[156b]

The work presented here was undertaken in order to obtain a more detailed understanding of the primary and secondary processes which take place in photochemically initiated reactions between O_3 and the chlorofluoromethanes.

5.02 Results and Discussion

Reaction mixtures containing 26 Nm^{-2} of O_3(0.2τ) and 2.4 kNm^{-2} of CF_3Cl, CF_2Cl_2 and $CFCl_3$ (18τ) were made up to a total pressure of 16.6 kNm^{-2} (125τ) with SF_6. Ozone was monitored in absorption using the method described previously in section 2.05. The amount of ozone removed was determined by flashing mixtures of O_3 in the presence of N_2 and SF_6. This had the added advantage of checking the stability of the experimental conditions. Absorption cross sections have been determined for Freons 11-13.[167] From these measurements it was determined that the extent of photolysis of $CFCl_3$, CF_2Cl_2 and CF_3Cl was < 5%, 0.02% and 0.0% respectively, and only in the case of Freon 11 was the release of free chlorine atoms of importance. Intermediate and final ozone depletions for freons 11-13 are presented in Table 13.

Table 13: Experimental O_3 depletions for various Freon/Ozone systems, measured at room temperature ($293^{o}K$).

CFM	concentration (Molecule cm^{-3})		Intermediate % depletion	Final % depletion	Φ_i	Φ_f
CF_3Cl	O_3	7.08×10^{15}	15.3	22.7	1.9	2.8
	SF_6	3.72×10^{18}	$\pm$	$\pm$	$\pm$	$\pm$
	CF_3Cl	6.37×10^{17}	0.9	1.4	0.2	0.2
CF_2Cl_2	O_3	7.08×10^{15}	14.5	35.0	1.8	4.4
	SF_6	3.72×10^{18}	$\pm$	$\pm$	$\pm$	$\pm$
	CF_2Cl_2	6.37×10^{17}	0.8	1.6	0.1	0.3
$CFCl_3$*	O_3	7.08×10^{15}	17.0	44.0	2.1	5.5
	SF_6	3.72×10^{18}	$\pm$	$\pm$	$\pm$	$\pm$
	CF_2Cl_2	6.37×10^{17}	0.6	1.0	0.4	0.3

*some photolysis of $CFCl_3$ (<5%) occurs in this system.

The corrected % O_3 photolysis was 8.0 $\pm$ 0.4%, determined using the $O_3/SF_6/N_2$ system.

It is immediately apparent from these results that the number of chlorine atoms in the CFM had a significant effect on the final ozone depletion, and on removal by secondary reactions in particular. The intermediate depletion was the same, within experimental error, for the three molecules studied, with almost as much ozone being removed by reaction as by photolysis. Since less than 1% of $O(^1D)$ produced by the flash reacts with O_3, this removal must be due to reaction either with methyl fragments [12] or with free halogen atoms [1]

$$CF_xCl_{3-x} + O_3 \longrightarrow CF_xCl_{3-x}O + O_2 \qquad [12]$$

For Freons 11 and 12, the alkoxyl radicals decompose to release free chlorine atoms into the system, thus accounting for the higher values of Φ_f observed in the presence of these CFMs. In the case of Freon 13, the chemistry is clearly different. Here, the release of a fluorine atom is the only possible decomposition route.

5.03 Computer Simulation

The model already presented for the photolysis of O_3 in the presence of SF_6 was used as the basis from which the CF_3Cl/O_3 and CF_2Cl_2/O_3 systems could be investigated.

CF_3Cl/O_3 system.

The reactions which were included in the CF_3Cl/O_3 model are listed in Table 14, together with the most accurate rate constants available in the current literature. The suggested channels for the reaction of $O(^1D)$ with CFMs [4-8] are of fundamental importance, as are the reactions of methyl radicals and the ClO_x cycle chain termination processes.

TABLE 14

SIMULATION OF THE PHOTOLYSIS OF OZONE IN PRESENCE OF CF3CL.
TEMPERATURE=300K. FINAL BEST FIT MODEL.

NO.	REACTION	K/CM3 MOLEC-1 S-1	<REF>
	7.08E15 O3 = O(1D) + O2(SD)	K1	<CALC>
	O(1D) + O3 = O(3P) + O(3P) + O2	2.7E-10	<130>
< 4 >	O(1D) + 6.37E17 CF3CL = CLO + CF3	1.62E-10	<156,158
< 8A>	O(1D) + CF3CL = CF2O + FCL	6.3E-11	<156,158
< 8B>	O(1D) + CF3CL = CL + F + CF2O	2.5E-11	<156,158
< 2 >	O(3P) + CLO = CL + O2	5.3E-11	<166B>
<24 >	O(3P) + O(3P) + 3.72E18 SF6 = O2 + SF6	84E-34	<CALC>
<23 >	O(3P) + 3.54E15 O2 + SF6 = O3 + SF6	250E-35	<CALC>
< 1 >	CL + O3 = CLO + O2	1.2E-11	<166B>
<13 >	CF3 + CF3 = C2F6	9.0E-12	<159>
<12 >	CF3 + O3 = CF3O + O2	1.0E-10	<EST>
<15 >	F + O3 = FO + O2	1.4E-11	<166A>
<16A>	CLO + CLO = CLOO + CL	1.2E-14	<161,162
<16B>	CLO + CLO = OCLO + CL	2.4E-15	<161,162
<16C>	CLO + CLO = CL2 + O2	9.6E-15	<161,162
<17 >	CLOO + SF6 = CL + O2 + SF6	6.0E-13	<163>
<19 >	FO + CLO = F + OCLO	3.3E-11	<EST,162
<20 >	FO + FO = F2 + O2	3.3E-11	<165>
<18A>	CL + CLOO = CL2 + O2	1.6E-10	<164>
<18B>	CL + CLOO = CLO + CLO	1.6E-11	<164>
<21 >	O2(SD) + O3 = O2 + O2 + O(3P)	1.11E-15	<136>
	O2(SD) + SF6 = O2 + SF6	6.02E-18	<EST>

INITIAL CONCENTRATIONS (MOLECULES/CM-3) ARE GIVEN IMMEDIATELY PRECEDING A PARTICULAR SPECIES. CALCULATED VALUES <23,24> REFER TO THOSE DETERMINED IN CHAPTER 4. K1 IS CALCULATED USING THE SUBROUTINE PATCHD.

A number of models were tried, using previous estimates of branching ratios to begin with.[153,155] Only the final and most satisfactory model will be discussed in detail here. All calculations were based on a temperature of 298°K.

Branching ratios determined by Garraway and Donovan[158] were used to obtain a fit to the experimental intermediate ozone depletion. $O(^1D)$ reacts with CF_3Cl via channels 4, 8a, 8b with branching ratios of 65%, 25% and 10% respectively. CF_3 radicals produced in reaction [4] were assumed to react rapidly with O_3 [12], although some recombination to form C_2F_6 may have occurred.[159]

$$Cl + O_3 \longrightarrow ClO + O_2 \qquad [1]$$

$$CF_3 + O_3 \longrightarrow CF_3O^{\ddagger} + O_2 \qquad [2]$$

$$CF_3 + CF_3 \longrightarrow C_2F_6 \qquad [13]$$

$$CF_3O^{\ddagger} \longrightarrow CF_2O + F \qquad [14]$$

$$F + O_3 \longrightarrow FO + O_2 \qquad [15]$$

Fluorine atoms produced via channel [8b] remove O_3 to form FO [15]. Although no direct evidence of the production of FO in the CF_3Cl/O_3 system has been produced, it has been detected mass spectrometrically in the CF_3Br/O_3 system.[160] In the former case it was impossible to distinguish between the FO and Cl m/e peaks, but it seems reasonable to assume that FO was indeed produced. It was not necessary to include the release of fluorine atoms by decomposition of CF_3O [14].

The rate constant for the reaction of CF_3 radicals with O_3 [12] was taken to be

$$k_{12} = 1.0 \times 10^{-10} \text{ cm}^3 \text{ molec}^{-1}\text{s}^{-1}$$

The final O_3 depletion must be determined by the reactions of $O(^3P)$, $O_2(^1\Delta_g)$ and halogen atoms with ozone. Rate constants for these processes are accurately known. One of the most poorly understood features of Freon/O_3 systems is the disproportionation reaction of ClO radicals, although it is generally accepted this reaction [16] is second order in ClO.

$$ClO + ClO \longrightarrow \text{products} \qquad [16]$$

Clyne et al.[161] have measured the overall second order rate constant mass spectrometrically, using molecular beam sampling, at low pressure - $k_{16} = (2.2 \pm 0.3) \times 10^{-14} cm^3 molec^{-1} s^{-1}$.

$$ClO + ClO \longrightarrow ClOO + Cl \qquad [16a]$$

$$\longrightarrow OClO + Cl \qquad [16b]$$

$$\longrightarrow Cl_2 + O_2 \qquad [16c]$$

$$ClOO + SF_6 \longrightarrow Cl + O_2 + SF_6 \qquad [17]$$

$$Cl + ClOO \longrightarrow Cl_2 + O_2 \qquad [18a]$$

$$\longrightarrow ClO + ClO \qquad [18b]$$

The major reaction channel has been shown to lead to the formation of ClOO [16a], while OClO has been identified as a minor product [13b]. In a recent study of the Cl/O_3 system, Champion and Donovan[162] found a branching ratio into channel [16a] of $50\% < k_a < 80\%$, with $20\% < k_b + k_c < 50\%$. ClOO rapidly dissociates to produce free chlorine atoms [17]. It was assumed that there was no third body contribution to the ClO decay, since no definite evidence has been found to support the flash photolysis studies of Johnston et al[163] who proposed a third order process leading to the formation of molecular chlorine and oxygen [16d].

$$ClO + ClO + M \rightleftharpoons Cl_2O_2 + M \qquad [16d]$$

$$Cl_2O_2 + M \longrightarrow Cl_2 + O_2 + M$$

These workers[164] have also shown that the major channel in the reaction of Cl with ClOO [18] leads to formation of Cl_2, ClO being only a minor product. Branching ratios into channels [16a,b and c] were taken to be 50%, 10% and 40% respectively.

OClO has been detected spectroscopically in the CF_3Cl/O_3 system.[162] Reaction [16b] alone was unable to account for the concentration of OClO observed. However, in the presence of a large excess of ethane, the OClO yield was substantially reduced, showing that its formation was only partially due to ClO disproportionation [16]. Thus some process involving free halogen atoms is inferred.

The presence of a free radical scavenger, such as molecular oxygen which should be more effective in removing CF_3 radicals than halogen atoms, reduced the OClO concentration by more than half. It was proposed that OClO formation resulted from the reaction of FO with ClO [19], thus supporting the production of free fluorine atoms [8b].

$$ClO + FO \longrightarrow OClO + F \qquad [19]$$

$$FO + FO \longrightarrow F_2 + O_2 \qquad [20]$$

$$O_2(^1\Delta_g) + O_3 \longrightarrow O_2 + O_2 + O(^3P) \qquad [21]$$

$$O(^3P) + O_3 \longrightarrow O_2 + O_2 \qquad [22]$$

Taking reactions [16-22] into consideration resulted in an excessively large final O_3 depletion. Even processes involving $O_2(^1\Delta_g)$ and $O(^3P)$ alone predicted final O_3 depletion of ca. 30% compared with an experimental value of 22.7 $\pm$ 1.4%. Thus it is clear that some removal of $O_2(^1\Delta_g)$ or $O(^3P)$ must occur.

Within the time scale of the reaction some diffusion of $O_2(^1\Delta_g)$ and $O(^3P)$ to the wall of the vessel may have occurred, although no evidence to support this was found in the other systems studied (Chapters 4 and 6). Since $O_2(^1\Delta_g)$ is the precursor of $O(^3P)$, the large difference in the experimental and simulated results suggests that it is the former which is removed, possibly by reaction with some radical species. Ultimately, substantial removal of $O_2(^1\Delta_g)$ must be included, and the results in table 16(a) demonstrate that it is possible to obtain a fit to the experimental values. Figure 25 shows a plot of simulated and experimental decays for 60% removal of $O_2(^1\Delta_g)$. These agree closely except for times shorter than 1 ms, where there is some divergence in the experimental and computed intermediate O_3 depletions, suggesting that the extrapolation procedure adopted is not applicable in this particular case. The simulation predicts rapid O_3 removal over 100 μs-1 ms, which is not accounted for by the extrapolation.

Recombination reactions of halogen atoms, as well as the reactions of $O(^1D)$ and $O(^3P)$ atoms with O_3, were found to have a negligible effect on the simulated decay. However recombination reactions involving oxygen atoms were found to have a significant influence on the final O_3 depletion [23,24]

$$O(^3P) + O_2 + SF_6 \longrightarrow O_3 + SF_6 \qquad [23]$$

$$O(^3P) + O(^3P) + SF_6 \longrightarrow O_2 + SF_6 \qquad [24]$$

This model does not support quenching of $O(^1D)$ [6], so that there are only two major channels in the reaction of $O(^1D)$ with CF_3Cl [4,8].

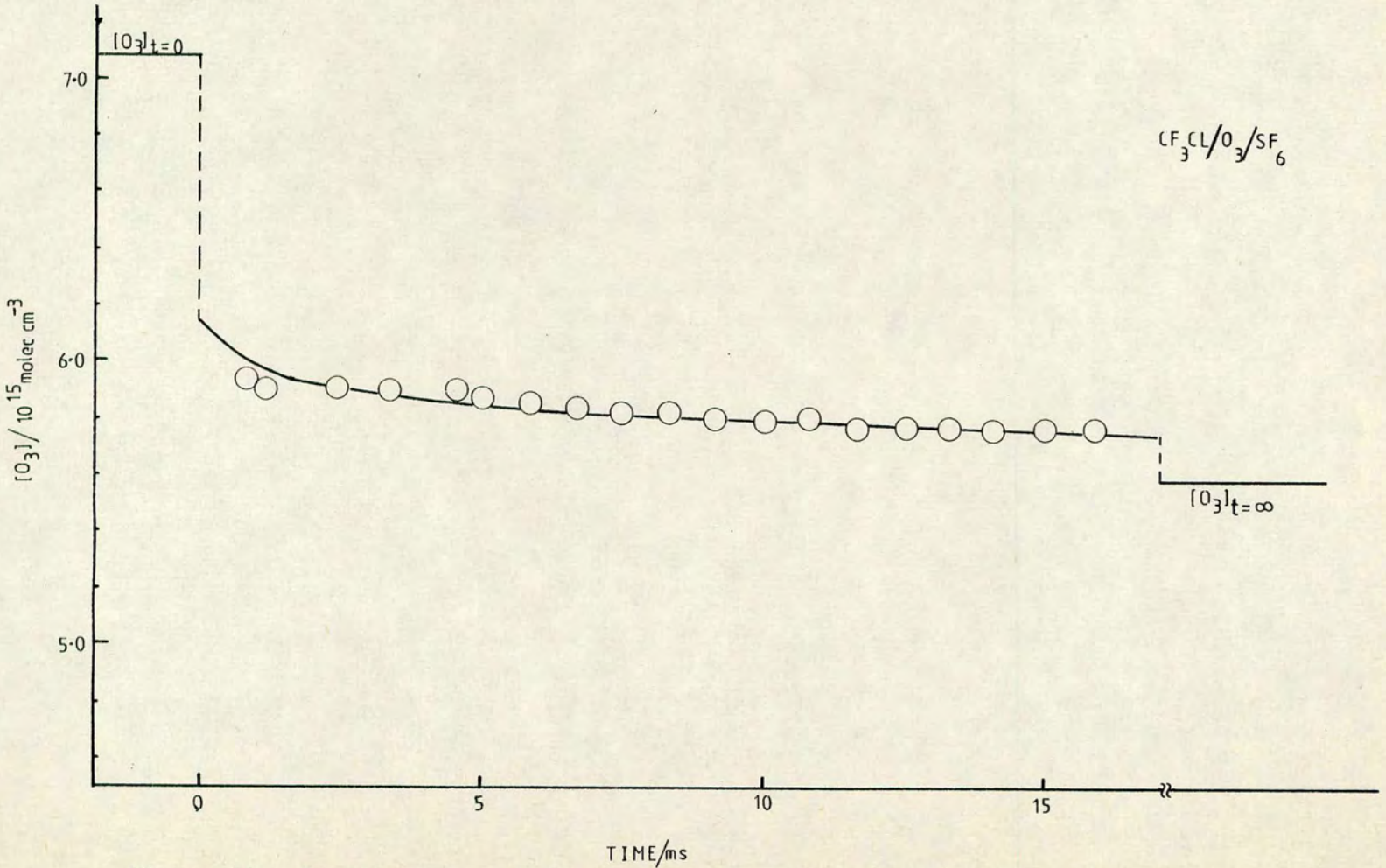

Figure 25: Simulated best fit profile (solid line) for the removal of O_3 following photolysis in the presence of CF_3Cl. Experimental decay is represented by ◯.

TABLE 15

SIMULATION OF THE PHOTOLYSIS OF OZONE IN PRESENCE OF CF2CL2.
TEMPERATURE=300K. FINAL BEST FIT MODEL.

NO.	REACTION	K/CM3 MOLEC-1 S-1	<REF>
	7.08E15 O3 = O(1D) + O2(SD)	K1	<CALC>
	O(1D) + O3 = O(3P) + O(3P) + O2	2.7E-10	<130>
< 4 >	O(1D) + 6.37E17 CF2CL2 = CLO + CF2CL	3.5E-10	<156,158
< 7 >	O(1D) + CF2CL2 = CF2O + CL2	1.3E-10	<156,158
	O2(SD) + SF6 = O2 + SF6	5.16E-18	<EST>
<21 >	O2(SD) + O3 = O2 + O2 + O(3P)	1.48E-15	<136>
< 2 >	O(3P) + CLO = CL + O2	5.3E-11	<166B>
<24 >	O(3P) + O(3P) + 3.72E18 SF6 = O2 + SF6	84E-34	<CALC>
<23 >	O(3P) + 3.54E15 O2 + SF6 = O3 + SF6	250E-35	<CALC>
< 1 >	CL + O3 = CLO + O2	1.2E-11	<166B>
<12 >	CF2CL + O3 = CF2CLO + O2	1.00E-10	<EST>
<13 >	CF2CL + CF2CL = C2F4CL2	9.0E-12	<EST>
<24 >	CF2CLO + SF6 = CF2O + CL + SF6	7.0E-17	<EST>
<16A>	CLO + CLO = CL2 + O2	9.6E-15	<161,162
<16B>	CLO + CLO = OCLO + CL	2.4E-15	<161,162
<16B>	CLO + CLO = CLOO + CL	1.2E-14	<161,162
<17 >	CLOO + SF6 = CL + O2 + SF6	6.0E-13	<163>
<18A>	CL + CLOO = CL2 + O2	1.6E-10	<164>
<18B>	CL + CLOO = CLO + CLO	1.6E-11	<164>

INITIAL CONCENTRATIONS (MOLECULES/CM-3) ARE GIVEN IMMEDIATELY PRECEDING A PARTICULAR SPECIES. CALCULATED VALUES <23,24> REFER TO THOSE DETERMINED IN CHAPTER 4. K1 IS CALCULATED USING THE SUBROUTINE PATCHD.

Table 16: Calculated and experimental intermediate and final ozone depletions for photolysis of O_3 in the presence of CF_3Cl and CF_2Cl_2

CFM	Ozone depletion							
	Experimental				Calculated			
	$\%_i$	$\%_f$	Φ_i	Φ_f	$\%_i$	$\%_f$	Φ_i	Φ_f
(a) CF_3Cl	15.3 ± 0.9	22.7 ± 1.4	1.9 ±0.1	2.8 ±0.2	13.6	21.3	1.8	2.8
(b) CF_2Cl_2	14.5 ± 0.8	35.0 ± 1.6	1.8 ±0.1	4.4 ±0.2	12.1	31.6	1.6	4.1
% O_3 photolysed	8.0 ± 0.5				7.7			

$\underline{CF_2Cl_2/O_3 \text{ system}}$

In modelling the CF_2Cl_2/O_3 system, the reaction scheme was similar to that described for CF_3Cl/O_3. Table 15 lists the reactions included, together with literature values of the rate constants. A branching ratio of 70% into the ClO channel [4] has been determined by Garraway and Donovan,[158] some 30% of $O(^1D)$ reacting via channels [7] and [8]. Reactions [1,12,13,15] were again taken into consideration in calculating the intermediate O_3 removal (Table 16b).

The final O_3 depletion was determined by reactions [16-21]. The secondary growth of ClO, observed by Donovan et al.,[152] was accounted for by the complete dissociation of CF_2ClO to release free chlorine atoms into the system [25].

$$CF_2ClO\ (+M) \longrightarrow CF_2O + Cl\ (+M) \qquad [25]$$

The rate constant k_{13} for the recombination of CF_2Cl radicals is not known and that for the recombination of CF_3 radicals was assumed.

Using the experimental method described here, it is impossible to distinguish between the channels leading to formation of CF_2O [7] and CFClO [8]. However, channel [7] is more exothermic by ca. 40 kJ $mole^{-1}$. Furthermore, Kaufman and Wolfrum[160] observed CF_2O, but not CFClO, in this system. Thus, it would seem reasonable to conclude that formation of CF_2O [7] entirely accounts for the branching ratio of 30%. The best simulated fit to the experimental O_3 decay is shown in Figure 26. Again, there is disagreement at short times as considered previously for the CF_3Cl/O_3 system. The computed final ozone depletion is slightly lower than the experimental value and may be due to an

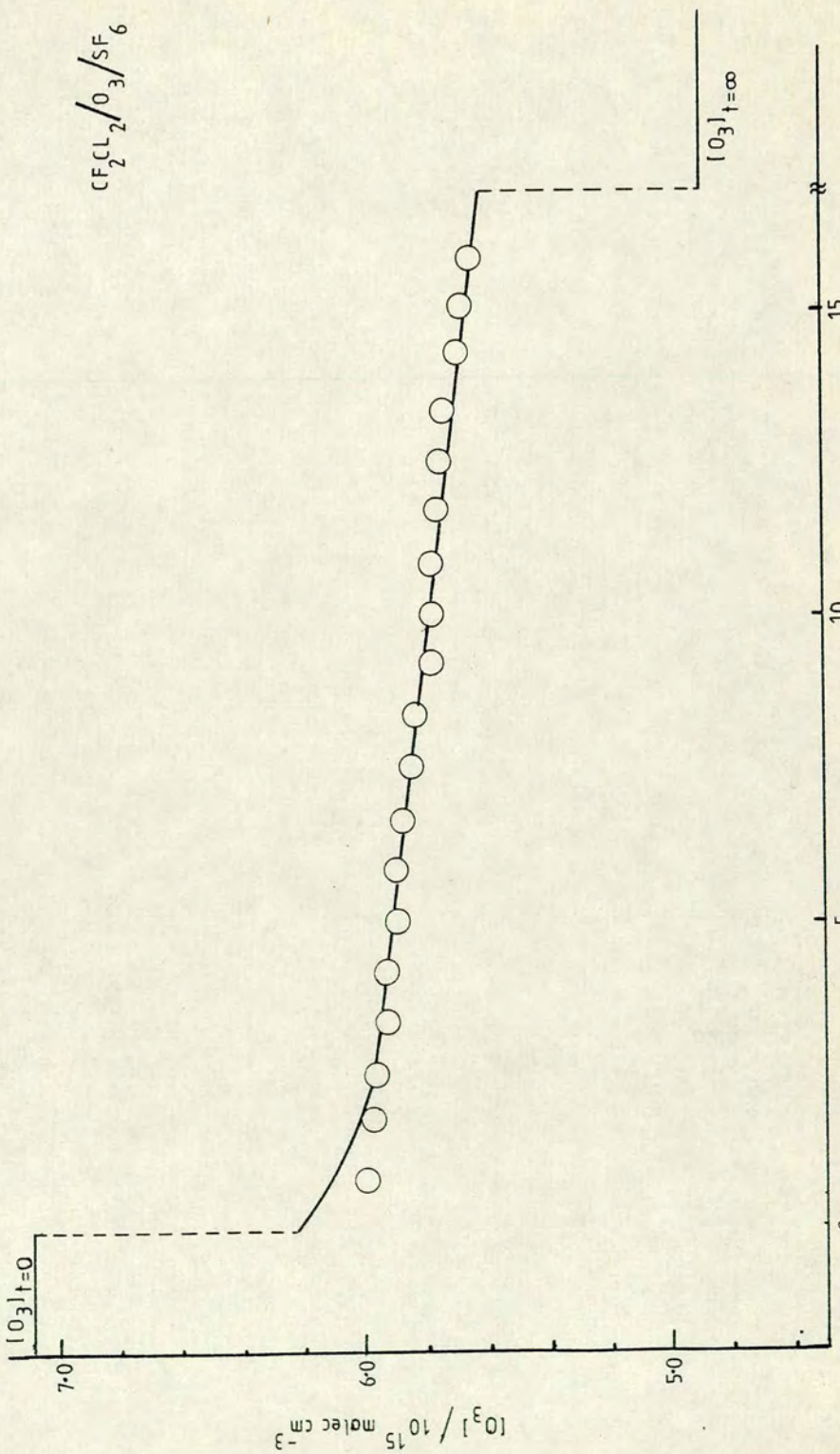

Figure 26: Simulated best fit profile (solid line) for the removal of O_3 following photolysis in the presence of CF_2Cl_2. Experimental decay is represented by ○.

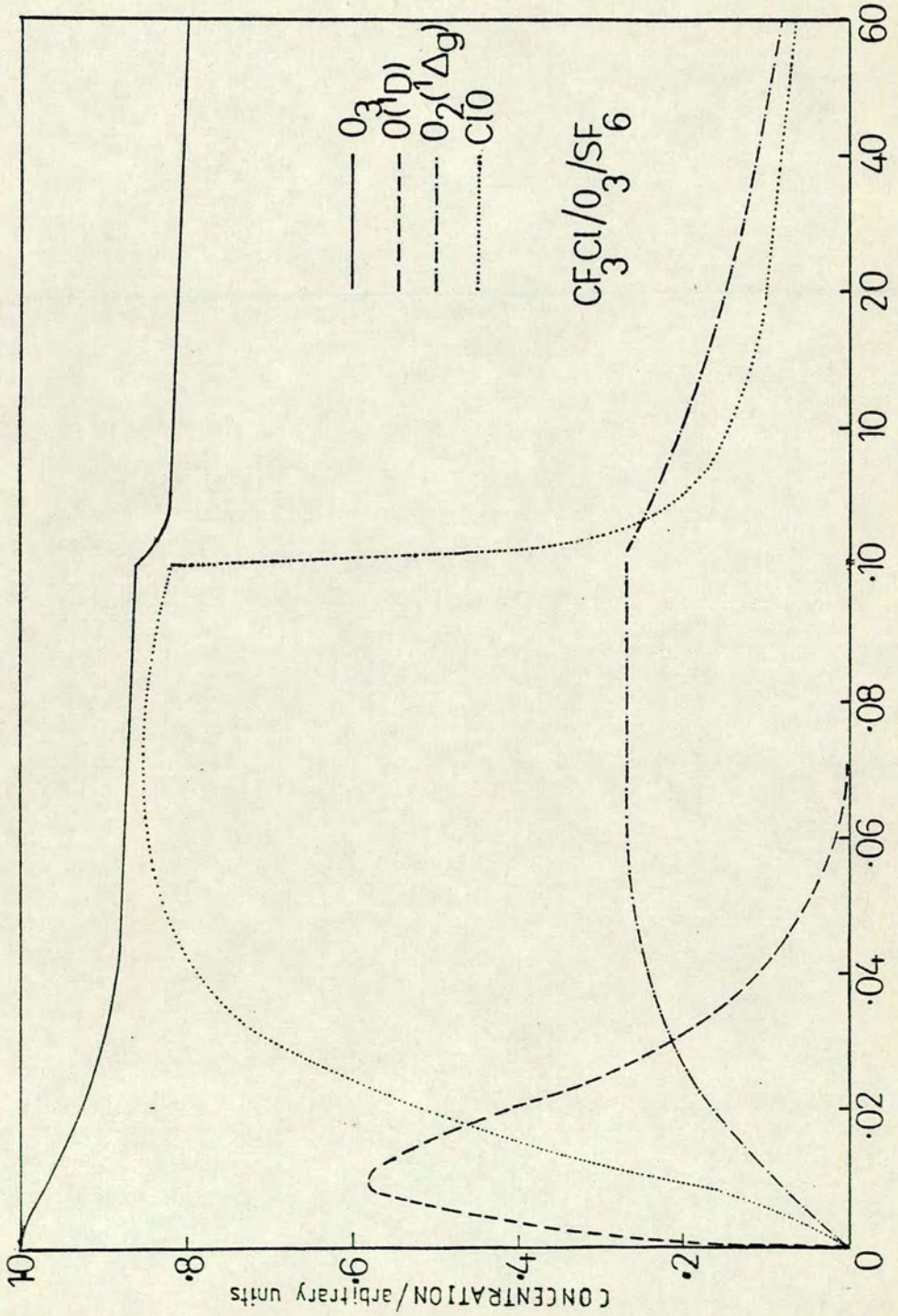

Figure 27: Simulated concentration profiles for O_3, $O(^1D)$, $O_2(^1\Delta g)$ and ClO following O_3 photolysis in the presence of CF_3Cl. The full scale value represents concentrations of 7.0×10^{15}, 2.0×10^{11}, 1.8×10^{15} and 4.0×10^{14} molecules cm^{-3} respectively.

overestimate of the importance of CF_2Cl recombination [13] or removal of $O_2(^1\Delta_g)$, again assumed to be 60% by processes other than reaction with O_3.

Comparing the models presented for Freons 12 and 13, it can be seen that a consistent scheme is presented. Both models predict quenching of $O(^1D)$ to be unimportant, accounting for <10% of the total removal of $O(^1D)$. Only two channels appear to be significant, those leading to the formation of ClO and CF_2O.

Figure 27 shows the computed concentration profiles for most of the transient species present following photolysis of O_3 in the presence of CF_3Cl, based on the model presented in table 14.

In conclusion, it must be stated that no unique model of these systems is possible, with the limited experimental evidence currently available. A more complete identification of species involved in O_3/CFM systems is required, together with a better understanding of their reaction kinetics, before this goal can be achieved.

Chapter 6

Singlet Sulphur Monoxide

6.01 Introduction

Both $SO(^1\Delta)$ and $SO(^1\Sigma^+)$ have been detected when the products of a microwave discharge in O_2 are mixed with small sulphur containing molecules (section 1.06).[74,75,76] Chemiluminescence studies have shown the $^1\Sigma^+$ state to lie 10,500 cm^{-1} above the ground state.[77] Recently, sensitized chemiluminescence at 6150 cm^{-1} has been assigned to the $a^1\Delta \rightarrow X^3\Sigma^-$ transition.[167] This value is close to that predicted by Colin et al.[77] and is in agreement with ab initio calculations which estimate that the $^1\Delta$ state lies between 5700 cm^{-1} and 6300 cm^{-1} above the ground state.[168] Dixon et al. have used SCF-type calculations to estimate the potential energy curves of the low lying bound states of SO.[169] SO chemiluminescence has been reported for reactions of sulphur and oxygen atoms produced in argon matrices.[170,171]

In this work the reaction of $O(^1D)$ with OCS [1] was used to produce $SO(^1\Delta)$. Ozone photolysis (λ < 310 nm) provided a suitable source of $O(^1D)$ atoms. A computer simulation model was developed in an attempt to understand the reactions of $SO(^1\Delta)$ in the OCS/O_3 system. The rate constant for the reaction of $SO(^1\Delta)$ with O_3 is reported and it is suggested that this process might be a possible stratospheric sink for O_3.

The removal of $O(^1D)$ atoms by carbonyl sulphide [1] has been discussed,[78] and it is predicted that this reaction yields SO in either the $^1\Delta$ or $^1\Sigma$ states. Taube and Jones,[172] in low temperature matrix studies, considered two possible reactive channels [1a,b].

$$O(^1D) + OCS \rightarrow SO(^1\Delta, ^1\Sigma) + CO \quad [1a]$$

$$\rightarrow S(^1D) + CO_2 \quad [1b]$$

$$O(^3P) + OCS \rightarrow SO(^3\Sigma) + CO \quad [2]$$

When S and SO are produced in the states ^1D and $^1\Delta$, the reactions are exothermic by ca. 311 and 307 kJ mole^{-1} respectively. Spin forbidden processes to form the ground states are correspondingly more exothermic. The formation of $SO(^1\Delta)$ was found to be the dominant channel. There was no evidence to support the formation of atomic sulphur. Tracer experiments show the isotopic course of reaction [1a] to be

$$O(^1D) + {}^*OCS \rightarrow C^*O + SO(^1\Delta) \quad [1a]$$

Crutzen[173] has recently suggested that OCS is possibly a significant source of SO_2 in the stratosphere. There are a number of photochemical reactions which remove OCS. By far the most important of these is the photodissociation of carbonyl sulphide to yield sulphur atoms [3]. Ground state $S(^3P)$ reacts rapidly with O_2 to form $SO(^3\Sigma)$ [6]. The products of the reaction of $S(^1D)$ with O_2 have not been confirmed experimentally. However, orbital correlation rules predict two channels[1] [4a,b], of which that yielding $SO(^1\Sigma^+)$ is exothermic. The detection of emission from $SO(^1\Sigma^+)$ in microwave discharge experiments[69] suggests that the reaction does proceed by this channel [4a].

$$OCS + h\nu \rightarrow CO + S(^1D, ^3P) \quad [3]$$

$$S(^1D) + O_2 \rightarrow SO(^1\Sigma^+) + O(^3P); \Delta H^o_{298} = -15.3 \text{ kJ mole}^{-1} \quad [4a]$$

$$\rightarrow SO(^3\Sigma^-) + O(^1D); \Delta H^o_{298} = 49.1 \text{ kJ mole}^{-1} \quad [4b]$$

$$S(^1D) + M \rightarrow S(^3P) + M \quad [5]$$

$$S(^3P) + O_2 \rightarrow SO(^3\Sigma) + O(^3P) \quad [6]$$

$$SO + O_2 \rightarrow SO_2 + O(^3P) \quad [7]$$

SO is rapidly oxidised [7] to form SO_2 by O_2, O_3, NO_2. Reaction of $O(^1D)$ and $O(^3P)$ atoms with OCS also ultimately leads to the formation of SO_2 [1a,2,7]. Thus SO_2 would appear to be the major product of OCS decay in the stratosphere.

6.02 Results and Discussion

Flash photolysis with both kinetic spectroscopy and kinetic spectrophotometry was used to study the OCS/O_3 system. These techniques are described in detail in sections 2.05 and 2.04. In experiments where ozone was monitored in absorption at 253.7 nm, 26 Nm^{-2} (0.2τ) of ozone was photolysed in the presence of 130, 270 or 530 Nm^{-2} (1,2,4τ) of OCS. Mixtures were made up to a total pressure of 16.7 k Nm^{-2} (125τ) with SF_6. The experimental procedure was the same as that described in chapter 4.

In the case of experiments using flash spectroscopy, reaction mixtures contained 13 or 26 Nm^{-2} of ozone, 270 Nm^{-2} (2τ)of OCS and 1.3 k Nm^{-2} (10τ) of SF_6. The lower pressure of O_3 was useful when the transient spectra being studied occurred in the region where O_3 is a strong absorber ($\lambda<270$ nm).

Ozone and carbonyl sulphide were found to react slowly in the absence of light. The resulting O_3 depletion was relatively small, even over the period of a complete experiment, and could be measured readily.

Investigation using the technique of kinetic spectroscopy showed that, within the first few micro-seconds of the photolytic flash, ozone was removed very rapidly. $S_2(^1\Delta_g)$ was observed at short delays (5-25 μs) and decayed to yield ground state $S_2(^3\Sigma_g^-)$. Since formation of $S_2(^1\Delta_g)$ was not noticeably

altered in the absence of ozone, its presence was entirely accounted for by the photolysis of OCS [3,8].

$$S(^1D) + OCS \rightarrow S_2(^1\Delta_g) + CO \qquad [8]$$

Sulphur dioxide was detected several milli seconds after the flash and was presumably formed by oxidation of SO. SO_2 may well have been produced in some vibrationally excited state, such that its absorption spectrum was diffuse and difficult to detect at short delays.

Table 17 shows the measured depletions, when ozone was monitored in absorption at 253.7 nm, for a range of OCS pressures. It is apparent that the initial ozone depletion during the photolysis flash was not significantly affected by variation in the concentration of carbonyl sulphide. Since only 9.4(7)% of O_3 was removed by photolysis, the remainder of this depletion must be accounted for by reaction. Crutzen[173] has suggested that the removal of $O(^1D)$ by OCS is fast, and it is not unreasonable to assume that the rate constant for this reaction should be similar to that for quenching of $O(^1D)$ by CO_2 (approx. 2.0×10^{-10} $cm^3 molec^{-1} s^{-1}$). Thus, in the present system, less then 1% of $O(^1D)$ reacted with O_3. Some product of reaction [1], such as SO, must have been responsible for O_3 removal during the flash. However, the reaction of ground state SO with O_3 [10] is slow, inferring that this species is formed in an electronically excited state. Both the $^1\Delta$ and $^1\Sigma$ states of SO are feasible products of reaction [1], as predicted by the correlation diagram illustrated in Figure 28. $SO(^1\Delta)$ is thermodynamically favoured, although $SO(^1\Sigma)$, if formed, would be rapidly quenched to yield

Table 17: Ozone depletions following the photolysis of $O_3/OCS/SF_6$ mixtures

Species	Pressure	Intermed. O_3 % depletion	Final O_3 % depletion	Φ_i	Φ_f
OCS O_3 SF_6	130 Nm^{-2} 26 Nm^{-2} 16.5 Nm^{-2}	16.1 ± 0.7	29.1 ± 0.7	1.7 ± 0.1	3.2 ± 0.2
OCS O_3 SF_6	270 Nm^{-2} 25 Nm^{-2} 16.4 k Nm^{-2}	16.8 ± 0.3	30.9 ± 0.8	1.8 ± 0.2	3.4 ± 0.2
OCS O_3 SF_6	530 Nm^{-2} 25 Nm^{-2} 16.0 k Nm^{-2}	17.4 ± 0.4	21.7 ± 1.6	1.9 ± 0.1	2.3 ± 0.2

Results averaged over 15 experiments.

Percentage O_3 photolysis = 9.4 (7) derived from $O_3/N_2/SF_6$ results corrected for incomplete quenching of $O(^1D)$ by N_2.

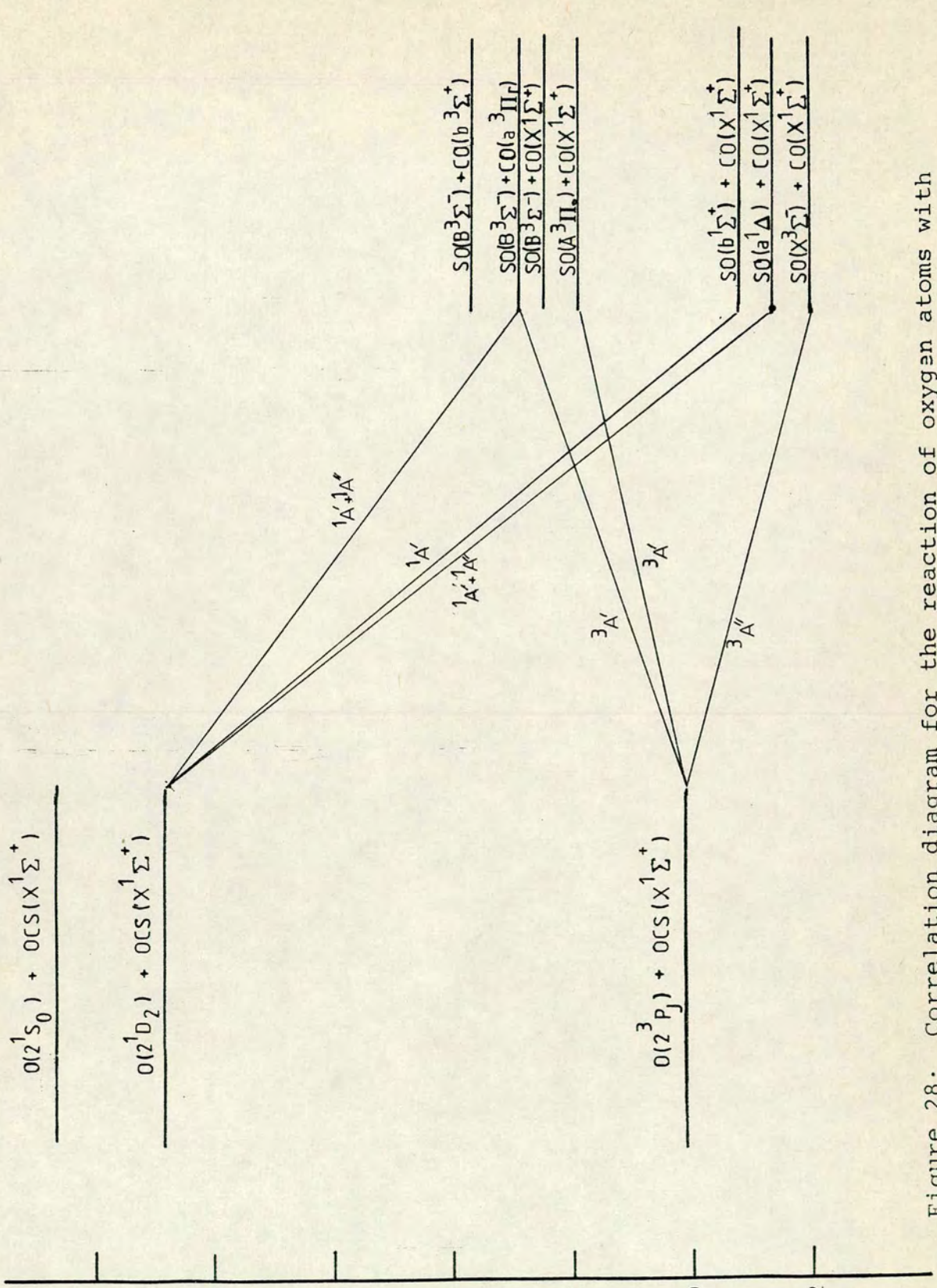

Figure 28: Correlation diagram for the reaction of oxygen atoms with carbonyl sulphide.

the $^1\Delta$ state. The reaction of $SO(^1\Delta)$ with O_3 [9] is predicted to be fairly fast to account for the observed depletion.

In an attempt to understand the O_3/OCS system more fully, and to obtain limits for the rate constants of the proposed reactions, computer simulation was employed (appendix 3). The model developed in Chapter 6 to account for O_3 photolysis was used as the basis of the present study. Reactions thought to be of importance are outlined below and rate constants, if known, are listed in Table 18. Photolysis of OCS was considered as having only a minimal effect in this system.

$$O(^1D) + OCS \rightarrow SO(^1\Delta) + CO \qquad [1]$$

$$\rightarrow O(^3P) + OCS \qquad [11]$$

$$O(^3P) + OCS \rightarrow SO(^3\Sigma) + CO \qquad [2]$$

$$SO(^1\Delta) + M \rightarrow SO(^3\Sigma) + M \qquad [12]$$

$$(M = OCS, SF_6)$$

$$SO(^1\Delta) + O_3(^1A) \rightarrow SO_2(^1A_1) + O_2(^1\Delta_g) \qquad [9a]$$

$$\Delta H^\circ_{298} \simeq -428 \text{ kJ mole}^{-1}$$

$$\rightarrow SO_2(^3B_1) + O_2(^3\Sigma_g^-) \qquad [9b]$$

$$\Delta H^\circ_{298} \simeq -214 \text{ kJ mole}^{-1}$$

$$\rightarrow SO(^3\Sigma) + O_2(^3\Sigma_g^-) + O(^3P) \qquad [9c]$$

$$\Delta H^\circ_{298} \simeq +29 \text{ kJ mole}^{-1}$$

$$SO(^3\Sigma) + O_3(^1A_1) \rightarrow SO_2(^1A_1) + O_2(^3\Sigma_g^-) \qquad [10]$$

$$\Delta H^\circ_{298} = -522 \text{ kJ mole}^{-1}$$

$$SO(^3\Sigma) + O(^3P) \xrightarrow{M} SO_2(^1A_1) \qquad [13]$$

$$SO_2(^3A_1) + O(^3P) \xrightarrow{M} SO_3 \qquad [14]$$

$$O_2(^1\Delta_g) + O_3 \rightarrow O_2 + O_2 + O(^3P) \qquad [15]$$

Table 18: Rate constants for reactions of importance in the simulation of the $OCS-O_3$ system

No.	Reaction	Rate/$cm^3 molec^{-1} s^{-1}$	Ref.
[2]	$O(^3P) + OCS \rightarrow SO(^3\Sigma) + CO$	$(0.8 - 1.2) \times 10^{-14}$	175, 177
[10]	$SO(^3\Sigma) + O_3 \rightarrow SO_2 + O_2$	7.5×10^{-14}	176
[11]	$SO(^3\Sigma) + O(^3P) \xrightarrow{M} SO_2$	2.2×10^{-11}	174
[12]	$SO_2(^1A_1) + O(^3P) \xrightarrow{M} SO_3$	2.0×10^{-14}	174
a	$SO_2 + O_3 \rightarrow SO_3 + O_2$	$<10^{-22}$	174
b	$SO + SO_3 \rightarrow SO_2 + SO_2$	2.0×10^{-15}	174
c	$SO_3 + O \rightarrow SO_2 + O_2$	5.6×10^{-17}	174

a, b and c are unlikely to be important in this system and not considered in the simulation model.

Assuming a value for k_1 of 2.0×10^{-10}, as previously discussed, the rate constant (k_9) for the removal of $SO(^1\Delta)$ by O_3 was varied until a good fit to the intermediate depletion was obtained. The range of values over which agreement was obtained within the experimental error limits was

$$3.0 \times 10^{-12} < k_9 < 1.0 \times 10^{-11} \text{ cm}^3\text{molec}^{-1}\text{s}^{-1}$$

For a value of k_9 less than the lower limit, reaction [9] would have had an effect on the O_3 decay within the period of experimental observation ($t > 600$ μs). No such effect was detected. A rate constant greater than the upper limit produced too large an O_3 depletion. The best fit was obtained for a value of

$$k_9 = (6.0 \pm 3.0) \times 10^{-12} \text{ cm}^3\text{molec}^{-1}\text{s}^{-1}$$

Quenching by OCS accounted for 15 ± 5% of the removal of $O(^1D)$, within experimental error. The model was insensitive to small changes in k_1.

The final ozone depletion, as determined by computer modelling, was dependent on the nature of the products of the reaction of O_3 with $SO(^1\Delta)$. Three channels merit consideration. That leading to the dissociation of O_3 [9c] is endothermic by 29 kJ mol^{-1}, compared with 12 kJ mol^{-1} for the analogous reaction of $O_2(^1\Delta_g)$ [15], and was thus unlikely to be important in this case. Channels leading to the formation of O_2 and SO_2 correlate with one of these species being produced in an electronically excited state [9a,b]. The more exothermic route [9a] leads to the formation of $O_2(^1\Delta_g)$. However, the yield of $O_2(^1\Delta_g)$ from O_3 photolysis, together with the subsequent reactions

[13,2,10], was more than sufficient to account for the observed final O_3 depletion. Thus, it is proposed that the reaction of $SO(^1\Delta)$ with O_3 leads to the production of SO_2 in the first electronically excited (a^3B_1) state. This channel is still exothermic by ca. -214 kJ $mole^{-1}$. A suitable means of confirming that this is indeed the preferred channel would be to monitor the chemiluminescence from the SO_2 (a^3B_1) state, since removal by physical and reactive quenching is slow.

Physical quenching of $SO(^1\Delta)$ is expected to be more efficient than for $O_2(^1\Delta_g)$, as the energy gap for the $^1\Delta \rightarrow {}^3\Sigma$ transition is considerably smaller in the case of the former, being ca. 6350 cm^{-1} and 7882 cm^{-1} respectively. However, the spin forbidden nature of the quenching process suggests that, for a given species, the value of the rate constant, k_q should lie somewhere between the observed values for quenching of $O_2(^1\Delta_g)$ and $O_2(^1\Sigma_g{}^+)$. Quenching rate constants of the order of magnitude 10^{-16} are expected for zero-spin species, and k_{11} was taken to be ca. $1.0 \times 10^{-16} cm^3 molec^{-1} s^{-1}$ where M = SF_6. Rate constants for reactions of SO were taken from the recent review by Graedel.[174]

Good simulated fits to the experimental ozone decay were obtained for OCS pressures of 130 Nm^{-2} (1τ) and 270 Nm^{-2} (2τ), assuming a temperature of 298°K. The final ozone depletion was particularly sensitive to the rate constant k_{10} for the removal of O_3 by ground state SO. The model predicted a value of $k_{10} = 7.5 \pm 2.5 \times 10^{-14} cm^3 molec^{-1} s^{-1}$ in agreement with that obtained by Hampson and Garvin.[174] The best simulated fits are shown in Figure 29.

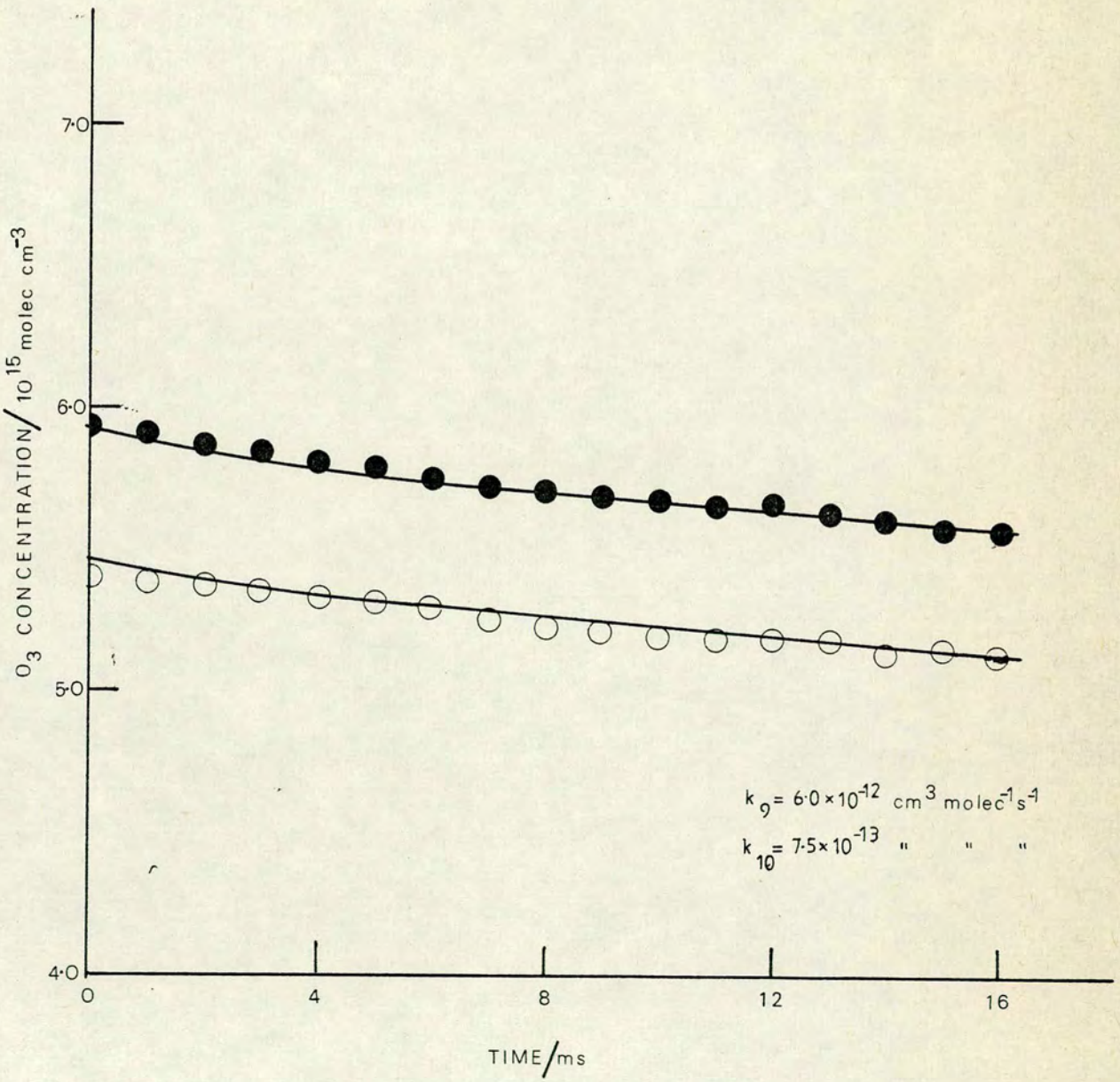

Figure 29: Simulated best fit profiles (solid lines) for the removal of ozone following photolysis in the presence of OCS. Experimental decays shown as ● (P_{OCS} = 130 Nm^{-2}) and ○ (P_{OCS} = 260 Nm^{-2})

The exceptionally low O_3 depletion obtained for the highest OCS pressure (530 Nm^{-2}) could not be accounted for in terms of the model presented above. To obtain such a value, some process involving the physical or reactive quenching of $O_2(^1\Delta_g)$ must be invoked. Quenching efficiency of $O_2(^1\Delta_g)$ by OCS is not expected to be very different from that observed in the case of CO_2.[50] Although reaction with OCS to produce ground state SO_2 and CO is exothermic (ΔH^o_{298} = -157 kJ $mole^{-1}$), this process [16] is also unlikely to occur. In the absence of a trend in experimental results on increasing the OCS pressure, no satisfactory explanation of this inconsistency could be found.

$$OCS(^1\Sigma) + O_2(^1\Delta_g) \rightarrow SO_2(^1A_1) + CO(^1\Sigma) \qquad [16]$$
$$\Delta H^o_{298} = -157 \text{ kJ mole}^{-1}$$

In conclusion, this work provides evidence that the removal of $O(^1D)$ by OCS to produce $SO(^1\Delta)$, is very fast, though no accurate determination of the rate could be made. Sulphur dioxide is clearly the major product of OCS decay. Crutzen[169] has estimated the input of SO_2 into the stratosphere due to OCS decay to be $6 \times 10^6 - 10^7$ molecules $cm^{-2}s^{-1}$. Industrial release from coal combustion is the main source of OCS in the troposphere.[175]

The rate constant for the removal of O_3 by $SO(^1\Delta)$ [9] has been determined

$$k_9 = 6.0 \pm 3.0 \times 10^{-12} cm^3 \text{ molec}^{-1}s^{-1}$$

That for the removal of O_3 by $SO(^3\Sigma^-)$ [10] was found to be in good agreement with other workers.

$$k_{10} = 7.5 \pm 2.5 \times 10^{-14} cm^3 molec^{-1}s^{-1}.$$

Assuming that the radiative lifetime of $SO(^1\Delta)$ is at least several seconds (section 1.06), reaction [9] may be a possible sink for stratospheric ozone if the level of OCS in the atmosphere continues to rise.

Chapter 7

Singlet Molecular Sulphur

7.01 Introduction

Formation of the first excited singlet state of sulphur has been observed spectroscopically in absorption via the $(f^1\Delta_u \leftarrow a^1\Delta_g)$ transition following photolysis of a number of sulphur containing compounds.[70,71] The mechanism for production of $S_2(^1\Delta_g)$ following photolysis of OCS is well understood[178] [1,2].

$$OCS(^1\Sigma^+) + h\nu(\lambda > 200\ nm) \rightarrow S(^1D) + CO(^1\Sigma^+) \qquad [1]$$

$$S(^1D) + OCS(^1\Sigma^+) \rightarrow S_2(^1\Delta_g) + CO(^1\Sigma^+) \qquad [2]$$

Although OCS is the cleanest source of $S(3^1D_2)$ atoms, it is unfortunately a weak absorber in the ultra-violet region. The kinetics of $S_2(^1\Delta_g)$ formation have yielded a lower limit for the rate constant of reaction [2] - $k_2 > 6 \times 10^{-11} cm^3 molec\ s^{-1}$.[178]

The $S_2(^1\Delta_g)$ spectrum is very short lived and closely follows the flash profile,[70] the rapid decay of this species contrasting markedly with that observed for $O_2(^1\Delta_g)$. As the radiative lifetime of $O_2(^1\Delta_g)$ is long (ca. 45 mins.), it is probable that $S_2(^1\Delta_g)$ also has a substantial lifetime. This decay must therefore be attributed to collisional deactivation to the triplet ground state. The resultant growth of $S_2(^3\Sigma_g^-)$ can be observed spectroscopically in absorption via the $(B^3\Sigma_u^- \leftarrow X^3\Sigma_g^-)$ transition. Removal of $S_2(^1\Delta_g)$ via some second order 'dimol' process, analogous to that observed for $O_2(^1\Delta_g)$, would only be important if the rate constant for such a process [4] was much greater than that for collisional quenching [3].

Other processes leading to the formation of ground state sulphur are relatively slow [6,7][179] as are those processes leading to its removal [8,9,10].[180]

$$S(^3P) + S(^3P) + M \rightarrow S_2(^3\Sigma_g^-) + M \quad [6]$$

$$S_2(^1\Delta_g) + M \rightarrow S_2(^3\Sigma_g^-) + M \quad [3]$$

$$S_2(^1\Delta_g) + S_2(^1\Delta_g) \rightarrow S_2(^3\Sigma_g^-) + S_2(^3\Sigma_g^-) \quad [4]$$

$$S(^1D) + M \rightarrow S(^3P) + M \quad [5]$$

$$S(^3P) + OCS \rightarrow S_2(^3\Sigma_g^-) + CO \quad [7]$$

$$S_2(^3\Sigma_g^-) + S_2(^3\Sigma_g^-) + M \rightarrow S_4 + M \quad [8]$$

$$S(^3P) + S_4 \rightarrow S_3 + S_2(^3\Sigma_g^-) \quad [9]$$

$$S(^3P) + S_3 \rightarrow S_2(^3\Sigma_g^-) + S_2(^3\Sigma_g^-) \quad [10]$$

7.02 Results and Computer modelling studies

The apparatus for flash photolysis with kinetic spectroscopy has been described previously (section 2.04). $S_2(a^1\Delta_g)$ was monitored via the (12,0) band of the $(f^1\Delta_u \leftarrow a^1\Delta_g)$ transition at 240.5 nm, while $S_2(^3\Sigma_g^-)$ was monitored via the (12,0) and (11,0) bands of the $(B^3\Sigma_u^- \leftarrow X^3\Sigma_g^-)$ transition at 271.5 nm and 279.9 nm respectively. Absolute concentrations of $S_2(X^3\Sigma_g^-)$ were obtained using the extinction coefficient measured by Gaydon et al.[181]

Experiments were carried out using 130 Nm^{-2}, 270 Nm^{-2} and 800 Nm^{-2} of OCS made up to a total pressure of 3.3 k Nm^{-2} with SF_6. Further investigations involved 267 Nm^{-2} of OCS made up to total pressures of 1.3 k Nm^{-2} and 12 k Nm^{-2} with SF_6.

$S(^1D)$ is the major product of OCS photolysis for $\lambda_{u.v.} > 200$ nm and reacts rapidly with OCS to form $S_2(^1\Delta_g)$. Absorption by $S_2(^1\Delta_g)$ was found to be weak and the species was only observed for low OCS pressures when a diluent gas was present, such that the absorption bands were pressure broadened. However, OCS itself absorbs in the same region of the spectrum as $S_2(^1\Delta_g)$, so that for the highest pressure of OCS, the absorption bands of the $S_2(^1\Delta_g)$ spectrum were saturated ($\lambda < 250$ nm).

Figure 30 is a photographic plate showing the rapid decay of the ($f^1\Delta_u \leftarrow a^1\Delta_g$) system and the subsequent growth of the ($B^3\Sigma_u^- \leftarrow X^3\Sigma_g^-$) system of S_2 for a typical experiment. On photolysis of OCS (270 Nm^{-2}), the maximum in the concentration profile of $S_2(^1\Delta_g)$ occurred at 10 μs, the approximate half life of the subsequent decay being 20 μs. An increase in the OCS pressure to 780 Nm^{-2} did not result in a larger absorption by $S_2(^1\Delta_g)$, the maximum occurring at ca. 15 μs, and was presumably the result of saturated absorption.

However, the rate of appearance of $S_2(^3\Sigma_g^-)$ was much more rapid at the highest pressure (780 Nm^{-2}) and resulted in a threefold increase in the yield of this species over that observed for 270 Nm^{-2} OCS. This suggests a similar increase in the yield of $S_2(^1\Delta_g)$ at the highest pressure of OCS.

The efficiency of SF_6 as a quencher of $S(^1D)$ or $S_2(^1\Delta_g)$ was found to be negligible, as is illustrated in Figure 31 by the comparable experimental results obtained with 270 Nm^{-2} OCS. for total pressures of 3.3 k Nm^{-2} and 12.0 k Nm^{-2}. Removal of $S_2(^1\Delta_g)$ appears to be due entirely to collisional quenching by OCS. First order plots of the growth of $S_2(^3\Sigma_g^-)$ at OCS pressures of 270 Nm^{-2} and 800 nm^{-2} are shown in Figure 32, yielding slopes of $(1.7 \pm 0.3) \times 10^4 s^{-1}$ and $(4.1 \pm 0.3) \times 10^4 s^{-1}$ respectively. Thus the second order rate constant for collisional quenching of $S_2(^1\Delta_g)$ by OCS, k_3, is given by

$$k_{OCS} = (2.4 \pm 0.6) \times 10^{-13} cm^3 molec\ s^{-1}$$

So as to determine that this rate constant was indeed that for collisional quenching of $S_2(^1\Delta_g)$ and not simply a lower limit imposed by the duration of the photolysis flash, a simple

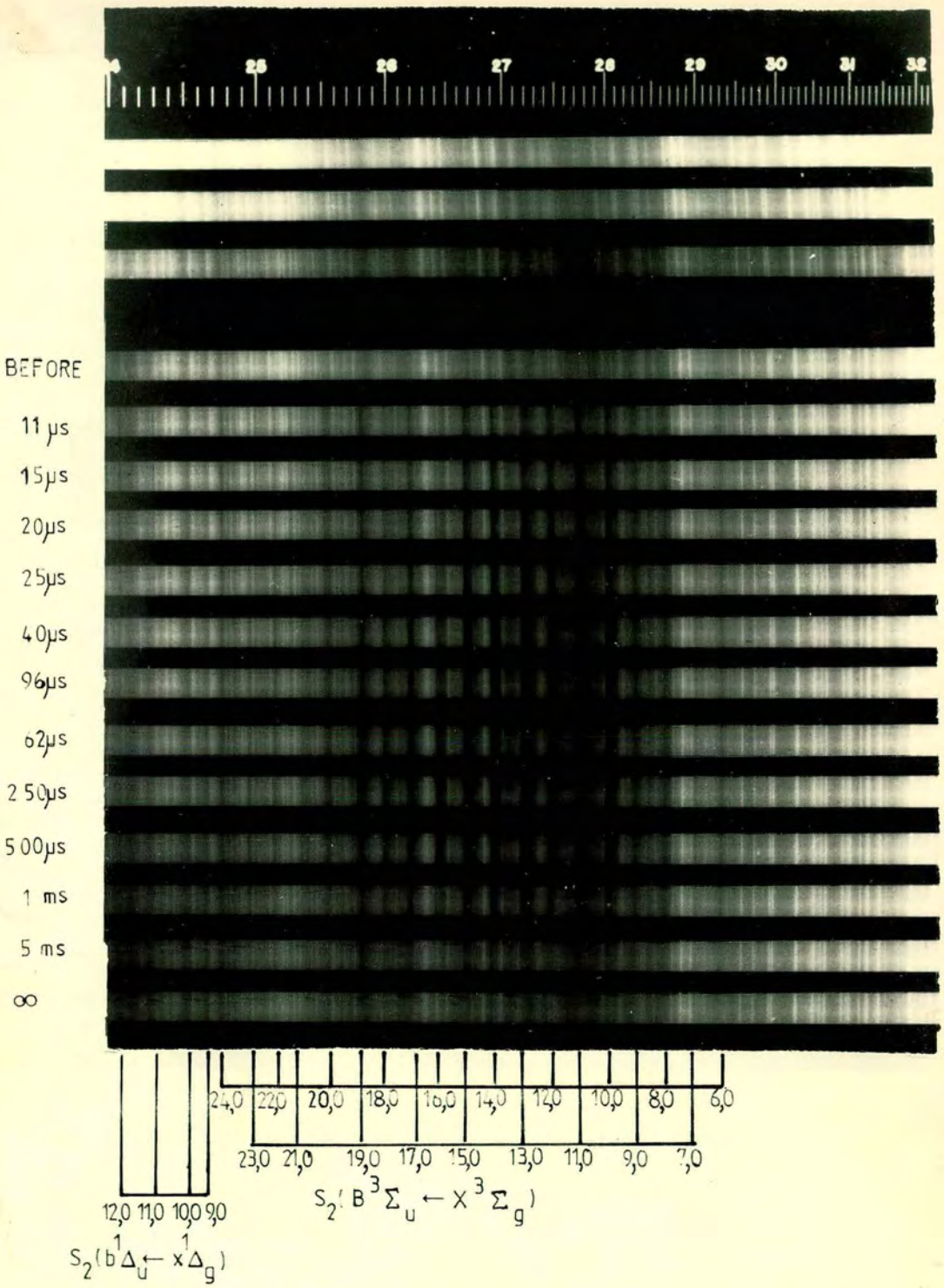

Figure 30: Photographic plate showing decay of $S_2(a^1\Delta g)$ and resulting growth of $S_2(X^3\Sigma_g^-)$. Following photolysis of OCS. (P_{OCS} = 750 Nm^{-2}, P_{tot} = 1.33 k N m^{-2})

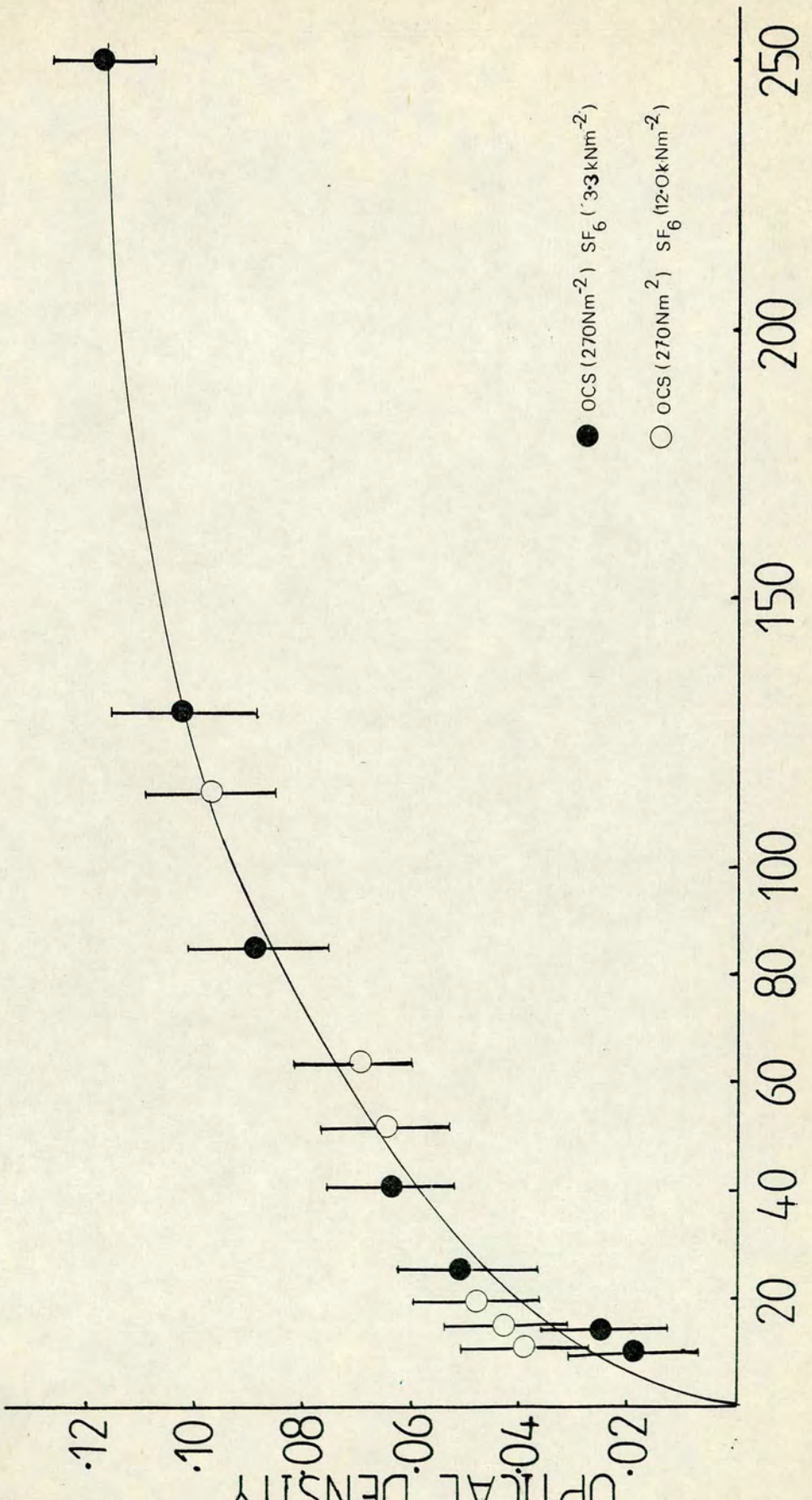

Figure 31: The growth of $S_2(X^3\Sigma_g^-)$ following photolysis of OCS for SF_6 pressures of 3.3 k N m^{-2} and 12.0 k N m^{-2}.

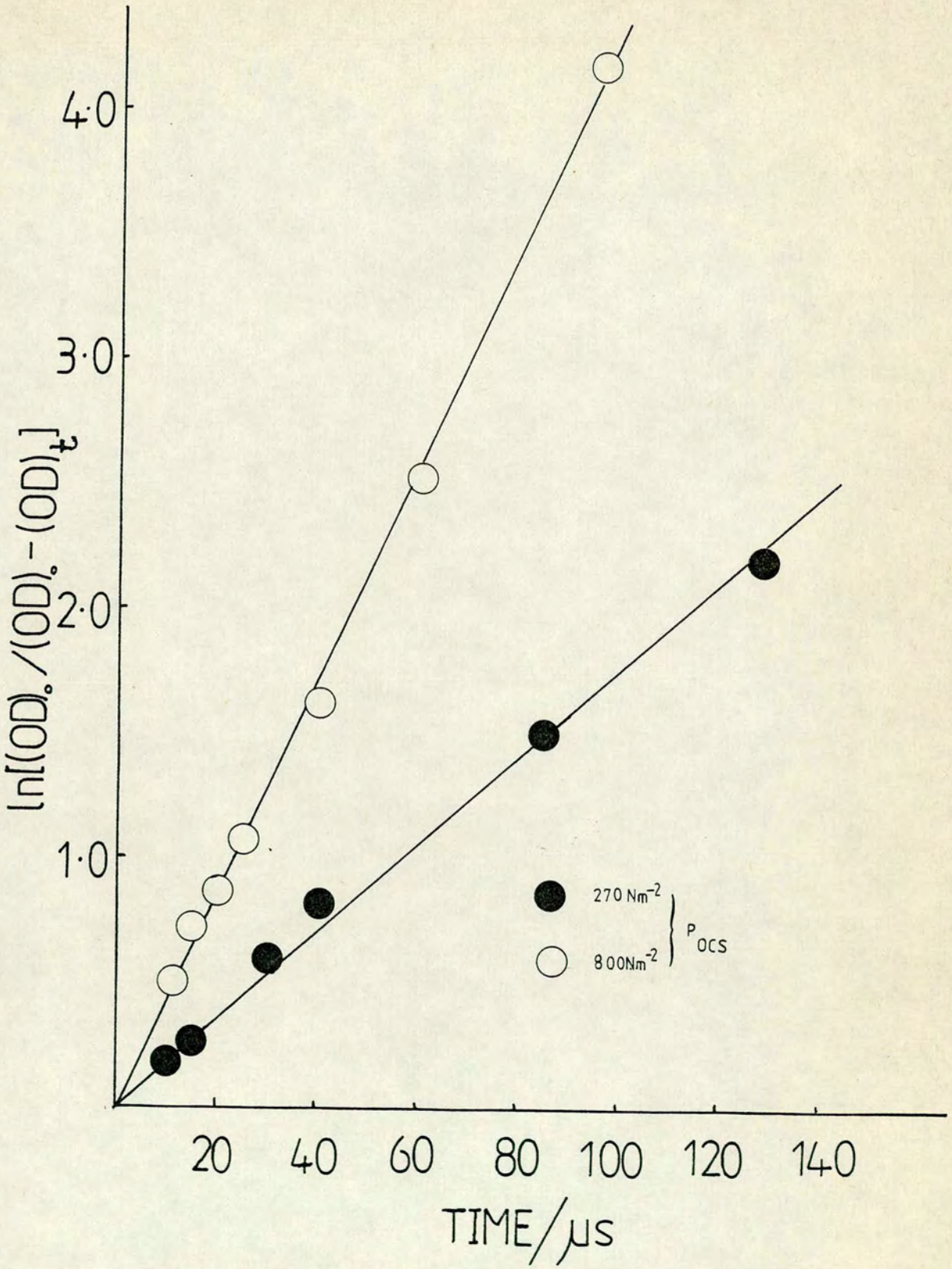

Figure 32: Pseudo first order plots of growth of $S_2(X^3\Sigma_g^-)$ versus time, following photolysis of OCS.

computer model of the system was again used. The rapid decay of the flash was found to fit a profile of the type

$$I = d[S(^1D)]/dt = A\ t\ \exp-(\beta t)^2$$

as described previously (section 2.04). From absolute measurements of the $S_2(^3\Sigma_g^-)$ concentration at long times (350 μs) and comparison with O_3 photolysis using the same apparatus, it was estimated that the extent of photolysis of OCS (270 Nm^{-2}) was 0.1(1)%.

$$OCS + h\nu \rightarrow S(^1D) + CO \qquad [1]$$

$$S(^1D) + OCS \rightarrow S_2(^1\Delta_g) + CO \qquad [2]$$

$$S_2(^1\Delta_g) + OCS \rightarrow S_2(^3\Sigma_g^-) + OCS \qquad [3]$$

Only three reactions [1,2,3] were considered in this model, since other processes should have had a negligible effect within the time scale considered ($t < 250$ μs). The lower limit for k_2 determined by Donovan et al.[178] was used to obtain a value of k_3 which provided a fit between the experimental and simulated curves of growth for $S_2(^2\Sigma_g^-)$. A flash rise time of 4 μs gave the best fit, this being somewhat shorter than the measured value of 10 μs which resulted in the simulated curve of growth being displaced along the time axis. This suggests that the time constant of the detector circuit was too high (section 2.04,Figure 6). The computed value of k_3 was in good agreement with experimental determination

$$k_{OCS} = (2.8 \pm 0.5) \times 10^{-13} cm^3 molec^{-1} s^{-1}$$

Figure 33 shows computed and experimental curves of growth over this range of values of k_3 for an OCS pressure of 270 Nm^{-2}.

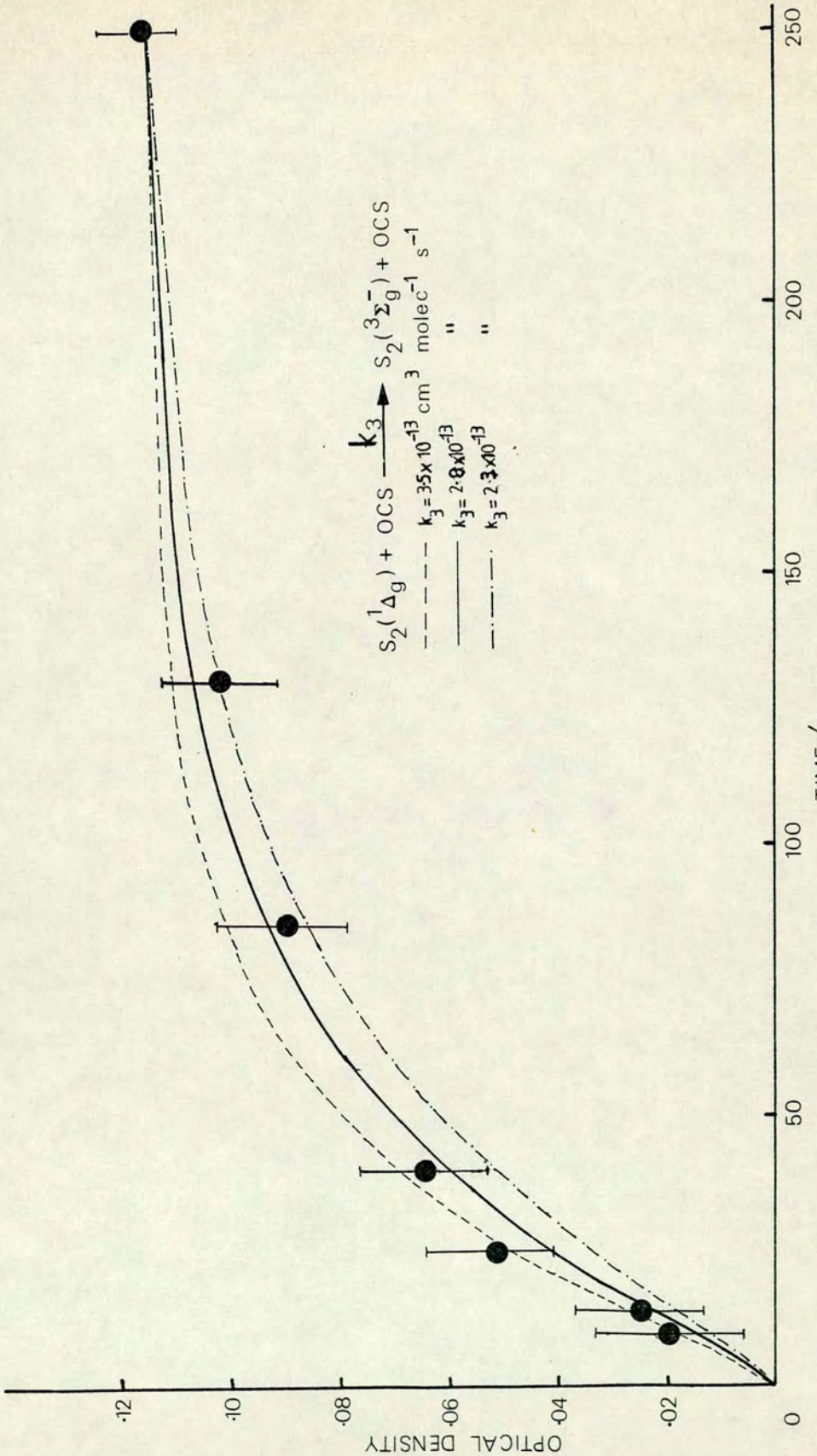

Figure 33: Calculated curves of growth for $S_2(^3\Sigma_g^-)$ following photolysis of OCS. Experimental points are shown as ●.

It is clear from these results that the growth of $S_2(^3\Sigma_g^-)$ does not follow the flash profile, the lower limit for such an occurrence being $k_3 = 1.0 \times 10^{-12} cm^3 molec^{-1} s^{-1}$. The model was insensitive to any increase in k_2, so that it was not possible to obtain a more accurate value for this rate constant.

7.03 Discussion

Recent studies of the quenching of $Br(4^2P_{\frac{1}{2}})$ ($T_e = 3685\ cm^{-1}$) by CO_2, OCS, CS_2 and H_2O have provided direct measurement of rate coefficients for electronic to vibrational (E → V) energy transfer into product states, where these are formed with at least one quantum of vibration in the ν_3 mode.[182,183] These results together with those of Donovan et al.[184] give clear evidence that as the number of vibrational quanta required to make the quenching process near resonant increases, quenching becomes less efficient. Quenching rate constants of $Br(4^2P_{\frac{1}{2}})$ by CO_2 and H_2O were shown to be more than an order of magnitude greater than for OCS and CS_2.

Excitation of $H_2O(\nu_1,\nu_3)$ and $CO_2(\nu_1,\nu_3)$ via Br* quenching are two examples of fast, mode specific, resonant energy transfer processes in which electronic and vibrational degrees of freedom are coupled by long range multipolar interactions, in this case quadrupole-dipole. For molecules such as OCS and CS_2, where larger numbers of vibrational quanta are required for near resonance, the observed quenching rates cannot be accounted for in terms of multipolar interactions. In these cases, non-resonant, non-adiabatic transitions from the electronic potential surface correlating to the $4^3P_{\frac{1}{2}}$ state must be involved.

Quenching of $S_2(^1\Delta_g)$ by an inert quencher is a spin-forbidden process. Thus, this species is expected to be much more resistant to quenching than $S_2(^1\Sigma_g^+)$, with the exception of paramagnetic quenchers, since the latter is quenched to the $^1\Delta_g$ state by a spin allowed process.

Merkel and Kearns[39] found a striking parallel between $O_2(^1\Delta_g)$ lifetime in solution and the solvent absorption intensity near 7880 and 6280 cm^{-1}, resonant with the (0,0) and (0,1) bands of the $^1\Delta_g \rightarrow {}^3\Sigma_g^-$ transition. Due to the nature of the electronic wave functions for oxygen, the $^1\Delta_g$ and $^3\Sigma_g^-$ states cannot couple in the absence of some spin-dependent perturbation. In non-heavy atom solvents there is no solvent induced mixing of these states. However, the $^1\Sigma_g^+$ and $^3\Sigma_g^-$ states are coupled by a spin-orbit matrix element of ca. 140 cm^{-1}. Consequently, in non-heavy atom solvents can induce direct mixing of the $^1\Delta_g$ and $^3\Sigma_g^-$ states, by causing mixing of the $^1\Delta_g$ and $^1\Sigma_g^+$ states, and thus provide a quenching route for the former. This argument was extrapolated to account for gas phase quenching of $O_2(^1\Delta_g)$ and gave values which were consistent with those measured experimentally.

Carleer[69] has estimated that the $^1\Delta_g$ state of S_2 lies ca. 4,700 cm^{-1} above the ground state, although this value could be in error by as much as 800 cm^{-1}. This is considerably lower than for $O_2(^1\Delta_g)$ (7882 cm^{-1}) and since spin selection rules are less rigorously held in the case of S_2, a much heavier molecule quenching of $S_2(^1\Delta_g)$ might be expected to be rather more efficient than for $O_2(^1\Delta_g)$. Figure 34 shows a partial energy diagram for CO_2 and OCS, where these molecules possess at least one quantum of ν_3 vibrational excitation. Over sixty infra-red absorption bands of OCS have been assigned[185] in the region 2400-7000 cm^{-1}. However, little information is available

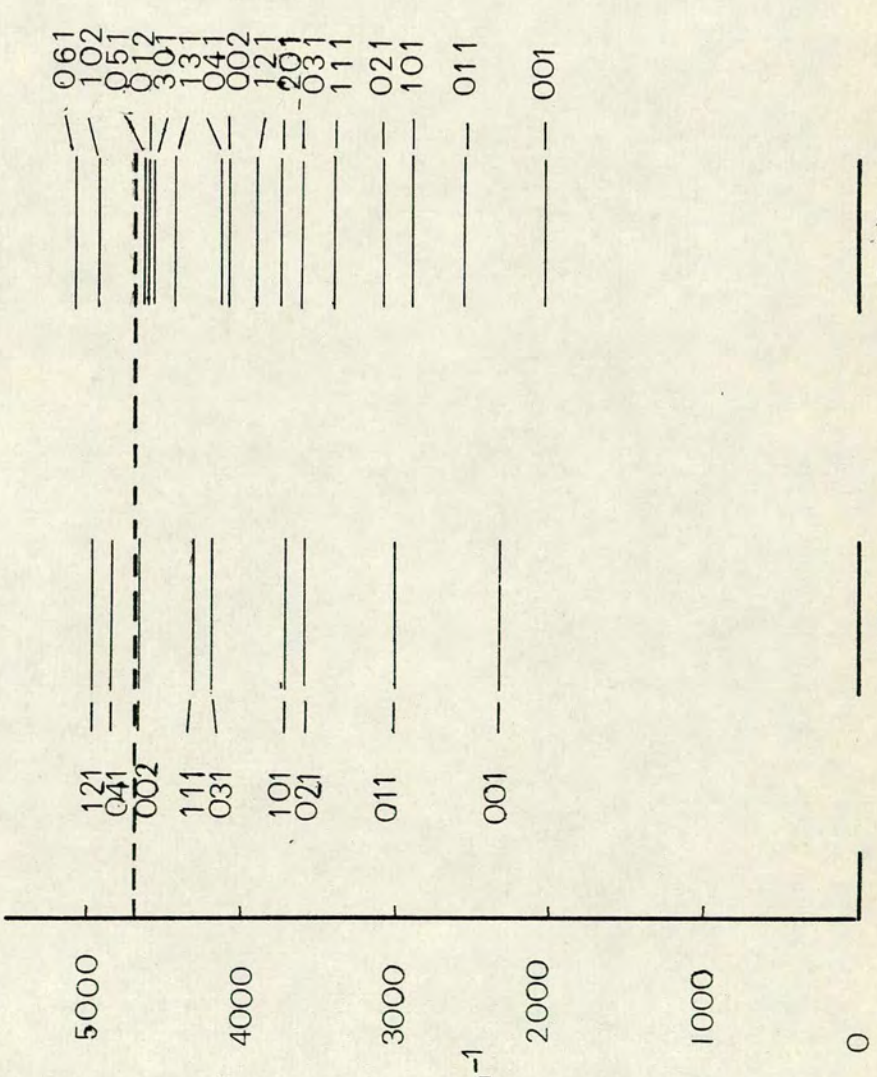

Figure 34: A partial energy diagram of CO_2 and OCS vibrational levels, including the estimated term value for $S_2(^1\Delta_g)$.

regarding their relative intensities,[186] especially for $\lambda > 4100\ cm^{-1}$.

If near resonant E → V transfer is to be important in the quenching of $S_2(^1\Delta_g)$ by OCS, only one channel can be considered as efficient, assuming $T_e = 4{,}700\ cm^{-1}$. In this case, the product state of OCS is the $(01^{o}2)$ vibrational level, involving the transfer of three quanta of energy and an energy defect of ca. $80\ cm^{-1}$. If, however, $S_2(^3\Sigma_g^-)$ is formed with one quantum of vibrational energy ($720\ cm^{-1}$) and OCS in the $(00^{o}2)$ product state, only two vibrational quanta are involved with an energy defect of ca. $100\ cm^{-1}$ - this transition is relatively strong in the IR absorption spectrum of OCS.

From Figure 34 it would appear that quenching of $S_2(^1\Delta_g)$ by CO_2, with E → V transfer into the $(00^{o}2)$ vibrational level, should be much more efficient than quenching by OCS ($\Delta E \sim 40\ cm^{-1}$). As CO_2 is an efficient quencher of $S(^1D)$,[1] it would be difficult to measure the rate constant, k_{CO_2}, for quenching of $S_2(^1\Delta_g)$. However, using equal concentrations of OCS and CO_2, an increase of an order of magnitude in the quenching efficiency of the latter should be detectable, even assuming up to 50% of $S(^1D)$ to be quenched by CO_2.

Appendices

Appendix I

Materials

CF_3Cl : ICI 'Arcton' liquified gas was thoroughly degassed by repeated trap to trap distillation at $77^{o}K$ with continuous pumping on the sample.

CF_2Cl_2: ICI 'Arcton' liquified gas was trapped in a cold finger at $77^{o}K$ and allowed to expand into a bulb before thoroughly degassing by repeated trapping at $77^{o}K$.

$CFCl_3$: As for CF_2Cl_2.

H_2O_2 : 100 volume (BDH 'Aristar') 30% w/v minimum assay, contained sodium stannate as a preservative.

He : 'Grade A' (B.O.C. Special Gases). O_2 < 1 p.p.m., N_2 < 1 p.p.m., H_2O < 5 p.p.m. Passed through liquid Nitrogen traps to remove any water.

Kr : 'Research Grade' (B.O.C. Ltd) used directly from glass break-seal container. Purity given as 99.99%.

N_2 : BOC 'white spot' grade (99.9%), passed through liquid nitrogen traps.

NaOCl : Fisons Technical Grade. 8% available chlorine (Cl). Total alkalinity (NaOH) 2% maximum.

O_2 : Cylinder grade (BOC) 99.5% minimum purity, was passed through CO_2 slush baths to remove any water present.

O_3 : See Appendix II.

OCS : Cylinder grade (Matheson Co. Inc.) purity 97.5% minimum, was thoroughly degassed by repeated trapping at $77^{o}K$.

SF_6 : Cylinder grade (Air Products Ltd) purity 99.9% was thoroughly degassed by repeated trap to trap distillation at $77^{o}K$ with continuous pumping on the sample.

Appendix II

Ozone Preparation and Handling

Ozone was prepared by a method similar to that described previously by Thrush and Clough.[128] The ozone trap was filled with 4-6 mesh silica gel and baked out, using an oil bath at 300°K, with continuous pumping until no further outgassing occurred (7-8 hours). Baking out was only necessary when the gel was fresh, or when it had been exposed to the atmosphere for any length of time.

The trap was first cooled using a solid CO_2/isopropanol slush bath (195°K) and connected to a Towers Ozone apparatus using PVC tubing and a minimal amount of silicon grease to make attachment easier. After flushing out the apparatus with O_2, dried over conc. H_2SO_4, having turned on the ozoniser, ozone was allowed to adsorb on the gel. After 30 minutes to one hour the trap was fully laden with O_3 and was closed off. The ozoniser was shut down and the apparatus flushed with O_2, the trap by-pass being open, so as to prevent oxidation of the PVC tubing. Pure ozone and mixtures with partial pressures of O_3 not exceeding 1.3 k Nm^{-2} were handled on a greaseless vacuum line, any joints being only lightly coated with silicon grease. Hydrocarbon grease was not used as this was highly dangerous and could have resulted in an explosive situation if in contact with liquid O_3. The freshly laden trap was attached to the line and pumped down slowly by a liquid N_2-trapped rotary pump. Any ozone was destroyed before reaching the pumps by passing over a hot glass tube containing a nickel catalyst. This process was repeated every few days so as to prevent a pressure build up of O_2 in the

trap. When fresh silica gel was used, several loads of ozone were required before the gel was deactivated.

When ozone was required on the line, the trap was first pumped on to remove O_2, after which the slush bath was removed so as to allow the gel to warm up and O_3 to desorb. The pressure was monitored continuously using the spiral guage and a safe upper limit of 4 k Nm^{-2} was not exceeded. With careful pumping O_3 purity of 95% was achieved.

Ozone was stored in the presence of helium in a blackened bulb and slowly decomposed at a rate of ca. 1% total O_3 pressure per day. Purity was checked daily by obtaining a u.v. absorption spectrum (section 4.02).

The safety aspects of this method of preparing and handling ozone have been carefully considered by Cook et al.[187]

Appendix III

Computer Programs

A 3.1. Introduction

The use of computers played an important part in the work reported in this thesis, and in this appendix the most important programs are described.

The computers used included the ICL 4/75 computers of the Edinburgh Regional Computer Centre (ERCC) and the IBM 370/158 computer of the Newcastle University Multi-Access System (NUMAC). The sophisticated interactive Edinburgh Multi-Access System (EMAS), run on the ICL 4/75, was used for the majority of programming tasks, whereas computer modelling programs were run on the IBM 370/158.

The programming language IMP was found to be particularly useful for EMAS, although FORTRAN IV was used for the IBM 370/158.

A 3.2. Programs to handle and process data from the transient recorder (Datalab DL905) and signal averager (Datalab DL4000).

Data stored in the memory of either the transient recorder or signal averager could be transferred to punch tape where it was formatted in ASCII code.

A program DIMOL was written to process data obtained by monitoring the decay in 'dimol' luminescence arising from the H_2O_2/NaOCl reaction. The intensity of light emitted at 633 nm was proportional to the square of the $O_2(^1\Delta_g)$ concentration. After determining the offset of the baseline from zero (see Fig. 1), by averaging over the last 200 channels, the concentration of $O_2(^1\Delta_g)$ was determined as follows:-

DELTA (I) = SQRT (INTEN(I)-BASE) [1]

By plotting the reciprocal of the singlet oxygen concentration (1/DELTA) versus time, the pseudo first order decay coefficient for quenching of $O_2(^1\Delta_g)$ could be determined. A weighted least squares routine was included to calculate the slope, the intercept and their respective errors. A graph subroutine was written to obtain a plot for each experiment on either the teletype or lineprinter.

This program was subsequently modified, with the help of Dr. H.M. Gillespie, to process data from either emission/fluorescence or absorption experiments. The program, known as EXPFITO, contains all the features of DIMOL such that detailed discussion of the former will serve to provide further information about the latter. EXPFITO is listed in table 19.

As well as including a linear weighted least squares routine, EXPFITO provides the alternative of fitting an exponential decay to the digital data in a non-linear least squares sense, using the ERCC IMP library routine IMPDAPRO.

For emission/fluorescence experiments the signal is directly proportional to concentration of the emitting species. Data will normally have been recorded in the pretrigger mode, in which case the baseline will be calculated from the pretrigger data. If, however, there should be no pretrigger information, the last 100 points are averaged to provide a baseline. For absorption studies two sets of data are needed for each experiment - one for the I=0 level and other for I_t during the experiment itself.

Data are read in input stream 1 (ST1). Various other streams are defined as follows.

ST2 - information file: contains experiment numbers, time full scale (seconds) and flash recovery time (seconds). Also (optionally) the first and last points of the decay to be processed if any particular portion is selected. A space separates each piece of data and a new line is required for each experiment to be processed.

ST3 - output file which lists the results.

ST4 - data to be read in at run time from the teletype or command file. DEFINE (ST4,.TT) will provide an explanation of each piece of data required, whereas DEFINE (ST4,.DATA) merely requires the user to enter the appropriate series of numbers separated by spaces.

ST10- output file for graph (optional).

An explanation of some of the data read in ST4 is given below.

(a) <u>signal + or -</u>

The program only processes negative-going signals. Thus if the signal is positive-going it is inverted by taking the negative of each data point. This feature is only important in the case of fluorescence data.

(b) <u>weighting code for linear least squares calculation</u>

This is only important when there is no subsequent optimisation run using the routine IMPDAPRO. Normally the linear least squares calculation simply provides initial values for the subsequent optimisation, which converges rapidly even for starting values which are far from the final best values. Thus it is sufficient to use weighting code 0.

(c) maximum number of iterations

The program usually converges within 5 or 6 iterations for reasonable tolerances. A suitable maximum might be 20, to allow for any particularly bad set of data.

(d) tolerances

DAPRO compares each value of the parameter of the model with the previous value; if the difference is less than the tolerance for that parameter, the values are returned to the calling program. If the difference is greater than the tolerance, the program enters another cycle. The tolerance is calculated as

$$V_o(i)/\text{TOL 1 or TOL 2} \quad (i = 1 \text{ or } 2) \qquad [2]$$

where $V_o(i)$ is the value of the parameter before commencing optimisation and TOL 1 and TOL 2 are integers read in. TOL 1 = TOL 2=10,000 is recommended for most data; however for quicker calculations, e.g. preliminary results, 500 is adequate. N.B. The program may use up to 30 seconds CPU time for a tolerance of 10,000.

(e) Number of lines of output

This will print out the required number of equally spaced values. Set to 0 unless particularly required.

Table 20 lists a specimen job together with an explanation of the data input instructions.

A 3.3 Computer Modelling Programs

In this work the programs CHEK and CHEKMAT, developed by Curtis and Chance[129], were used. Program CHEK simulates chemical kinetics for well mixed gas and solution phase systems on an IBM system/360 or 370 computer. Program CHEKMAT simulates chemical kinetics with matching of observed data by automatically fitting selected rate constants. Input data is prepared in natural, free-format language. Adequate information is available on preparation of data for both programs, on the methods used in them and on how to modify their action by supplying user subroutines Integration steps are taken by Gear's (1971) predictor corrector method, which is suitable for stiff sets of differential equations. Table 21 lists the typical input information, in this case for the CF_3Cl/O_3 model. Only two user subroutines will be discussed, since these were the only adaptations of the programs required for this work.

PATCHD was used to calculate the flash intensity profile and hence the rate of O_3 photolysis [3].

$$d[O_3]/dt = k\,[O_3]_t \propto I[O_3]_t \qquad [3]$$

For most purposes the intensity of the flash (I) is best expressed in the form [4], where A and B are

$$I = A\,t\,\exp(-\beta t) \qquad [4]$$

constants - β is the inverse of the time at which the flash intensity is at its maximum, i.e. $\beta = 1/t_{max}$.
By integration of equations [3] and [4] an expression can be derived which relates k_1 to P_∞, the percentage photolysis at $t = \infty$, A, β and t. This subroutine is included in Table 21.

$$k_1 = \ln (100/100-P_o).A.t.\exp(-\beta t) \qquad [5]$$

PATCH 1 was developed to simulate the expected experimental ozone decay converting calculated concentrations into transmitted light intensities (I_t) using the Beer-Lambert Law. This subroutine is shown in Table 21.

TABLE 19 PROGRAM EXPFITO

```
1    %BEGIN
2        %INTEGER P,PT,M,IMIN,DPT,SIGNAL
3        %INTEGER PTS,IATMIN,END,STORE,MINSTOR
4        %INTEGER NUMBER,IATMAX,IFINAL
5        %INTEGER OUTPUT,PORTION,TYPE
6        %INTEGER MM,NA,NB,MN
7        %INTEGER FIRST,LAST,WEIGHT
8        %INTEGER NF,U,N,ZERO,DELAY
9        %INTEGER I,B,LIMIT,OUT
10       %REAL TOL1,TOL2
11       %REAL MAXSOFAR,TOTAL,T,SLOPE
12       %REAL DT,DEVSLOPE,MINSOFAR
13       %REAL DEVINT,BASE,EXPT,TFS
14       %REAL INTER,SIGW,SIGWX,RECOV
15       %REAL SIGWY,SIGWX2,SIGWY2,SIGWXY
16       %REAL SIGWDD,DEN,CLOSE,GROUND
17       %REAL ALPHAA,ALPHAB,ALPHA2,CALCY,ENDINT
18       %LONGREAL SS,DD
19       %LONGREALARRAY VV(1:2),TOLL(1:2)
20       %REALARRAY X(1:1000),Y(1:1000),W(1:1000)
21       %REALARRAY AVG(1:2),INTEN(1:1024)
22       %LONGREALARRAY TIME(1:1024),DELTA(1:1024)
23       %REALARRAY LRECIP(1:1024),PLOTX(1:1000),PLOTY(1:1000)
24       %REALARRAY PY(1:1000)
25       %REAL MAXY,MINY,DY
26       %STRING(10) XAXIS,YAXIS
27       %EXTERNALROUTINESPEC IMP DAPRO(%LONGREALFN F    %C
C        %INTEGER KO,MA,ME,N,%INTEGERNAME M    %C
C        %LONGREALNAME S,D,%LONGREALARRAYNAME X,Y,V,TOL,SF)
28       !
29       !INFORMATION
30       !
31       SELECTOUTPUT(4)
32       NEWLINE
33       %PRINTTEXT'THIS PROGRAM IS ONLY FOR USE IN CONJUNCTION
34'      WITH DATA FROM A TRANSIENT RECORDER.'
35       %PRINTTEXT'OUTPUT4=INSTRUCTIONS,OUTPUT3=RESULTS
36'      OUTPUT10=GRAPH,INPUT1=DATA,INPUT2=INSTRUCTIONS'
37       NEWLINE
38       %PRINTTEXT'THE INSTRUCTIONS FILE(ST2) SHOULD CONTAIN
39'      THE EXPERIMENT NO., TFS(SECS), FLASH RECOVERY TIME(SECONDS),
40'      AND(OPTIONALLY) THE FIRST AND LAST CHANNELS TO BE PROCESSED,
41'      WITH A SPACE BETWEEN EACH PIECE OF DATA AND A NEWLINE FOR
42'      EACH EXPERIMENT'
43       NEWLINES(2)
44       %PRINTTEXT'HOW MANY EXPERIMENTS ARE TO BE PROCESSED?'
45       NEWLINE
46       READ(NUMBER)
47       NEWLINE
48       %PRINTTEXT'IS A GRAPH OUTPUT REQUIRED?
49'      IS THIS TO BE ON THE LINEPRINTER(1)'
50       %PRINTTEXT' OR ON THE TELETYPE(2)?
51'      IF NO GRAPH OUTPUT IS REQUIRED TYPE(0).'
52       NEWLINE
53       READ(OUT)
54       NEWLINE
55       %PRINTTEXT'IS THE SIGNAL +(8) OR -(9)?'
56       NEWLINE
57       READ(SIGNAL)
58       NEWLINE
59       %PRINTTEXT'ABSORPTION(1) OR FLUORESCENCE(2) DATA?'
60       NEWLINE
61       READ(TYPE)
62       %PRINTTEXT'DO YOU WISH TO SELECT A PORTION OF THE DECAY
63'      CURVE WHICH IS TO BE PROCESSED? YES(2) OR NO(1)?'
64       NEWLINE
65       READ(PORTION)
66       NEWLINE
67       %PRINTTEXT'
68'      WAS A PRETRIGGER DELAY SET? IF SO, HOW MANY CHANNELS?
69'      IF NOT TYPE(0).'
70       NEWLINE
71       READ(DELAY)
72       %PRINTTEXT'WEIGHTING CODE FOR L.L.S. CALC.'
73       NEWLINE
74       %PRINTTEXT'0: NO WEIGHTING'
75       NEWLINE
76       %PRINTTEXT'1: WEIGHTING PROP. TO EXPTL CONCS'
77       NEWLINE
78       %PRINTTEXT'2: WEIGHTING PROP. TO EXPTL CONCS SQUARED'
79       NEWLINE
80       READ(WEIGHT)
81       %PRINTTEXT'MAX NO OF ITERATIONS TO BE PERFORMED'
82       NEWLINE
83       READ(MN)
84       %PRINTTEXT'THE TOLS X(K) ARE DEFINED SUCH THAT THE CALC.'
85       NEWLINE
86       %PRINTTEXT'IS TAKEN TO HAVE CONVERGED '
87       %PRINTTEXT'IF THE CHANGE IN EACH PARAMETER'
88       NEWLINE
89       PRINTSTRING('IS < 1 PART IN X(K) OF ITS STARTING VALUE')
90       NEWLINE
91       %PRINTTEXT 'TOLERANCE FOR INTERCEPT'
92       NEWLINE
93       READ(TOL1)
94       %PRINTTEXT'TOLERANCE FOR RATE CONSTANT'
95       NEWLINE
96       READ(TOL2)
97       %PRINTTEXT'
98'      HOW MANY LINES OF OUTPUT ARE REQUIRED PER EXPT.?'
99       NEWLINE
```

```
      READ(OUTPUT)
      XAXIS='TIME(SECS)'
      YAXIS='L(CONC)'
      !INPUT!
      %CYCLE U=1,1,NUMBER
      MM=MN
      SELECTINPUT(2)
      READ(EXPT)
      READ(TFS)
      READ(RECOV)
      %IF PORTION=2 %THENSTART
      READ(FIRST)
      READ(LAST)
      %FINISH
      SELECTOUTPUT(3)
      %PRINTTEXT'EXPERIMENT NUMBER '
      PRINT(EXPT,2,2)
      NEWLINES(3)
      !
      !READING DATA
      !
      SELECTINPUT(1)
      %IF TYPE=1 %THENSTART
      GROUND=0
      READ(INTEN(1))
      READ(INTEN(2))
      %CYCLE I=3,1,1024
          READ(INTEN(I))
          GROUND=GROUND+INTEN(I)
      %REPEAT
      GROUND=GROUND/1022
      %IF SIGNAL=8 %THENSTART
      GROUND=-GROUND
      %FINISH
      %FINISH
      READ(INTEN(1))
      READ(INTEN(2))
      %IF SIGNAL=8 %THENSTART
      INTEN(2)=-INTEN(2)
      %FINISH
      MAXSOFAR=INTEN(2)
      MINSOFAR=INTEN(2)
      %CYCLE I=3,1,1024
          READ(INTEN(I))
      %IF SIGNAL=8 %THENSTART
      INTEN(I)=-INTEN(I)
      %FINISH
      %REPEAT
      !
      !BASELINE
      !
      TOTAL=0
      %IF DELAY=0 %THENSTART
          %CYCLE I=925,1,1024
              TOTAL=TOTAL+INTEN(I)
          %REPEAT
      BASE=TOTAL/100
      %FINISH
      %IF DELAY≠0 %THENSTART
          %CYCLE I=2,1,DELAY-2
              TOTAL=TOTAL+INTEN(I)
          %REPEAT
      BASE=TOTAL/(DELAY-3)
      %FINISH
      !
      !PROCESSING!
      !
      !FORM ARRAY OF I OR I(O)/I VALUES
      !
      DT=TFS/1000
      IATMAX=DELAY+INT(RECOV/DT)
      END=1024
      %IF PORTION=2 %THEN %START
      %IF FIRST>=1 %THEN %START
      IATMAX=FIRST
      %FINISH
      END=LAST
      %FINISH
      T=((IATMAX-DELAY)*DT)
      %CYCLE I=IATMAX,1,END
      %IF TYPE=2 %THEN %START
      DELTA(I)=BASE-INTEN(I)
      %FINISH
      %IF TYPE=1 %THEN %START
      DELTA(I)=(BASE-GROUND)/(INTEN(I)-GROUND)
      %FINISH
      TIME(I)=T
      T=T+DT
      %REPEAT
      !
      !FORM ARRAY OF CONCS
      !
      I=IATMAX
      %IF TYPE=1 %THEN %START
      %WHILE DELTA(I)>1 %THEN %CYCLE
      LRECIP(I)=LOG(LOG(DELTA(I)))
      %IF I=END %THEN %EXIT
      I=I+1
      %REPEAT
      IFINAL=I-1
      %FINISH
      %IF TYPE=2 %THEN %START
      %WHILE DELTA(I)>0 %THEN %CYCLE
      LRECIP(I)=LOG(DELTA(I))
      %IF I=END %THEN %EXIT
      I=I+1
      %REPEAT
      IFINAL=I-1
      %FINISH
      !
```

```
      !WEIGHTED LEAST SQUARES!
      !
      %CYCLE I=IATMAX,1,IFINAL
      N=I-IATMAX+1
      %IF WEIGHT=0 %THEN %START
      W(N)=1
      %FINISH
      %IF WEIGHT=1 %THEN %START
      %IF TYPE=2 %THENSTART
      W(N)=DELTA(I)
      %FINISH
      %IF TYPE=1 %THENSTART
      W(N)=(DELTA(IATMAX)/DELTA(I))
      %FINISH
      %FINISH
      %IF WEIGHT=2 %THEN %START
      %IF TYPE=2 %THEN %START
      W(N)=(DELTA(I))**2
      %FINISH
      %IF TYPE=1 %THEN %START
      W(N)=(DELTA(IATMAX)/DELTA(I))**2
      %FINISH
      %FINISH
      Y(N)=LRECIP(I)
      X(N)=TIME(I)
      %REPEAT
      NF=IFINAL-IATMAX+1
      SIGW=0
      SIGWX=0
      SIGWY=0
      SIGWX2=0
      SIGWY2=0
      SIGWXY=0
      SIGWDD=0
      %CYCLE I=1,1,NF
           SIGW  =SIGW  +W(I)
           SIGWX =SIGWX +W(I)*X(I)
           SIGWY =SIGWY +W(I)*Y(I)
           SIGWX2=SIGWX2+W(I)*X(I)*X(I)
           SIGWY2=SIGWY2+W(I)*Y(I)*Y(I)
           SIGWXY=SIGWXY+W(I)*X(I)*Y(I)
      %REPEAT
         DEN=SIGW*SIGWX2 - SIGWX*SIGWX
      SLOPE=(SIGW*SIGWXY - SIGWX*SIGWY)/DEN
      INTER=(SIGWY*SIGWX2-SIGWX*SIGWXY)/DEN
      %CYCLE I=1,1,NF
           SIGWDD=SIGWDD+((Y(I) - SLOPE*X(I) -INTER)**2)*W(I)
      %REPEAT
      ALPHA2=SIGWDD/(NF-2)
      ALPHAA=SQRT(!ALPHA2*SIGW/DEN!)
      ALPHAB=SQRT(!ALPHA2*SIGWX2/DEN!)
      DEVSLOPE=ALPHAA
      DEVINT  =ALPHAB
      !
      !COMMENCE OPTIMISATION!
      !
      !USING THE INITIAL VALUES OF THE SLOPE AND INTERCEPT
      !CALC. ABOVE TO DERIVE STARTING VALUES OF THE OPTIMISATION
      !PARAMETERS, THE APPROP MODEL RELATING INTENSITY OR I(O)/I
      !VALUES AND TIME IS FITTED TO THE DATA IN A NON-L.L.S.
      !SENSE,USING THE IMP LIBRARY ROUTINE IMP DAPRO.
      !
      NA=IATMAX
      NB=END
      %IF TYPE=1 %THEN ->100
      VV(1)=EXP(INTER)
      VV(2)=-SLOPE
      TOLL(1)=VV(1)/TOL1
      TOLL(2)=VV(2)/TOL2
      %BEGIN
          %LONGREALARRAY TIMEA(NA:NB),DELTAA(NA:NB),SFF(NA:NB)
          %CYCLE I=NA,1,NB
          TIMEA(I)=TIME(I)
          DELTAA(I)=DELTA(I)
          %REPEAT
          %LONGREALFN F(%LONGREAL C,%LONGREALARRAYNAME V)
              %RESULT=V(1)*EXP(-V(2)*C)
              %END
          IMP DAPRO(F,0,NA,NB,2,MM,SS,DD,TIMEA,DELTAA,VV,TOLL,SFF)
          %END
      ->200
      100:              VV(1)=EXP(EXP(INTER))
      VV(2)=EXP(-SLOPE)
      TOLL(1)=VV(1)/TOL1
      TOLL(2)=VV(2)/TOL2
      %BEGIN
          %LONGREALARRAY TIMEA(NA:NB),DELTAA(NA:NB),SFF(NA:NB)
          %CYCLE I=NA,1,NB
          TIMEA(I)=TIME(I)
          DELTAA(I)=DELTA(I)
          %REPEAT
          %LONGREALFN F(%LONGREAL C,%LONGREALARRAYNAME V)
              %RESULT=EXP(V(1)*EXP(-V(2)*C))
              %END
          IMP DAPRO(F,0,NA,NB,2,MM,SS,DD,TIMEA,DELTAA,VV,TOLL,SFF)
          %END
      200:              !OUTPUT!
      !
      %IF OUTPUT=0 %THEN ->300
      NEWLINES(3)
      %PRINTTEXT'INTENSITY          CONC    LOG(CONC)   TIME(S)'
      B=((IFINAL-IATMAX)//OUTPUT)
      LIMIT=B*OUTPUT+IATMAX-B
      NEWLINE
      %CYCLE I=IATMAX,B,LIMIT
      PRINT(INTEN(I),6,0)
      SPACES(5)
      PRINT(DELTA(I),6,2)
      SPACES(4)
      PRINT(LRECIP(I),2,4)
```

```
      SPACES(6)
      PRINTFL(TIME(I),4)
      NEWLINE
      %REPEAT
      300:              NEWLINES(2)
      %PRINTTEXT'FOR L.L.S. CALC.(WEIGHTING CODE='
      WRITE(WEIGHT,1)
      %PRINTTEXT'):-'
      NEWLINE
      %PRINTTEXT'SLOPE='
      PRINTFL(SLOPE,4)
      %PRINTTEXT' +OR- '
      PRINTFL(DEVSLOPE,4)
      NEWLINE
      %PRINTTEXT'INTERCEPT='
      PRINTFL(INTER,4)
      %PRINTTEXT' +OR-'
      SPACE
      PRINTFL(DEVINT,4)
      NEWLINE
      %PRINTTEXT'T.F.S.='
      PRINTFL(TFS,4)
      %PRINTTEXT'SECS'
      NEWLINE
      %PRINTTEXT'FLASH RECOVERY TIME ='
      PRINTFL(RECOV,4)
      %PRINTTEXT'SECS'
      NEWLINE
      %PRINTTEXT'RESULT AFTER OPTIMISING FIT:-'
      NEWLINE
      %PRINTTEXT'NUMBER OF ITERATIONS PERFORMED='
      WRITE(MM,5)
      NEWLINE
      %IF TYPE=1 %THEN %START
      DD=LOG(DD)
      VV(1)=LOG(VV(1))
      VV(2)=LOG(VV(2))
      %FINISH
      %PRINTTEXT'FIRST ORDER RATE CONSTANT ='
      PRINTFL(VV(2),4)
      %PRINTTEXT' +OR- '
      PRINTFL(DD,4)
      %PRINTTEXT' /SECOND'
      NEWLINE
      %PRINTTEXT'CONCN AT T=0    '
      PRINTFL(VV(1),4)
      NEWLINE
      %PRINTTEXT'VARIANCE=   '
      PRINTFL(SS,4)
      NEWLINE
      %IF PORTION=1 %START
      NEWLINE
      %PRINTTEXT'TOTAL DECAY PROCESSED'
      %FINISH
      %IF PORTION=2 %START
      %IF FIRST=0 %THEN %START
      FIRST=IATMAX
      %FINISH
      NEWLINE
      %PRINTTEXT'PROCESSED FROM CHANNEL '
      WRITE(FIRST,4)
      %PRINTTEXT' TO CHANNEL '
      WRITE(LAST,4)
      %FINISH
      NEWLINE
      NEWPAGE
      NEWLINE
      %IF OUT=1 %OR OUT=2 %THENSTART
      !GRAPH OUTPUT!
      %IF NF>60 %THENSTART
      PT=60
      DPT=NF//PT
      PTS=PT
      %IF DPT*PTS>NF %THENSTART
      PTS=NF//(DPT-1)
      %FINISH
      P=0
      NF=PTS*DPT
      %CYCLE I=DPT,DPT,NF
      P=P+1
      PLOTX(P)=X(I)
      PLOTY(P)=Y(I)
      %REPEAT
      %FINISH
      %IF NF<=60 %THENSTART
      %IF NF<=60 %THEN PT=60 %AND M=1
      %IF NF<=30 %THEN PT=30 %AND M=2
      %IF NF<=20 %THEN PT=20 %AND M=3
      %IF NF<=15 %THEN PT=15 %AND M=4
      %IF NF<=10 %THEN PT=10 %AND M=6
      PTS=NF
      P=NF
      %CYCLE I=1,1,NF
      PLOTX(I)=X(I)
      PLOTY(I)=Y(I)
      %REPEAT
      %FINISH
      !SCALE OF GRAPH!
      IMIN=1
      MAXY=PLOTY(1)
      MINY=PLOTY(1)
      %CYCLE I=1,1,P
      %IF PLOTY(I)>MAXY %THEN MAXY=PLOTY(I)
      %IF PLOTY(I)<MINY %THEN MINY=PLOTY(I) %AND IMIN=I
      %REPEAT
      DY=(MAXY-MINY)*(OUT/100)
      !.LP OUT=1: .TT OUT=2!
      %CYCLE I=1,1,P
      %IF I≠IMIN %THENSTART
      PY(I)=((PLOTY(I)-MINY)/DY)+1
```

```
        %FINISH
        %IF I=IMIN %THEN PY(I)=1
        %REPEAT
        !OUTPUT!
        SELECTOUTPUT(10)
        %IF U=1 %AND OUT=1 %THENSTART
        NEWLINES(47)
        %FINISH
        NEWLINES(2)
        %PRINTTEXT'EXPERIMENT NO. '
        PRINT(EXPT,3,2)
        SPACES(3)
        %PRINTTEXT'SLOPE='
        PRINTFL(SLOPE,4)
        SPACES(2)
        %PRINTTEXT'INTERCEPT='
        PRINTFL(INTER,4)
        %IF PORTION=1 %START
        NEWLINE
        SPACES(20)
        %PRINTTEXT'TOTAL DECAY PROCESSED'
        %FINISH
        %IF PORTION=2 %START
        %IF FIRST=0 %THEN %START
        FIRST=IATMAX
        %FINISH
        NEWLINE
        SPACES(20)
        %PRINTTEXT'PROCESSED FROM CHANNEL '
        WRITE(FIRST,4)
        %PRINTTEXT' TO CHANNEL '
        WRITE(LAST,4)
        %FINISH
        NEWLINE
        SPACES(20)
        PRINTSTRING(YAXIS)
        SPACES(2)
        %PRINTTEXT'(1 UNIT='
        PRINTFL(DY,4)
        %PRINTTEXT').'
        %IF OUT=2 %THENSTART
        NEWLINE
        SPACES(18)
        %FINISH
        SPACES(2)
        %PRINTTEXT'THE VALUE AT 0 IS '
        PRINTFL((PLOTY(IMIN)-DY),4)
        NEWLINE
        SPACES(10)
        %PRINTTEXT'0    5    10   15   20   '
        %PRINTTEXT'25   30   35   40   45   50'
        %IF OUT=1 %THENSTART
        %PRINTTEXT'   55   60   65   70   75'
        %PRINTTEXT'   80   85   90   95   100'
        %FINISH
        NEWLINE
        SPACES(10)
        %PRINTTEXT'!----'
        %CYCLE I=5,5,100?/OUT
        %PRINTTEXT'!----'
        %REPEAT
        %IF PT=60 %THENSTART
        NEWLINE
        %CYCLE I=1,1,PTS
        SPACES(7)
        WRITE(I,2)
        %IF I=10 %OR I=50 %THENSTART
        CALCY=0
        CALCY=(((2*PLOTX(1))-PLOTX(2))+(I*(PLOTX(2)-PLOTX(1))))
        CALCY=(CALCY*SLOPE)+INTER
        PY(I)=(((CALCY-MINY)/DY)+1
        SPACES(INT(PY(I))-1)
        PRINTSTRING('X')
        NEWLINE
        ->1
        %FINISH
        SPACES(INT(PY(I))-1)
        PRINTSTRING('*')
        NEWLINE
        1: %REPEAT
        %IF PTS<60 %THENSTART
        %CYCLE I=PTS+1,1,60
        SPACES(7)
        WRITE(I,2)
        NEWLINE
        %REPEAT
        %FINISH
        %FINISH
        %IF NF<=30 %THENSTART
        %CYCLE I=1,1,NF
        NEWLINES(M)
        SPACES(7)
        WRITE(I,2)
        SPACES(INT(PY(I))-1)
        PRINTSTRING('*')
        %REPEAT
        NEWLINES(60-(NF*M))
        %FINISH
        SPACES(20)
        PRINTSTRING('THE X AXIS REPRESENTS ')
        PRINTSTRING(XAXIS)
        SPACES(2)
        %IF OUT=2 %THENSTART
        NEWLINE
        SPACES(5)
        %FINISH
        %PRINTTEXT'THE VALUE AT 0 IS '
        PRINTFL((2*PLOTX(1))-PLOTX(2),4)
        %PRINTTEXT'(1 UNIT='
        PRINTFL(PLOTX(2)-PLOTX(1),4)
        %PRINTTEXT'(SECS).)'
        %FINISH
        NEWLINE
        %REPEAT
        %ENDOFPROGRAM
```

TABLE 20 PROGRAM EXPFITO

INPUT/OUTPUT

```
COMMAND:DEFINE(ST1,DATA01)

COMMAND:DEFINE(ST2,INF001)

COMMAND:DEFINE(ST3,RES01)

COMMAND:DEFINE(ST4,*TT)

COMMAND:RUN(EXPFITO)

THIS PROGRAM IS ONLY FOR USE IN CONJUNCTION
WITH DATA FROM A TRANSIENT RECORDER.OUTPUT4=INSTRUCTIONS,
OUTPUT3=RESULTS,OUTPUT10=GRAPH,INPUT1=DATA,INPUT2=INSTRUCTIONS
THE INSTRUCTIONS FILE(ST2) SHOULD CONTAIN
THE EXPERIMENT NO., TFS(SECONDS), FLASH RECOVERY TIME(SECONDS)
AND(OPTIONALLY) THE FIRST AND LAST CHANNELS TO BE PROCESSED,
WITH A SPACE BETWEEN EACH PIECE OF DATA AND A NEWLINE FOR
EACH EXPERIMENT

HOW MANY EXPERIMENTS ARE TO BE PROCESSED?
DATA:2

IS A GRAPH OUTPUT REQUIRED?
IS THIS TO BE ON THE LINEPRINTER(1) OR ON THE TELETYPE(2)?
IF NO GRAPH OUTPUT IS REQUIRED TYPE(0).
DATA:0

IS THE SIGNAL +(P) OR -(N)?
DATA:N

ABSORPTION(1) OR FLUORESCENCE(2) DATA?
DATA:2
DO YOU WISH TO SELECT A PORTION OF THE DECAY
CURVE WHICH IS TO BE PROCESSED? YES(2) OR NO(1)?
DATA:1


WAS A PRETRIGGER DELAY SET? IF SO, HOW MANY CHANNELS?
IF NOT TYPE(0).
DATA:400
WEIGHTING CODE FOR LINEAR LEAST SQUARES CALCULATION
0: NO WEIGHTING
1: WEIGHTING PROPORTIONAL TO EXPTL CONCENTRATIONS
2: WEIGHTING PROPORTIONAL TO EXPTL CONCENTRATIONS SQUARED
DATA:2
MAX NO OF ITERATIONS TO BE PERFORMED.
DATA:30
THE TOLERANCES X(K) ARE DEFINED SUCH THAT THE CALCULATION
IS TAKEN TO HAVE CONVERGED IF THE CHANGE IN EACH PARAMETER
IS LESS THAN 1 PART IN X(K) OF ITS STARTING VALUE
TOLERANCE FOR INTERCEPT
DATA:10000
TOLERANCE FOR RATE CONSTANT
DATA:10000

HOW MANY LINES OF OUTPUT ARE REQUIRED PER EXPT.
DATA:0
 STOPPED AT LINE 536

COMMAND:LIST(RES01)



EXPERIMENT NUMBER   1.03



TOLERANCES    TOL(1)= 2.101833@ -1     TOL(2)= 5.403200@ -2

ITERATIONS    V(1)            V(2)            B(1)            B(2)

    1         2.476144@  3    6.407268@  2    2.843107@  2    9.139700@  1
    2         2.610322@  3    6.686658@  2    1.341785@  2    2.793899@  1
    3         2.632938@  3    6.729547@  2    2.261624@  1    4.288887@  0
    4         2.635590@  3    6.735172@  2    2.651132@  0    5.624653@ -1
    5         2.635921@  3    6.735895@  2    3.311599@ -1    7.227880@ -2
    6         2.635963@  3    6.735887@  2    4.227726@ -2    8.254674@ -3


FOR LINEAR LEAST SQUARES CALCULATION(WEIGHTING CODE= 2):-
SLOPE=-5.403300@  2 +OR-  7.950700@  0
INTERCEPT= 7.692500@  0 +OR-  1.624400@ -2
T.F.S.= 2.000000@ -2SECS
FLASH RECOVERY TIME = 1.000000@ -3SECS
RESULT AFTER OPTIMISING FIT:-
NUMBER OF ITERATIONS PERFORMED=      6
FIRST ORDER RATE CONSTANT = 6.736000@  2 +OR-  8.116700@  0 /SECOND
CONCN AT T=0     2.636000@  3
VARIANCE=    4.966200@  1

TOTAL DECAY PROCESSED
```

TABLE 21 PROGRAM CHEK — INPUT DATA

```
//EDCHOSEL JOB (REGION=250K,T=2M,L=5,),'JME-CHEMISTRY'
// EXEC FORTRANG,REGION.G=250K
//C.SYSIN DD *
      SUBROUTINE PATCHD
      REAL*8 XX,DELTA,RATE,A,B,P,Q
      INTEGER*2 INCSET
      COMMON/GNRL/XX,DELTA
      COMMON/CMPL/IMAX
      COMMON/COEFF/RATE(250),INCSET(250)
      DATA A/9.25E9/,B/-1.00E5/,P/7.70/
      Q=XX+1.0E-9
      RATE(INCSET(1))=(DLOG(100/(100-P)))*A*Q*DEXP(B*Q)
      RETURN
      END
//L.LIB DD DSN=QXPLU.CHEKMAT,DISP=SHR
//L.SYSIN DD *
    INCLUDE LIB(CHEK)
    ENTRY MAIN
//G.FT09F001 DD SYSOUT=A
//G.SYSIN DD *
* SIMULATION OF THE PHOTOLYSIS OF OZONE IN PRESENCE OF CF3CL. ;
* TEMPERATURE=300K. FINAL BEST FIT MODEL. ;
**;
7.08E15 O3 = O(1D) + O2(SD)              / 1.00E-10 ;
O(1D) + O3 = O(3P) + O(3P) + O2          / 2.7E-10  ;
O(1D) + 6.37E17 CF3CL = CLO + CF3        / 1.62E-10 ;
O(1D) + CF3CL = CF2O + FCL               / 6.3E-11  ;
O(1D) + CF3CL = CL + F + CF2O            / 2.5E-11  ;
O(3P) + CLO = CL + O2                    / 5.3E-11  ;
O(3P) + O(3P) + 3.72E18 SF6 = O2 + SF6 / 84E-34   ;
O(3P) + 3.54E15 O2 + SF6 = O3 + SF6      / 250E-35  ;
CL + O3 = CLO + O2                       / 1.2E-11  ;
CF3 + CF3 = C2F6                         / 9.0E-12  ;
CF3 + O3 = CF3O + O2                     / 1.0E-10  ;
F + O3 = FO + O2                         / 1.4E-11  ;
CLO + CLO = CLOO + CL                    / 1.2E-14  ;
CLO + CLO = OCLO + CL                    / 2.4E-15  ;
CLO + CLO = CL2 + O2                     / 9.6E-15  ;
CLOO + SF6 = CL + O2 + SF6               / 6.0E-13  ;
FO + CLO = F + OCLO                      / 3.3E-11  ;
FO + FO = F2 + O2                        / 3.3E-11  ;
CL + CLOO = CL2 + O2                     / 1.6E-10  ;
CL + CLOO = CLO + CLO                    / 1.6E-11  ;
O2(SD) + O3 = O2 + O2 + O(3P)            / 1.48E-15 ;
O2(SD) + SF6 = O2 + SF6                  / 5.16E-18 ;
**;
MAX -7.08E15 O3 ;
MAX -0.00 FCL ;
MAX -0.00 CF2O ;
MAX -0.00 CF3O ;
MAX -0.00 CL2 ;
MAX -6.37E17 CF3CL ;
MAX -0.00 CLO ;
MAX -0.00 CL ;
MAX -0.00 FO ;
MAX -0.00 F ;
MAX -0.00 CF3 ;
MAX -0.00 C2F6 ;
MAX -3.54E15 O2 ;
MAX -4.35E18 SF6 ;
MAX -7.08E14 O(1D) ;
MAX -7.08E14 O2(SD) ;
MAX -7.08E14 O(3P) ;
MAX -0.00 OCLO ;
MAX -0.00 CLOO ;
MAX -0.00 F2 ;
GSTREAM 9 100 ;
GRAPH CLO 4.0E14 C ;
GRAPH O(1D) 2.0E11 1 ;
GRAPH O2(SD) 1.8E15 D ;
GRAPH CF3 2.0E13 F ;
GRAPH O3 7.10E15 Z ;
TIME 2.0E-6 2.0E-6 ;
NSTEP 50 ;
DELTA 2.0E-6 ;
BEGIN 2 ;
SAVE ;
TIME 1.0E-4 1.0E-3 ;
NSTEP 199 ;
DELTA 1.0E-3 ;
BEGIN 2 ;
STOP ;
//

SUBROUTINE PATCH1
REAL*8 VAR,EL,D,AIO
COMMON/VAR/VAR(100)
DATA EL/1.43E-16/,AIO/135.4/
D=VAR(1)*EL
VAR(4)=AIO*(DEXP(-D))
RETURN
END
```

References

References

1. R.J. Donovan and D. Husain, Chem.Rev. 489,70,(1970).

2. H.E. Gunning and O.P. Strausz, Adv.in Photochem.143,4,(1966).

3. R.J. Donovan and H.M. Gillespie, Specialist Periodical Reports (Chemical Society) Gas Kinetics Vol 1, (1975).

4. R.G.W. Norrish and G. Porter, Nature 164, 658, (1949).

5. P.M. Rentzepis and C.J. Mitchele, Anal.Chem. 20A, 42, (1970).

6. M.J. Berry in "Molecular Energy Transfer", ed. by J.Jortner and R.D. Levine, p.114, Wiley (1976).

7. R.P.Wayne Adv.in Photochem. 311, 7, (1969).

8. R.J. Donovan, K. Kaufmann and J. Wolfrum, Nature 204, 262, (1976).

9. A.A. Westenberg and N. de Haas, J.Chem.Phys. 3087, 40, (1964).

10. M.A.A Clyne, Phys.Chem.of fast Reactions, Vol. 1, p.245, (Plenum) (1971).

11. L.F. Phillips and H.I. Schiff, J.Chem.Phys. 1233, 37, (1962).

12. E.A. Ogryzlo and A.E. Pearson, J.Phys.Chem.2913, 72, (1968).

13. N. Jonathan, K.Ross and D.J. Smith, J.Chem.Phys. 3758, 53, (1970).

14. R.H. Newman, L.F. Phillips et al., Trans.Farady Soc.2827, 66, (1970).

15. H.S. Johnston et al., Proc.Natl.Acad.Sci.(US) 1146, 57,(1967).

16. H.S. Johnston and E.D. Morris, J.Am.Chem.Soc. 1918, 90, (1968).

17. D.A. Parkes, D.M. Paul and C.P. Quinn, J.Chem.Soc.Faraday Trans.I 1935, 72, (1976).

18. L.F. Phillips, Rev.Scient.Instrum. 1098, 42, (1971).

19. K. Kayama and J.C. Baird, J.Chem.Phys. 2604, 46, (1967).

20. D. Zamani-Khamira and H.F. Hameka, J.Chem.Phys.2191, 55, (1971).

21. D.R. Kearns, Chem.Rev. 395, 71, (1971).

22. B. Rosen (ed), Int. Table of Selected Constants vol.17, Spectroscopic Data, Pergamon, (1970).

23. U. Schurath,J.Photochem. 215, 4, (1975).

24. E. McKeown and W.A. Waters, J.Chem.Soc.(B) 1040, (1966).

25. M. Kasha and A.U.Khan, Annal.N.Y.Acad.Sci 5, 71,(1970).

26. R.J. Browne and E.A. Ogryzlo, Proc.Chem.Soc. 117, (1964).

27. T. Kajiwara and D.R. Kearns, J.Am.Chem.Soc. 5886, 95,(1973).

28. I.B.C. Mathesen, J.B. Lee, B.S. Yamanashi and M.L. Wolbarsho, Chem.Phys.Lett.355, 27, (1974).

29. J.N. Pitts et al., J.Am.Chem.Soc.3299, 97, (1975).

30. A.A. Krasmovskii and E.A. Vendiktov, Biophyzika, 387, 23, (1978).

31. H.W.-S. Chan, J.Am.Chem.Soc. 4632, 93, (1971).

32. L.L. Smith and J.I. Teng, J.Am.Chem.Soc. 4060, 95, (1973).

33. D.J.T. Porter and L.L. Ingraham, Biochim.Biophys.Acta, 97, 334, (1974).

34. L.L. Smith and M.J. Kulig, J.Am.Chem.Soc. 1027, 98, (1976).

35. W. Adam, Chem.Z. 142, 99, (1975).

36. K. Sugioka et al., J.Biol.Chem. 2404, 250, (1975).

37. K. Sugioka and M. Nakano, Biochim.Biophysica Acta 203, 423, (1976).

38. P.B. Merkel and D.R. Kearns, Chem.Phys.Lett. 120, 12, (1971).

39. P.B. Merkel and D.R. Kearns, J.Am.Chem.Soc.7244, 94, (1972).

40. I.B.C. Matheson, A.D. King and J. Lee, Chem.Phys.Lett.49, 55, (1978).

41. A.A. Gorman and M.A.J. Rogers, Chem.Phys.Lett.52, 55, (1978).

42. C.A. Long and D.R. Kearns, J.Am.Chem.Soc.2018, 97, (1975).

43. K. Kear and E.W. Abrahamson, Abstracts of 2nd Noyes Photochemistry Symposium (1972).

44. J.A. Davidson and E.A. Ogryzlo, Chemiluminescence and Bioluminescence (Plenum Press, N.Y., 1973).

45. M. Braithwaite, J.A. Davidson and E.A. Ogryzlo, J.Chem.Phys., 771, 65, (1976).

46. K. Kear and E.W.Abrahamson, J.Photochem. 409, 3,(1974).

47. R.G.O. Thomas and B.A. Thrush, Proc.Roy.Soc.A 307, 356, (1977).

48. E.A. Ogryzlo, Ber. Bunsengesellschaft Phys. Chem.177, 81, (1977).

49. E.A. Ogryzlo and B.A. Thrush, Chem.Phys.Lett.34, 23,(1973).

50. E.A. Ogryzlo and B.A. Thrush, Chem.Phys.Lett.314, 24, (1974).

51. S. Madronich, J.R. Weisenfeld and G.J. Wolga, Chem.Phys.Lett. 267, 46, (1977).

52. K. Furukawa and E.A. Ogryzlo, J.Photochem. 163, 1, (1972).

53. R.D. Ashford and E.A. Ogryzlo, Can.J.Chem.5344, 52, (1974).

54. R.D. Ashford and E.A. Ogryzlo, J.Am.Chem.Soc.3604, 97,(1975).

55. R.D. Kenner and A.U. Khan, J.Chem.Phys.1877, 64, (1976).

56. D.R. Kearns and A.U. Khan, J.Chem.Phys.3272, 48, (1968).

57. R.D. Kenner and A.U. Khan, Chem.Phys.Lett.643, 36, (1975).

58. R.D. Kenner and A.U. Khan, Chem.Phys.Lett.340, 45, (1977).

59. I.T.N. Jones and K.D. Bayes, J.Chem.Phys.3119, 59, (1973).

60. T. Frankiwicz and R.S. Berry, Env.Sci.Tech.365, 6, (1972).

61. M. Sukigawa, Seyan Kenkyu 387, 23, (1977).

62. J.J. Deakin, D. Husain and J.R. Weisenfeld, Chem.Phys.Lett. 146, 10, (1971).

63. R.G. Derwent and B.A. Thrush, Chem.Phys.Lett.591, 9,(1971)

64. A.T. Phitt, R.D. Coombe et al., App.Phys.Lett.,745,31, (1977).

65. M.A.A. Clyne and A.H. Curran, Gas Kinetics and Energy Transfer (vol 2), p.253, The Chemical Society, (1977).

66. V.S. Zeiev, L.D. Mikheev and V.I. Yalvoi, Soviet J.Quantum Electronics 442, 5, (1975).

67. R.F. Barrow and R.P. Duparc, Elemental Sulphur, Ed. B. Meyer, Interscience, (1965).

68. R.F. Barrow et al. J.Physics B, Ser 2 283, 1, (1968).

69. M. Carleer and R. Colin, J.Phys B 175, 3, (1970).

70. O.P. Strauz, R.J. Donovan and M.de Sorgo, Ber.Bunsengesellschaft Phys.Chem., 253, 72, (1968).

71. R.J. Donovan, D. Husain and P.T. Jackson, J.Chem.Soc.Trans. Far.Soc. 1798, 64, (1967).

72. W.D. McGrath, J.J. McGarvey and D.N. Dempster, Can.J.Chem. 2454, 45, (1967).

73. F.A. Cotton and G. Wilkinson, Adv.Inorg.Chem. (3rd Ed.) Interscience (1972).

74. W.H. Breckenridge and T.A. Millar. J.Chem.Phys.465, 56, (1972).

75. A. Carrington, D. Levy and T.A. Millar, J.Chem.Soc., Trans.Farad.Soc.2994, 62, (1966).

76. W.W. Clarke and F.C. De Lucia, J.Mol.Spec.332, 60, (1976).

77. R. Colin, Can.J.Phys. 1539, 46, (1968).

78. M.C. Linn and R.G. Shortridge, Chem.Phys.Lett.146, 35, (1975).

79. R.J. Donovan and D.J. Little, Chem.Phys.Lett. 394, 53, (1978).

80. R.J. Donovan, D.J. Little and J. Konstantatos, J.Photochem. 86, 1, (1973).

81. S.J. Arnold and E.A. Ogryzlo, Can.J.Phys. 2053,45, (1967).

82. G. Porter and M.A. West in 'Investigation of Rates and Mechanisms of Reactions' (2nd ed.) part 2,edited by G.G. Hammes (Wiley-Interscience).

83. D.J. Little, Ph.D. thesis, University of Edinburgh (1974).

84. L. Mallet, Compt.Rendu 352, 185, (1927).

85. P. Groh and K.A. Kirrmann, Compt.Rendu 275, 215, (1942).

86. A.U. Khan and M. Kasha, J.Am.Chem.Soc. 3293, 92, (1970).

87. A.E. Cahill and H. Taube, J.Am.Chem.Soc. 2313, 74,(1953).

88. T. Kajiwara, Bussei 15, 15, (1974).

89. S.J. Arnold, M. Kubo and E.A. Ogryzlo, Adv.Chem. 133, 71, (1968).

90. H.H. Seliger, J.Chem.Phys.3133, 40, (1964).

91. D.L. Heustis, G. Black, S.A. Edelstein, R.L. Sharpless, J.Chem.Phys.4471, 50, (1974).

92. S.J. Arnold and E.A. Ogryzlo, Can.J.Phys.2053, 45, (1967).

93. R.G. Derwent and B.A. Thrush, Trans.Far.Soc.2036, 67, (1971).

94. K.H. Becker, W. Groth and U. Schurath, Chem.Phys.Lett. 259, 8, (1971).

95. Handbook of Chemistry and Physics (55th Edn.) page D-159, Ed. R.G. Weast (CRC Press, 1974).

96. P.H. Vidaud, R.P. Wayne and M. Yaron, Chem.Phys.Lett. 306, 38, (1976).

97. A. Lieff, U. Schurath, K.H. Becker and E.H. Fink, J. Photochem.211, 8, (1978).

98. F.D. Finlay and D.R. Snelling, J.Chem.Phys. 545, 55,(1971).

99. P.R.H. Speakman,personal communication.

100. E.J. Bowen, Pure and App. Chem., 447, 9, (1964).

101. T.D. Clarke and R.P. Wayne, Proc. Roy. Soc. A 111, 314 (1969).

102. P.D. Steer, R.A. Ackerman and J.N. Pitts, J.Chem.Phys. 843, 55, (1969).

103. K.G. Vohra, J.P.S. Chatha, P.K.Arova and N. Raja, Proc.Symp. on Singlet Molecular Oxygen, 1975 (1976) p.35.

104. P.M. Borrell, P. Borrell and M.D. Pedley, Chem.Phys.Lett. 300, 51, (1977).

105. M. Griggs, J.Chem.Phys., 857, 49, (1968).

106. E. Castellano and H.J.Schumacher, J.Chem.Phys. 2238, 36, (1962).

107. D.R. Stuhl, JANAF Thermochemical Tables, 2nd Ed. (1971).

108. I.T.N. Jones and R.P. Wayne, Proc.Roy.Soc. A 273, 319, (1970).

109. O. Kajimoto and R.J. Cvetanovic., Chem.Phys.Lett. 533, 37, (1976).

110. D.L. Philen, R.T. Watson and D.D. Davis, J.Chem.Phys. 3316, 67, (1977).

111. G.K. Moortgat, I. Arnold and J.M. Comes, Chemical Physics, 211, 24, (1977).

112. C.L. Lin and W.B. DeMore, J.Photochem. 161, 2, (1973).

113. W.B. DeMore and O.F. Raper, J.Chem.Phys.1780, 44, (1966).

114. E. Lissi and J. Heicklen, J.Photochem. 39, 1, (1970).

115. R.F. Hampson, J.Phys.Chem. Ref. Data 267, 2, (1973).

116. C.E. Fairchild, E.J. Stone and G.M. Lawrence, J.Chem.Phys. 3632, 69, (1978).

117. L.J. Heidt and G.S. Forbes, J.Am.Chem.Soc. 2365, 56, (1934).

118. R.G.W. Norrish and R.P. Wayne, Proc.Roy.Soc.A 200, 288, (1965).

119. G. von Ellenreider, E. Castellano and H.J. Schumacher, Chem.Phys.Lett. 152, 9, (1971).

120. W.D. McGrath and R.G.W. Norrish, Proc.Roy.Soc.A 265, 242, (1957).

121. V.D. Biamonte, L.G. Hartshorn and E.J. Bair, J.Chem.Phys. 3617, 55, (1971).

122. H. Webster and E.J. Bair, J.Chem.Phys. 4532, 53, (1970).

123. M. Gunther and D.R. Snelling, Chem.Phys.Lett. 93, 5, (1970).

124. D.J. Giachardi and R.P. Wayne, Proc.Roy.Soc.A 131, 330, (1971).

125. L. Wallace and D.M. Hunten, J.Geophys.Res. 4813, 73, (1968).

126. R.A. Young and G. Black, J.Chem.Phys. 2311, 47, (1967).

127. E. Lissi and J. Heicklen, J.Geophys.Res. 4248, 77, (1972).

128. P.N. Clough and B.A. Thrush, Chem. and Ind. 1971 (1966).

129. A.R. Curtis and E.M. Chance, A.E.R.E. (Harwell)-R7345 H.M.S.O. (1974).

130. R.F. Heidner, D. Husain and J.R. Weisenfeld, J.C.S. Faraday Trans. II 827, 69, (1973).

131. R.J. Cvetanovic, Can.J.Chem. 1452, 52, (1974).

132. G.E. Streit, G.J. Howard, A.L. Schomaltekopf, J.A. Davidson and H.I. Schiff, J.Chem.Phys. 4761, 65, (1976).

133. D. Husain and R.F. Heidner, Int.J.Chem.Kin. 819, 5, (1973).

134. D.R. Snelling, Can.J.Chem. 257, 52, (1974).

135. K.L. Demerjian, J.A. Kerr and J.G. Calvert, Adv.Env.Sci.Tech.1, 4, (1974).

136. K. Schofield, Int.J.Chem.Kin. 255, 4, (1974).

137. R.J. Donovan et al., J.C.S. Faraday II 145, 69, (1973).

138. K. Schofield, Planet.Space Sci. 643, 15, (1967).

139. D. Husain, L.J. Kirsch and R.J. Donovan, J.Photochem., 1, (1972).

140. D. Davis, Chem.Phys.Lett. 273, 22, (1973).

141. M.J. McEwan and L.F. Phillips
Chemistry of the Atmosphere.
Arnold (1968).

142. H.S. Johnston, NBS-NSRDS-20 (1968).

143. J.E. Morgan and H.I. Schiff, J.Chem.Phys. 1495, 38, (1963).

144. I.M. Campbell and C.N. Gray, Chem.Phys.Lett. 607, 18, (1973).

145. S.W. Benson and A.E. Axworthy, J.Chem.Phys. 2614, 42, (1965).

146. M.F.R. Mulcahy and D.J. Williams, Trans.Faraday Soc. 59, 64, (1968).

147. F. Kaufman, J.Chem.Phys. 4541, 46, (1967).

148. R.E. Huie, J.Phys.Chem. 2643, 76, (1972).

149. F. Kaufman, Ann.Rev.Phys.Chem. 45, 20, (1969).

150. F.S. Rowland and M.J. Molina, Nature 810, 249, (1974).

151. J.E. Lovelock et al. Nature 194, 241, (1973).

152. H.M. Gillespie and R.J. Donovan, Chem.Phys.Lett.468, 37, (1976).

153. H.M. Gillespie, R.J. Donovan and J.G. Garraway, J.Photochem. 29, 7, (1977).

154. R.J. Donovan, K. Kaufmann and J. Wolfrum, Nature, 204, 262, (1976).

155a. J.N. Pitts, H.L. Sandoval and R. Atkinson, Chem.Phys.Lett., 31, 29, (1974).

155b. R.K.M. Jayority, R. Simoniatis and J. Heicklen, J.Photochem. 203, 4, (1975).

156a. I.S. Fletcher and D. Husain, J.Phys.Chem. 1837, 80, (1976).

156b. J.A. Davidson, H.I. Schiff, T.J. Brown and C.J. Howard. J.Chem.Phys.4277, 69, (1978).

157. A.M. Bass and A.E. Ledford, 12th Informal Conference on Photochemistry, Maryland, U.S. (1976).

158. J.G. Garraway and R.J. Donovan, personal communication.

159. T. Ogawa, G.A. Carlson and G.C. Pimentel, J.Phys.Chem. 2090, 74, (1970).

160. K. Kaufmann and J. Wolfrum, to be published.

161. M.A.A. Clyne, D.J. McKenny and R.T. Watson, J.C.S. Faraday I, 322, 71, (1975).

162. R.J. Donovan and J. Champion, personal communication.

163. H.S. Johnston, E.D. Morris and J. van den Bogaerde, J.Am.Chem.Soc. 7712, 91, (1976).

164. M.A.A. Clyne and R.T. Watson, J.C.S. Faraday I 1169, 73, (1977).

165. R. Foon and M. Kaufman, Progr. Reaction Kinetics, 81, 8, (1975).

166a. M.A.A. Clyne and R.T. Watson, J.C.S. Faraday I 2250, 70, (1974).

166b. M.A.A. Clyne and Wing S. Nip, J.C.S. Faraday II 838, 72, (1976).

167. T. Ishiwata and I. Tanaka. 'Sensitised Chemiluminescence by $SO(^1\Delta)$' 13th informal conference on Photochemistry. Clearwater Beach FL (1978).

168. W. Swepe, Y.-P. Lee and H.F. Schaefer (to be published, see ref. 171)

169. R.N. Dixon, P.W. Tasker and G.G. Balint-Kurti Molec.Phys. 1455, 34, (1977).

170. D.E. Tevault and R.R. Smardzewski J.Chem.Phys. 3182, 69, (1978).

171. Y.-P. Lee and G.C. Pimental J.Chem.Phys. 306, 69, (1978).

172. P.R. Jones and H. Taube J.Phys.Chem. 1007, 77, (1973).

173. P.J. Crutzen Geophys.Res.Lett. 73, 3, (1976).

174. I.E. Graedel Geophys. and Space Phys.Rev. 421, 15, (1977) and ref. therein.

175. J.P. Friend 'The Global Sulphur Cycle' in "Chemistry of the lower atmosphere" p.177 Ed. S.I. Rasool, Plenum, N.Y. (1973).

176. K. Schofield J.Chem.Phys.Ref. Data 25, 2, (1973).

177. D.C. Kresenski, R. Simoniatis and J. Heicklen Int.J.Chem.Kin. 467, 3, (1971).

178. R.J. Donovan, L. Kirsch and D. Husain Nature 1164, 222, (1969).

179. R.B. Klemm and D.D. Davis, J.Chem.Phys. 1137, 78, (1974).

180. R.B. Langford and G.A. Oldershaw J.C.S. Faraday Trans.I. 1389, 69, (1973).

181. A.G. Gaydon, G.H. Kimbell and H.B. Palmer
Proc.Roy.Soc.A. 313, 279, (1964).

182. A. Hariri and C. Wittig. J.Chem.Phys. 4454, 67, (1977).

183. A. Hariri and C. Wittig J. Chem.Phys. 2109, 68, (1978).

184. R.J. Donovan, C. Fotakis and M.F. Golde
J.C.S.Faraday Trans II 2055,
72, (1976).

185. A. Fayt, Annales Soc.Sci.Bruxelles 69, 84, (1970).

186. T.D. Kolaniitseva and D.N. Slichepkin
Opt.Spectrosk 51, 38, (1975).

187. G.A. Cook, A.D. Kiffer, C.V. Klump, A.H. Malik and L.A. Spence
Adv. in Chem.Ser., Am.Chem.Soc.
44, 21, (1957).

Lectures attended

In accordance with the regulations of the University of Edinburgh, Department of Chemistry, the post-graduate lecture courses etc. attended during the period of study are listed here.

They were: Chemistry of the upper atmosphere; Molecular collisions; Aspects of nuclear magnetic resonance spectroscopy; Computer programming; History of the chemistry department; The gaseous environment and Scientific German tutorials.

In addition, many of the regular departmental seminars in the chemistry department and discussions organised by the gas kinetics research group were attended.